3-1-2012

The Impact of Nucleoside Sugar Modification on Biochemical DNA Transactions

Adides Williams
Loma Linda University

LOMA LINDA UNIVERSITY
School of Medicine
in conjunction with the
Faculty of Graduate Studies

The Impact of Nucleoside Sugar Modification on Biochemical DNA Transactions

by

Adides Anthwon Williams

A Dissertation submitted in partial satisfaction of
the requirements for the degree of
Doctor of Philosophy in Biochemistry

March 2012

Each person whose signature appears below certifies that this dissertation in his/her opinion is adequate, in scope and quality, as a dissertation for the degree Doctor of Philosophy.

_____, Chairperson

Lawrence C. Sowers, Professor and Chair, Department of Pharmacology & Toxicology, University of Texas Medical Branch, Galveston, TX

_____

John Buchholz, Professor of Physiology and Pharmacology

_____

Penelope Duerksen-Hughes, Professor of Biochemistry

_____

Jonathan Neidigh, Assistant Professor of Biochemistry

_____

Kangling Zhang, Associate Research Professor of Biochemistry

ACKNOWLEDGEMENTS

I would like to express my thanks and gratitude to Dr. Lawrence Sowers who provided both the time and resources to make all this possible. I am grateful for his mentorship and am thankful that he dedicated his personal time and interest into my development as a scientist.

I would also like to extend a loving thanks to my mom, Margaret Kearney, who has stood by me and encouraged me to attain my goals. She continues to be an invaluable support system. I would also like to thank my sister, Kadijah Rhinehart, and my brother, Tajh Rhinehart, for all of their encouragement and support.

I would like to say a special thanks to Dr. Jonathan Neidigh for his guidance and co-mentorship both in and out of the lab. I would also like to extend a special thanks to my committee members for their guidance and support.

CONTENTS

TABLES

Tables Page

FIGURES

Figures Page

ABBREVIATIONS

dU	2’-deoxyuridine
$U^{2'F(ara)}$	2’-deoxy-2’-fluoroabinofuranosyl uracil
$U^{2'F(ribo)}$	2’-deoxy-2’-fluororibofuranosyl uracil
rU	Uridine
araU	1-β-D-arabinofuranosyluracil
dFdU	2’-deoxy-2’,2’-difluorouridine (Gemcitabine metabolite)
FIAU (Fialuridine)	5-iodo-(2'-deoxy-2'-fluoro-β-D-arabinosyl) uracil
5IdU	5-iodo-2’-deoxyuridine
araC	1-β-D-arabinofunanosylcytosine
dFdC (Gemcitabine)	2’-deoxy-2’,2’-difluorocytidine
pol β	DNA polymerase Beta (β)
AMVRT	avian myeloblastosis viral reverse transcriptase
Klenow (exo-)	*Escherichia coli* (Klenow Fragment) exonuclease deficient
T_m	Melting Temperature
ΔG°	Gibbs free energy
ΔH°	Enthalpy change
ΔS°	Entropy change
Km	Michaelis-Menten constant
kcat	Catalytic turnover number
kcat/Km	Enzyme catalytic efficiency
rN	ribonucleoside
araN	arabinonucleoside

HPLC	high performance liquid chromatography
MALDI-TOF	matrix-assisted laser desorption/ionization time-of-flight
ESI-MS	electrospray ionization mass spectrometry
MeCN	acetonitrile
MeOH	methanol
DCM	dichloromethane
EtOAc	ethyl acetate
UV/Vis	ultraviolet-visible light

ABSTRACT OF THE DISSERTATION

The Impact of Nucleoside Sugar Modification on Biochemical DNA Transactions

by

Adides Anthwon Williams

Doctor of Philosophy, Graduate Program in Biochemistry
Loma Linda University, March 2012
Dr. Lawrence C. Sowers, Chairperson

Discrimination by DNA polymerases controls the fidelity of DNA replication, and reduced fidelity results in mutations essential in the etiology of cancer. Polymerase discrimination operates at both dNTP insertion and subsequent elongation steps, and involves several energetic and structural factors that are as yet incompletely understood. While base pairing interactions have been studied extensively, substantially less is known about the role of sugar structure and conformation for polymerase incorporation and extension. In these studies we examined, systematically, the role of sugar structure and conformation on polymerase selection of the dNTP for insertion and polymerase elongation. To accomplish these goals, we have developed methods for the synthesis of oligonucleotides with nucleoside analogues with biased sugar conformations at the 3'-end (growing end) as well as at internucleotide positions. Through a series of thermodynamic, structural and functional studies, we reveal how sugar structure and conformational properties impact polymerase incorporation and extension behavior. The analogues proposed for this study allow an examination of structural and conformational properties, but also, this group of analogues comprises an important class of cytotoxic, antitumor and antiviral agents. The results of these studies will likely provide a clearer understanding of the role of sugar conformation in the fidelity of DNA synthesis and replication as well

as reveal important insights into the activity and toxicity of several nucleoside analogues and allow prediction of the biological properties of future analogues.

CHAPTER ONE

INTRODUCTION

DNA Synthesis and Fidelity

Fidelity of DNA synthesis is necessary to maintain genomic integrity, and errors made during replication and repair can lead to mutations and stalled replication forks [1]. DNA polymerases ensure the fidelity of DNA replication in both eukaryotes and prokaryotes. Nucleotide insertion, exonucleolytic proofreading and extension of primer termini are three distinct steps that contribute to overall replication fidelity [2]. Substantial work has focused on the importance of "base pairing fidelity" in the selection of the correct nucleotide [3-8]. But, relatively little work has been devoted to the impact of nucleoside ribose conformation on polymerase incorporation and extension. It is well known, however, that under endogenous conditions, DNA polymerases preferentially select 2'-deoxyribonucleoside triphosphates (dNTPs) for DNA replication whereas RNA polymerases select ribonucleoside triphosphates (rNTPs).

Polymerase Incorporation and Extension

For a given DNA sequence position, polymerase discrimination must occur in two distinct steps. During the insertion step a candidate nucleotide is chosen that is complimentary to the template base and is able to bind to the primer-template complex with sufficient stability [3-8]. Differences in the base-pairing and base-stacking energy

between correct and incorrect nucleotides, as measured in oligonucleotide melting studies, have been proposed to account for polymerase discrimination at the insertion step. Indeed, Goodman and co-workers [9] explained how polymerases could discriminate against mispairs by amplifying free energy differences ($\Delta\Delta G°$) between correct and incorrect base pairs. Following insertion, the polymerase must select the next correct nucleotide during the extension step. Surprisingly, polymerase extension beyond a mispair is very difficult, even for the insertion of a correct dNTP and even though base-pairing and geometry conditions are met [9-13]. Thus, extension fidelity contributes nearly as much to the overall replication fidelity as the initial insertion step. Both the insertion and extension steps require a correctly positioned terminal 3'-hydroxyl (3'-OH) to attack the α-phosphate (αP) of an incoming nucleotide. In the case of geometrically aberrant base pairs, such as a purine-purine mispair, the 3'-OH would be shifted several angstroms from the correct position, potentially preventing polymerase extension. With purine-pyrimidine mispairs, however, the geometry is closer to that of a normal Watson-Crick base pair, so that more subtle differences, such as sugar conformation, might become important. While sugar conformation can be biased by sugar structure, sugar conformation can also be influenced by base pair configuration.

Nucleoside Ribose Conformation

Sugar conformation, and therefore 3'-OH position, can change due to mispair formation, as well as from changes in the glycosidic torsion angle [14-18]. Sugar conformation can also be biased by the presence of substituents in the furanose ring. The conformational difference between deoxyribose and ribose sugars is attributed primarily

to the presence of the 2'-OH in the ribonucleosides. Other substituents, in particular, electron-withdrawing substituents including fluorine, are known to profoundly influence sugar conformation [19-22]. Nucleoside analogues bearing C2' (sugar) fluoro (F) and OH modifications comprise an important class of antitumor and antiviral agents [23, 24, 25, 26], and existing evidence indicates that the activity of these analogues results largely from interfering with DNA synthesis following misincorporation. Although the mechanism of action of these agents is incompletely understood, they are primary agents for the treatment of several human maladies including viral infections and tumors. For example, 2'-deoxy-2',2'-difluorocytidine (Gemcitabine, dFdC), in combination with platinum-containing drugs, is successfully used in the treatment of metastatic breast cancer [27], bladder cancer [28], and pancreatic adenocarcinoma [29]. 1-β-D-arabinofuranosylcytosine (Cytarabine, araC), in combination with daunorubicin, is commonly used as a chemotherapeutic for the treatment of acute myeloid leukemia (AML) and lymphomas [30] and has demonstrated activity against both herpes simplex and herpes zoster viruses [31, 32]. 5-iodo-(2'-deoxy-2'-fluoro-β-D-arabinosyl) uracil (Fialuridine, FIAU) is perhaps the most infamous of the nucleoside analogue family as it was once used in the treatment of hepatitis B virus infection in NIH clinical trials where unexpected hepatotoxicity, progressive lactic acidosis and pancreatitis resulted in two patients receiving emergency liver transplants in addition to the deaths of five patients [33]. The mechanism of action of each nucleoside analogue is varied but ultimately involves inhibition of DNA synthesis following incorporation by a DNA polymerase. In the triphosphate form, nucleoside analogues are incorporated into DNA and, in the case of dFdC, araC and FIAU, act as (pseudo) chain terminators.

Clinically Relevant Nucleoside Analogues and their Metbolites

In addition to phosphorlyation, nucleoside analogues can undergo additional metabolic processing. For example, FIAU is further metabolized to 1-(2-deoxy-2-fluoro-β-D-arabinofuranosyl)uracil ($U^{2'F(ara)}$). Interestingly, studies have shown that incubation of human hepatoma HepG2 cell lines with $U^{2'F(ara)}$ resulted in decreased mitochondrial DNA content [34] suggesting that $U^{2'F(ara)}$ may contribute to the cytotoxic profile of FIAU. Further, intra- and extracellular cytidine deaminases rapidly deaminate dFdC and araC to 2'-deoxy-2',2'-difluorouridine (dFdU) and 1-β-D-arabinofuranosyluracil (araU) metabolites. Surprisingly, little work has been done with these uracil analogues, yet they could account for much of the activity or cytotoxicity of these agents. Indeed, recent studies have demonstrated that dFdU nucleotides are formed and accumulate in the liver of mice and humans after multiple dosings of dFdC [35]. In addition, dFdUTP was observed in the DNA of HepG2 treated cells and the incorporation of dFdUTP correlated with dFdU cytotoxicity suggesting that liver accumulation of dFdU and subsequent misincorporation of dFdUTP might be associated with observed liver toxicity in patients following continuous oral and/or intravenous administration of dFdC [36]. In all, these studies highlight the biological importance of these sugar modified nucleoside analogues and the contribution of their metabolites to observed cytotoxicity.

The Purpose and Goals of these Studies

In this project we designed a series of experiments that allowed us to systematically examine the role of sugar structure and conformation on sugar-modified NTP (modNTP) incorporation and extension. To accomplish this we chemically

synthesized sugar-modified triphosphates and a series of synthetic oligonucleotides with C2'-F and C2'-OH substituted ribose sugars in arabino and ribo configurations at both an internucleotide position, and for the first time, at the 3'-end in a model replication fork. The results of our polymerase kinetics and thermal denaturation studies provided a systematic understanding of the energetic impact of nucleoside sugar substitution on polymerase incorporation and extension. Further, these studies lend insight into the mechanism of action and toxicity of clinically relevant nucleoside analogues and their metabolites.

References

(1) Kunkel, T. A. (2004) DNA replication fidelity. J. Biol. Chem. 279, 16895-16898.

(2) Goodman, M. F., Creighton, S., Bloom, L. B., and Petruska J. (1993) Biochemical basis of DNA replication fidelity. Crit. Rev. Biochem. Mol. Biol. 28, 1559-1562.

(3) Petruska, J., Sowers, L.C. and Goodman, M.F. (1986). Comparison of nucleotide interactions in water, protein, and vacuum: Model for DNA polymerase fidelity. Proc. Natl. Acad. Sci. USA. 83, 1559-1562.

(4) Joyce, C.M., Sun, X.C. and Grindley, N.D.F. (1992). Reactions at the polymerase active site that contribute to the fidelity of Escherichia coli DNA polymerase I (Klenow Fragment). J. Biol. Chem. 267, 24485-24500.

(5) Johnson, K.A. (1993). Conformational coupling in DNA polymerase fidelity. Annu. Rev. Biochem. 62, 685-713.

(6) Goodman, M.F. and Fygenson, D.K. (1998). DNA polymerase fidelity: From genetics toward a biochemical understanding. Genetics 148, 1475-1482.

(7) Beard, W.A. and Wilson, S.H. (2003). Structural insights into the origins of DNA polymerase fidelity. Structure 11, 489-496.

(8) Joyce, C. M. and Benkovic, S.J. (2004). DNA polymerase fidelity: Kinetics, structure, and checkpoints. Biochemistry 43, 14318-14324.

(9) Petruska, J., Goodman, M.F., Boosalis, M.S., Sowers, L.S., Cheong, C. and Tinoco, I. (1988). Comparison between DNA melting thermodynamics and DNA polymerase fidelity. Proc. Natl. Acad. Sci. USA. 85, 6252-6256.

(10) Perrino, F.W., Preston, B.D., Sandell, L.L. and Loeb, L.A. (1989). Extension of mismatched 3' termini of DNA is a major determinant of the infidelity of human immunodeficiency virus type 1 reverse transcriptase. Proc. Natl. Acad. Sci. 86, 8343-8347.

(11) Zinnen, S., Hsieh, J-C. and Modrich, P. (1994). Misincorporation and mispaired primer extension by human immunodeficiency virus reverse transcriptase. J. Biol. Chem. 269, 24195-24202.

(12) Mendelman, L.V., Petruska, J., and Goodman, M.F. (1990). Base pair extension kinetics. Comparison of DNA polymerase alpha and reverse transcriptase. J. Biol. Chem. 265, 2338-2346.

(13) Shah, A.M., Maitra, M. and Sweasy, J.B. (2003). Variants of DNA polymerase β extend mispaired DNA due to increased affinity for nucleotide substrate. Biochemistry 42, 10709-10717.

(14) Harvey, S.C. and Prabhakaran, M. (1986). Ribose puckering: structure, dynamics, energetics, and the pseudorotation cycle. J. Am. Chem. Soc. 108, 6128-6136.

(15) Boulard, Y., Cognet, J.A., Gabarro-Arpa, J., Le Bret, M., Sowers, L.C. and Fazakerley, G.V. (1992). The pH dependent configurations of the C.A mispair in DNA. Nucleic Acids Res. 20, 1933-1941.

(16) Cullinan, D., Johnson, F., Grollman, A. P., Eisenberg, M. and De Los Santos, C. (1997). Solution structure of a DNA duplex containing the exocyclic lesion 3, N4-etheno-2'-deoxycytidine opposite 2'-deoxyguanosine. Biochemistry 36, 11933-11943.

(17) Allawi, H.T. and SantaLucia, J., Jr. (1998). NMR solution structure of a DNA dodecamer containing single G•T mismatches. Nucleic Acids Res. 26, 4925-4934.

(18) Tonelli, M. and James, T.L. (1998). Insights into the dynamic nature of DNA duplex structure via analysis of nuclear overhauser effect intensities. Biochemistry 37, 11478-11487.

(19) Berger, I., Tereshko, V., Ikeda, H., Marquez, V.E. and Egli, M. (1998). Crystal structure of B-DNA with incorporated 2'-deoxy-2'-fluoro-arabino-furanosyl thymines: implications of conformational preorganization for duplex stability. Nucleic Acids Res. 26, 2473-2480.

(20) Damha, M.J., Wilds, C.J., Noronha, A., Brukner, I., Borkow, G., Arion, D. and Parniak, M.A. (1998). Hybrids of RNA and arabinonucleic acids (ANA and 2'F-ANA) are substrates of Ribonuclease H. J. Am. Chem. Soc. 120, 12976-12977.

(21) Ikeda, H., Fernandez, R., Wilk, A., Barchi, J.J., Jr., Huang, X. and Marquez, V.E. (1998). The effect of two antipodal fluorine-induced sugar puckers on the conformation and stability of the Dickerson-Drew dodecamer duplex [d(CGCGAATTCGCG)]2. Nucleic Acids Res. 26, 2237-2244.

(22) Wilds, C.J. and Damha, M.J. (1999). Duplex recognition by oligonucleotides containing 2'-Deoxy-2'-fluoro-D-arabinose and 2'-Deoxy-2'-fluoro-D-ribose. Intermolecular 2'-OH- phosphate contacts versus sugar puckering in the stabilization of triple-helical complexes. Bioconjugate Chem. 10, 299-305.

(23) Kuchta, R.D., Ilsley, D., Kravig, K.D., Schubert, S., Harris, B. (1992). Inhibition of DNA primase and polymerase alpha by arabinofuranosylnucleoside triphosphates and related compounds. Biochemistry 31, 4720-4728.

(24) Perrino, F.W. and Mekosh, H.L. (1992). Incorporation of cytosine arabinoside monophosphate into DNA at internucleotide linkages by human DNA polymerase α. J. Biol. Chem. 267, 23043-23051.

(25) Perrino, F.W., Mazur, D.J., Ward H. and Harvey, S. (1999). Exonucleases and the incorporation of aranucleotides into DNA. Cell. Biochem. Biophys. 30, 331-352.

(26) Pankiewicz K.W. (2000) Fluorinated nucleosides. Carbohyd. Res. 327, 87-105.

(27) Heinemann V. (2002) Gemcitabine plus cisplatin for the treatment of metastatic breast cancer. Clin. Breast Cancer 3, Suppl. 1, S24-s29.

(28) von der Maase, H., Hansen, S.W., Roberts, J.W., Dogliotti, L., Oliver, T., Moore, M.J., Bodrogi, I., Albers, P., Knuth A., Lippert, C.M., Kerbrat, P., Sanchez Rovira, P., Wershall, P., Cleall, S.P., Roychowdhury, D.F., Tomlin, I., Visseren-Grul, C.M., and Conte, P.F. (2000) Gemcitabine and cisplatin versus methotrexate, vinblastine, doxorubicin, and cisplatin in advanced or metastatic bladder cancer: Results of a large, randomized, multinational, multicenter, phase III study. J. Clin. Oncol. 17, 3068-3077.

(29) Colucci, G., Giuliani, F., Gebbia, V., Biglietto, M., Rabitti, P., Uomo, G., Cigolari, S., Testa, A., Maiello, E., and Lopez, M. (2002) Gemcitabine alone or with cisplatin for the treatment of patients with locally advanced and/or metastatic pancreatic carcinoma: A prospective, randomized phase III study of the Gruppo Oncologico dell'Italia Meridonale. Cancer 94, 902-910.

(30) Frei, E 3rd, Bickers, J.N., Hewlett, J.S., Lane, M., Leary, W.V., Talley, R.W. (1969) Dose schedule and antitumor studies of arabinosyl cytosine (NSC 63878). Cancer Res. 29, 1325-1332.

(31) Leopold, I.H. (1965) Clinical experience with nucleosides in herpes simplex eye infections in man and animals. Ann. N.Y. Acad. Sci. 130, 181-191; Renis, H.E. (1973) Antiviral activity of cytarabine in herpesvirus-infected rats. Antimicrob. Agents Chemother. 4, 439-444.

(32) Rapp, F. (1964) Inhibition by metabolic analogues of plaque formation by herpes zoster and herpes simplex viruses. J.Iimmunol. 93, 643-648.

(33) McKenzie R., Fried M.W., Sallie R., et al. (1985) Hepatic failure and lactic acidosis due to Fialuridine (FIAU), an investigational nucleoside analogue for chronic hepatitis B. N Engl. J. Med. 333, 1099–1105.

(34) Lewis, W., Levine, E.S., Griniuviene, B., Tankersley, K.O., Colacino, J.M., Sommadossi, J.P., Watanabe, K.A., Perrino, F.W. Fialuridine and its metabolites inhibit DNA polymerase gamma at sites of multiple adjacent analog

incorporation, decrease mtDNA abundance, and cause mitochondrial structural defects in cultured hepatoblasts. Proc. Natl. Acad. Sci. USA 93, 3592-3597.

(35) Veltkamp, S.A., Jansen, R.S., Callies, S., Pluim, D., Visseren-Grul, C.M., Rosing, H., Kloeker-Rhoades, S., Andre, V.A.M., Beijnen, J.H., Slapak, C.A., and Schellens, J.H.M. (2008) Oral administration of gemcitabine in patients with refactory tumors: A clinical and pharmacologic study. Clin. Cancer Res. 14, 3477-3485.

(36) Veltkamp, S.A., Pluim, D., van Eijndhoven, M.A.J., Bolijn, M.J, Ong, F.H.G., Govindarajan, R., Unadkat, J.D. Beijnen, J.H., and Schellens, J.H.M., (2008) New insights into the pharmacology and cytotoxicity of gemcitabine and 2',2'-difluorodeoxyuridine. Mol. Cancer Ther. 7, 2415-2425.

(37) Petruska, J., Sowers, L.C. and Goodman, M.F. (1986). Comparison of nucleotide interactions in water, protein, and vacuum: Model for DNA polymerase fidelity. *Proc. Natl. Acad. Sci. USA. 83*, 1559-1562.

CHAPTER TWO

IMPACT OF SUGAR PUCKER ON BASE PAIR AND MISPAIR STABILITY

*Adides A. Williams, Agus Darwanto, Jacob A. Theruvathu, Artur Burdzy, Jonathan W. Neidigh and Lawrence C. Sowers**

Department of Basic Sciences, Loma Linda University School of Medicine

Loma Linda, CA 92350

Running Title: sugar constraint and duplex stability

Adapted from Williams, A. A., Darwanto, A., Theruvathu, J.A., Burdzy, A., Neidigh, J. W., Sowers, L. C. (2009) Biochemistry 48, 11994-12004

Abstract

The selection of nucleoside triphosphates by a polymerase is controlled by several energetic and structural features, including base pairing geometry as well as sugar structure and conformation. Whereas base pairing has been considered exhaustively, substantially less is known about the role of sugar modifications for both nucleotide incorporation and primer extension. In this study, we synthesized oligonucleotides containing 2'-fluoro modified nucleosides with constrained sugar pucker in an internucleotide position and, for the first time, at a primer 3'-end. The thermodynamic stability of these duplexes was examined. The nucleoside 2'-deoxy-2'-fluoroarabinofuranosyl uracil ($U^{2'F(ara)}$) favors the 2'-endo conformation (DNA-like) while 2'-deoxy-2'-fluororibofuranosyl uracil ($U^{2'F(ribo)}$) favors the 3'-endo conformation (RNA-like). Oligonucleotides containing $U^{2'F(ara)}$ have slightly higher melting temperatures (T_m's) than those containing $U^{2'F(ribo)}$ when located in internucleotide positions or at the 3'-end and when correctly paired with adenine or mispaired with guanine. However, both modifications decrease the magnitude of ΔH^o and ΔS^o for duplex formation in all sequence contexts. In examining the thermodynamic properties for this set of oligonucleotides, entropy-enthalpy compensation is apparent. Our thermodynamic findings led to a series of experiments with DNA ligase that reveal, contrary to expectation based upon observed T_m's, that the duplex containing the $U^{2'F(ribo)}$ analog is more easily ligated. The 2'-fluoro-2'-deoxynucleosides examined here are valuable probes of the impact of sugar constraint and are also members of an important class of antitumor and antiviral agents. The data reported here may facilitate understanding the

biological properties of these agents, as well as the contribution of sugar conformation to replication fidelity.

Footnotes

[1]Abbreviations

T_m, Melting Temperature; dU, 2'-deoxyuridine; $U^{2'F(ara)}$, 2'-deoxy-2'-fluoroabinofuranosyl uracil; $U^{2'F(ribo)}$, 2'-deoxy-2'-fluororibofuranosyl uracil; araC, 1-β-D-arabinofunanosylcytosine

Introduction

The accurate replication of nucleic acids requires that polymerases select the correct nucleotide at each successive step of replication. Substantial work has focused on the importance of "base pairing fidelity" in the selection of the correct nucleotide (1-6). Polymerases must also choose among potential nucleoside triphosphates, even when the base pairing condition has been met. For example, RNA polymerases select ribonucleotide triphosphates (rNTPs) whereas DNA polymerases select 2'-deoxyribonucletide triphosphates (dent's) upon the basis of sugar structure and conformation. The selection of nucleotide triphosphates (NTP's) based upon differences in sugar structure and conformation has led to a suggested role for "sugar fidelity" among polymerases although the mechanisms have not been extensively explored (7-10).

For a given DNA sequence position, polymerase discrimination must occur in two distinct steps. In the insertion step, a candidate nucleotide is interrogated for its capacity to bind to the primer-template-enzyme complex with sufficient stability in an acceptable geometry (1-6). Differences in the base-pairing and base-stacking energy between correct and incorrect nucleotides, as measured in oligonucleotide melting studies, have been proposed to account for polymerase discrimination at the insertion step. Following insertion, the polymerase must select the next correct nucleotide during the extension step. Surprisingly, polymerase extension beyond a mispair is very difficult, even for the insertion of a correct NTP and even though base-pairing and geometry conditions are met (11-15). Extension fidelity contributes nearly as much to the overall replication fidelity as the initial insertion step. Although polymerase pausing at the extension step following a nucleotide misinsertion event would reduce overall mutation frequency by facilitating

proofreading or other repair, the mechanistic basis for extension fidelity is as yet unknown.

Polymerase insertion and extension require a terminal 3'-hydroxyl (3'-OH) in the correct position to attack the α-phosphate of a candidate NTP. In the case of geometrically aberrant base pairs, such as a purine-purine mispair, the 3'-OH would be shifted several angstroms from the correct position, potentially preventing polymerase extension. With purine-pyrimidine mispairs, however, the geometry is closer to that of a normal Watson-Crick base pair, so that more subtle differences, such as sugar conformation, might become important. The furanose sugar component of nucleic acids is non-planar and adopts a number of potential conformations that can be described by the pseudorotation angle, P (16-18). There are several conformations that correspond to energy minima as a function of P, and the value of P can significantly change the position of the 3'-OH. Ribonucleotides in RNA are biased toward a 3'-endo conformation whereas 2'-deoxynucleosides in DNA assume preferentially a 2'-endo pucker, potentially explaining, in part, polymerase sugar fidelity (Figure 1).

While sugar conformation can be biased by sugar structure, sugar conformation can also be influenced by base pair configuration. Sugar conformation, and therefore 3'-OH position, can change due to mispair formation, as well as from changes in the glycosidic torsion angle (19-23). While a correct base pair at the 3'-end of a template-primer complex would likely be found predominantly in a correct conformation with the 3'-OH in the correct position, mispair formation could modify sugar pucker and distort the position of the 3'-OH potentially explaining, in part, polymerase extension fidelity.

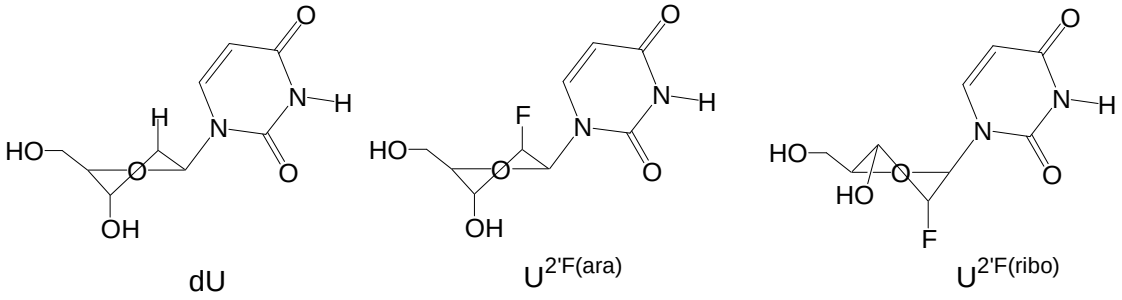

Figure 1. Nucleoside analogs examined in this study.

Sugar conformation can also be biased by the presence of substituents in the furanose ring. The conformational difference between deoxyribose and ribose sugars is attributed primarily to the presence of the 2'-OH in the ribonucleosides. Other substituents, in particular, electron-withdrawing substituents including fluorine, are known to profoundly influence sugar conformation (24-33). Evidence exists that sugar pucker can influence both nucleotide incorporation and extension by polymerases (34-41). Nucleotides that are constrained to a 3'-endo conformation - for example, 2'-fluororibo nucleotides - are preferentially incorporated by RNA polymerases (34). Conversely, 2'-fluoroarabino nucleotides that prefer the 2'-endo pucker are preferentially incorporated by DNA polymerases, yet surprisingly, are very difficult to extend (38). The physical basis for this selectivity has not as yet been established.

For this study, we constructed oligonucleotides with 2'-deoxyuridine (dU) and the 2'-fluoro analogs 2'-deoxy-2'-fluoroarabinofuranosyl uracil ($U^{2'F(ara)}$) and 2'-deoxy-2'-fluororibofuranosyl uracil ($U^{2'F(ribo)}$) in both internucleotide and 3'-end positions (Figure 1). The sugar pucker equilibrium for the $U^{2'F(ara)}$ and $U^{2'F(ribo)}$ analogs studied here has been previously studied by NMR spectroscopy (25-32). The reference nucleoside analog, dU, is in a rapid equilibrium between 2'-endo and 3'-endo conformations, with a

preference (61%) for the 2'-endo conformation (32). The $U^{2'F(ara)}$ analog is 57% 2'-endo whereas the $U^{2'F(ribo)}$ analog is 69% 3'-endo (33). When located in oligonucleotides and constrained by internucleotide linkages, the conformational preference of dU and $U^{2'F(ara)}$ shifts more toward 2'-endo whereas $U^{2'F(ribo)}$ shifts more toward 3'-endo (26).

The analogs described here were incorporated into an internucleotide position, as well as on the 3'-end. While both analogs have been incorporated previously into internucleotide positions, this is the first report of incorporation into the 3'-position. The analogs have been incorporated into duplex structures either properly paired with adenine or mispaired with guanine in an internucleotide position, as well as at a 3'-end position creating a model polymerase replication fork or ligase junction. The thermal and thermodynamic stability of these duplex structures has been studied. With this set of analogs, we could probe the energetic advantage or penalty for each analog and base pair, as well as probe for a potential interaction between base pairing and sugar conformation. Thermodynamic results reported here led to a series of experiments with DNA ligase that demonstrate, unexpectedly, that the duplex containing the $U^{2'F(ribo)}$ analog is more easily ligated. The thermodynamic parameters and results obtained are discussed within the context of the available literature on polymerase preferences for both nucleotide insertion and extension. Due to the importance of sugar-modified nucleosides as anticancer and antitumor drugs, the results reported here may provide new insight into the mechanisms of activity and the potential adverse effects of these analogs.

Materials and Methods

Solvents and Reagents

The solvents dichloromethane (CH_2Cl_2), methanol (MeOH), ethyl acetate (EtOAc) and hexanes were purchased from Fisher Scientific (Pittsburgh, PA). Pyridine, triethylamine (TEA) and acetonitrile (MeCN) were purchased from Sigma-Aldrich (St. Louis, MO). Dimethoxytrityl chloride (DMT-Cl) and 2-cyanoethyl tetraisopropyl phosphorodiamidite were purchased from Sigma-Aldrich (St. Louis, MO). 1,3,5-tri-O-benzoyl-2'-deoxy-2'-fluoro-D-arabinofuranose was purchased from MP Biomedicals (Aurora, OH). Thin layer chromatography (TLC) was performed on precoated silica gel 60 F_{254}, 5x20 cm, 250 μm thick plates purchased from EMD (Gibbstown, NJ).

Synthesis of 5'-dimethoxy-2'-deoxy-2'-fluoro-1-β-D-arabinofuranosyluracil, 3'-[(2-cyanoethyl)-(N,N-diisopropyl)]-phosphoramidite

Commercially available 1,3,5-tri-O-benzoyl-2'-deoxy-2'-fluoro-D-arabinofuranose was brominated to the corresponding bromosugar in 100% yield (42,43). The bromosugar was then coupled to 2,4-bis-*O*-trimethylsilyluracil to give 1-β-D-(3,5,-di-O-benzoyl-2-fluoroarabinofuranosyl)uracil as a solid residue (44). The dibenzoyl derivative was then deprotected to give 2'-deoxy-2'-fluoro-1-β-arabinofuranosyluracil ($U^{2'F(ara)}$) in a 30% yield (45). $U^{2'F(ara)}$ was then tritylated to give 5'-dimethoxytrityl-2'-deoxy-2'-fluoro-1-β-arabinofuranosyluracil in 48% yield and subsequently converted to its phosphoramidite derivative, 5'-dimethoxy-2'-deoxy-2'-fluoro-1-β-D-arabininofuranosyluracil, 3'-[(2-cyanoethyl)-(N,N-diisopropyl)]-phosphoramidite in 49% yield (46).

Oligonucleotide Synthesis and Characterization

Standard oligonucleotide synthetic procedures (47) were used to produce oligonucleotides with normal and modified analogs including dU, $U^{2'F(ara)}$ and $U^{2'F(ribo)}$ residues located at an internucleotide site. Oligonucleotide synthesis was conducted with a Gene Assembler Plus (Pharmacia LKB) automated DNA synthesizer. Oligonucleotides were deprotected with concentrated NH_3 (aq) at 60°C for 24 hours. In general, following synthesis and deprotection, oligonucleotides were purified by HPLC using a Hamilton PRP-1 column and a gradient of 10 – 40% MeCN in potassium phosphate buffer (10mM, pH 6.8) and examined by MALDI-TOF-MS. Oligonucleotides were then detritylated with 80% aqueous acetic acid at room temperature for 30 minutes. Following detritylation, oligonucleotides were purified by HPLC using a C-18 Vydac column and a gradient of 0 – 20% MeCN in water. Oligonucleotide purity was examined by MALDI-TOF-MS (48), and the free base composition was verified by HPLC, following enzymatic digestion (49) using a Supelcosil LC-18-S column and a gradient of 0 – 15% MeCN in water.

Synthesis of Oligonucleotides with 3'-terminally Located 2'-deoxyuridine Analogues

To insert dU, $U^{2'F(ara)}$ and $U^{2'F(ribo)}$ residues at the primer terminus, three synthetic approaches were investigated using the following universal supports available from Glen Research: 1) Glen UnySupport CPG 500, 2) Universal Support II and 3) Universal Support III PS (50,51). In each of the three approaches, it was necessary to increase the coupling times to 10 min (from 3 min) for insertion of $U^{2'F(ara)}$ and $U^{2'F(ribo)}$ residues at the primer terminus. Following detritylation, overall purity of the oligonucleotides produced using each of the three universal supports was determined by MALDI-TOF-MS and

denaturing polyacrylamide gel (20% (v/v) polyacrylamide, 8M urea). Upon the basis of MALDI-TOF-MS analysis, oligonucleotides synthesized using Universal Support III PS were of greater purity than those synthesized using Universal Support II or Glen UnySupport CPG 500. In particular, the mass spectra for oligonucleotides containing $U^{2'F(ara)}$ and $U^{2'F(ribo)}$ residues, produced using Universal Support III PS, revealed single peaks corresponding to the expected oligonucleotide masses. Following synthesis using Glen UnySupport CPG 500, several unidentified impurities in $U^{2'F(ara)}$ containing oligonucleotides (M-50, 221, 307, 360 and 619) and in $U^{2'F(ribo)}$ containing oligonucleotides (M+18 and M-227) were observed. Upon the basis of purity assessment following gel electrophoresis, Universal Support III PS was again determined to produce oligonucleotides of greater purity. In all, synthesis using Universal Support III PS produced oligonucleotides in greater quantity and of higher purity and was thus used exclusively for subsequent syntheses of oligonucleotides with dU, $U^{2'F(ara)}$ and $U^{2'F(ribo)}$ residues at the 3'-end.

Determination of Duplex Melting Behavior

Samples containing non self-complementary oligonucleotides were prepared in buffer containing 0.1 M NaCl, 0.01 M sodium phosphate, and 0.1mM EDTA, pH 7.0. Complexes were prepared by mixing equimolar amounts of interacting strands, and concentration dependent T_m measurements were conducted with total strand concentration (C_T) between 2 and 60 μM in cuvettes with path lengths between 1 and 10 mm. Molar extinction coefficients of oligonucleotides were calculated (52) to determine single strand concentrations. Oligonucleotide melting temperatures (T_m) were determined using a Varian Cary 300 Bio UV-visible spectrophotometer (Varian, Walnut Creek, CA).

Five temperature ramps were performed on each sample per run while observing the absorbance at 260 nm: 1) 12 °C to 90 °C at a rate of 0.5 °C/min, 2) 90 °C to 12 °C at a rate of 0.5 °C/min, 3) 12 °C to 90 °C at a rate of 0.5 °C/min, 4) 90 °C to 12 °C at a rate of 0.5 °C/min, and 5) 12 °C to 90 °C at a rate of 0.5 °C/min. The sample was held for 3 min when the temperature reached 90 °C and for 10 min when it reached 12 °C and started the next cycle. Data were collected at 0.5 °C intervals while monitoring the temperature with a probe inserted into a cuvette containing only buffer. The T_m of each duplex was determined using Cary WinUV Thermal software (Varian). Theoretical T_m values for control duplexes (A:dU and G:dU) were determined (53,54) and compared against values obtained using the Cary WinUV Thermal software. Thermodynamic parameters for non self-complimentary duplexes were calculated in two ways: 1) averages from fits of individual melting curves at different concentrations using Van't Hoff calculation in the Cary WinUV Thermal software; 2) the 1/ T_m *versus* ln (C_T/4) plots fitted to the following equation for the non self-complementary sequences examined here.

$$T_m^{-1} = \frac{R}{\Delta H^0} \ln\left(\frac{C_T}{4}\right) + \frac{\Delta S^0}{\Delta H^0} \qquad \text{Eq. 1}$$

Both methods assume a two-state model and $\Delta C_p = 0$ for the transition equilibrium. The two-state approximation was assumed to be valid for sequences in which the ΔH° values derived from the two methods agreed within 15% (54). The ΔH° values derived from the two methods agree within 15%, indicating that the two-state approximation is valid for all other sequences employed in this study.

Ligase Assays

The *E. coli* DNA ligase was obtained from New England Biolabs (Ipswich, MA) and human DNA ligase III was obtained from Enzymax (Lexington, KY). Oligonucleotide 5'-end radiolabeling was performed using adenosine 5'-[γ-^{32}P]-triphosphate ([γ-^{32}P]-ATP) (MP Biomedical, Costa Mesa, CA) and T4 polynucleotide kinase (New England BioLabs) under conditions recommended by the enzyme supplier. Labeled mixtures were subsequently centrifuged through G-25 Sephadex columns (Roche Applied Science, Indianapolis, IN) to remove excess unincorporated nucleotide. Duplex oligonucleotides containing a ligase junction were generated by mixing the labeled single strand (5'-GGCCACGACGG-3') with a 2-fold molar excess of CTTTGCCCGAAX, where X is dU, $U^{2'F(ara),}$ $U^{2'F(ribo)}$, and the template strand CCGTCGTGGCCATTCGGGCAAAG in the appropriate enzyme buffer as previously described (55). The *E. coli* DNA ligase buffer contained 30 mM Tris-HCl pH 8.0, 4 mM $MgCl_2$, 1 mM DTT, 26 µM NAD^+, 50 µg/ml BSA. The human DNA ligase III buffer contained 50 mM Tris-HCl pH 7.5, 10 mM $MgCl_2$, 10 mM DTT, 1 mM ATP. Annealing mixtures were heated at 95ºC for 5 min and then cooled slowly to room temperature. Standard *E. coli* DNA ligase assays were performed using 50 nM substrate with 500 nM *E. coli* DNA ligase in buffer, as above, in a total volume of 10 µl at 16ºC for selected time periods. Substrates (50 nM) were incubated with 50 nM human DNA ligase III in buffer, as above, in 10 µl total volume at 26.5ºC for selected time periods. The reactions were terminated by adding an equal volume of Maxam-Gilbert loading buffer (98% formamide, 0.01 M EDTA, 1 mg/ml xylene cyanole and 1 mg/ml bromophenol blue). Samples were denatured by heating at 95ºC for 5 min and quickly placed on ice for 2 min

before electrophoresis on 20% denaturing polyacrylamide gels (8 M urea). The bands corresponding to substrate and products were visualized and quantified using a Molecular Dynamics PhosphorImager (Molecular Dynamics, Sunnyvale, CA, now part of GE Healthcare) and quantified using ImageQuant software. Reaction rate constants (k_{obs}) for ligation reactions were determined by fitting time course data to a single exponential ($y = a(1-a^{-bx})$) using Sigma Plot 10.0, where "a" is the maximum product ratio and "b" is the reaction rate constant, k_{obs}.

Results

Oligonucleotide Synthesis

The phosphoramidite analog of $U^{2'F(ribo)}$ is commercially available; however, the corresponding phosphoramidite of $U^{2'F(ara)}$ is not available and was prepared in this laboratory by previously described methods as shown in Figure 2A. Oligonucleotides containing both analogs were prepared by standard solid phase synthesis methods. Sequences of oligonucleotides used in this study are shown in Figure 3.

Although the synthesis of oligonucleotides with $U^{2'F(ara)}$ and $U^{2'F(ribo)}$ have been previously reported, oligonucleotides with these analogs at the 3'-end are reported here for the first time. We considered two methods: the synthesis of solid phase supports linked to the analogs of interest or the use of solid supports containing linkers or "universal supports" for the preparation of 3'-end modified oligonucleotides (Figure 2B). As the needed phosphoramidites were available in our lab, we proceeded to test a series of commercially available solid supports. Although we did not exhaustively examine all of the supports, we found that Universal Support III PS provided the highest consistent coupling yields and purity.

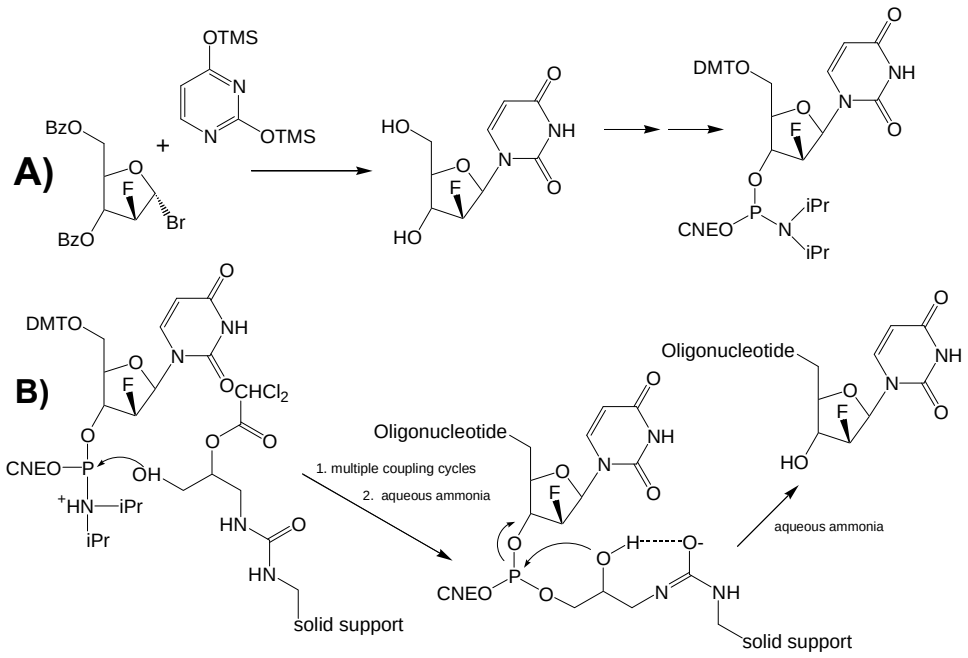

Figure 2. Oligonucleotide synthesis. A) Abbreviated scheme showing the synthesis of phosphoramidites for the incorporation of $U^{2'F(ara)}$ into oligonucleotides. B) Modified coupling conditions were used to attach $U^{2'F(ara)}$ to the 3'-terminus of oligonucleotides as described in the Materials and Methods.

A
5'-CTTTGCCCGAAX-3'
3'-TAGGAAACGGGCTTPCAATAA-5'

B
5'-CCGAAXGTTATT-3'
3'-GGCTTPCAATAA-5'

X = dU, $U^{2'F(ara)}$, $U^{2'F(ribo)}$
P = A, G

C
5'-CTTTGCCCGAAX^{OH} ^{P}GGCCACGACGG-3'
3'-GAAACGGGCTTA-----CCGGTGCTGCC-5'

Figure 3. Oligonucleotide duplexes examined in this report. The sequence of duplexes with sugar-modified nucleotides at A) the 3'-terminus or B) an internucleotide position used in this report. C) The sequences for oligonucleotide duplexes used as substrates for the ligase assays described in the Materials and Methods section.

Oligonucleotide Characterization

Synthetic oligonucleotides were characterized by MALDI-TOF-MS following deprotection and purification by HPLC. The mass spectra of the oligonucleotides containing the $U^{2'F(ara)}$ analog in both an internucleotide position and at a 3'-end are shown in Figures 4A and B, respectively. The observed mass in each case was consistent with the expected mass and demonstrated that the 3'-phosphate of the original phosphoramidite had been removed (Figure 2B). Oligonucleotides were also characterized by enzymatic digestion and analysis of the liberated nucleosides by HPLC. We considered this important as the mass of the two 2'-fluoro analogs is identical, and we needed an additional method to confirm that the oligonucleotides contained the correct isomer. As shown in Figure 5A, dU, $U^{2'F(ara)}$ and $U^{2'F(ribo)}$ are separable by HPLC and resolvable from the standard DNA nucleosides (Figure 5B).

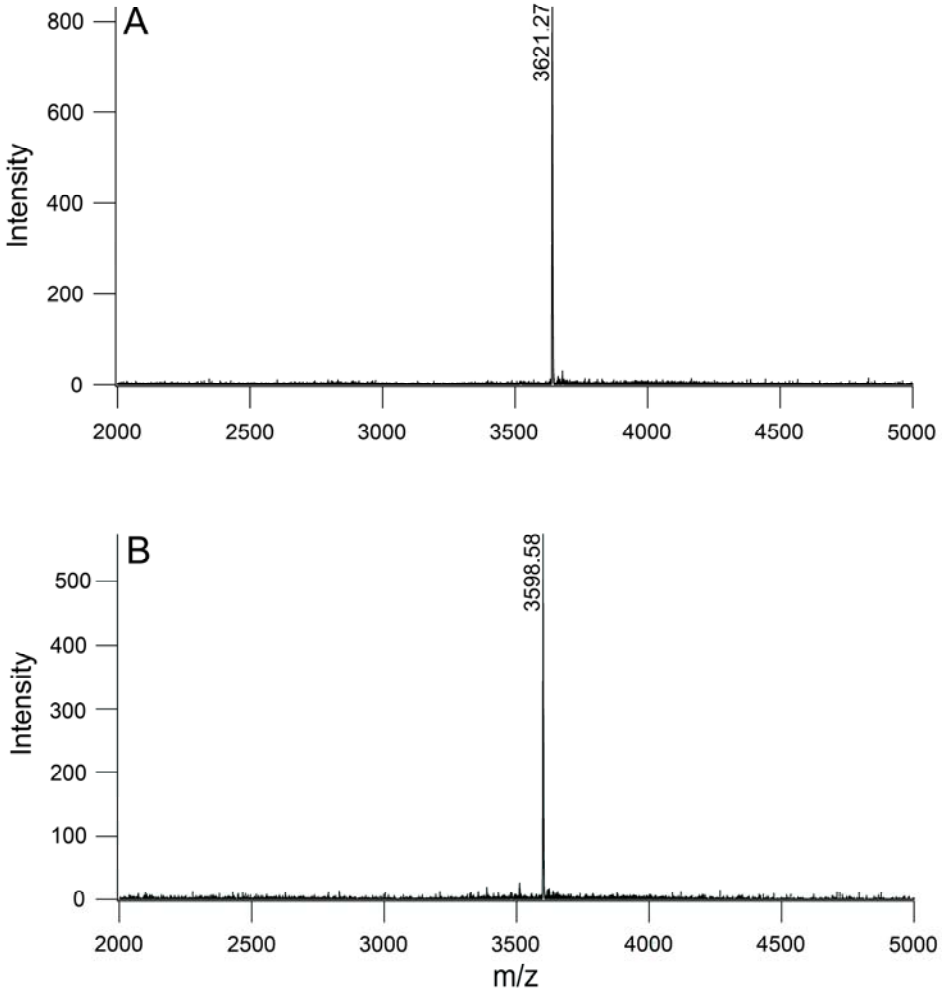

Figure 4. MALDI-TOF-MS spectra for $U^{2'F(ara)}$ containing oligonucleotides. A) The mass spectrum observed for the oligonucleotide with sequence 5'-CCGAA**X**GTTATT-3' where **X** is a $U^{2'F(ara)}$ residue at an internucleotide site. B) The mass spectrum observed for the oligonucleotide of sequence 5'-CTTTGCCCGAA**X**-3' where **X** is a $U^{2'F(ara)}$ residue at the 3'-end.

Measurement of Duplex Thermal and Thermodynamics Stability

Oligonucleotide duplexes were prepared in buffered solution by mixing equimolar amounts of the two strands, as indicated in Figure 3. Strands were annealed by heating to

90°C, followed by slow cooling. Melting profiles were obtained by observing UV absorbance at 260 nm as a function of temperature as described in Materials and Methods. Melting temperatures and corresponding thermodynamic parameters were obtained by analysis of the UV-temperature profiles as previously described (53, 54). Melting temperatures and thermodynamic parameters are presented in Table 1. Example melting curves are shown in Figure 6.

Analysis of Thermodynamic Data

Thermal and thermodynamic data obtained for the ensemble of oligonucleotides examined here were expressed as the corresponding differences by comparing the measured value for the substituted duplexes with the standard A:dU containing duplex for the 3'-end and internucleotide series. This data and the corresponding values of ΔT_m, $\Delta\Delta G^o_{37}$, $\Delta\Delta H^o$ and $\Delta\Delta S^o$ are presented in Table 1. Values of $\Delta\Delta H^o$ and $\Delta\Delta S^o$ appeared to correlate with one another, and this relationship is presented in Figure 7. Energy differences between base pairs examined in this study are shown diagrammatically in Figure 8.

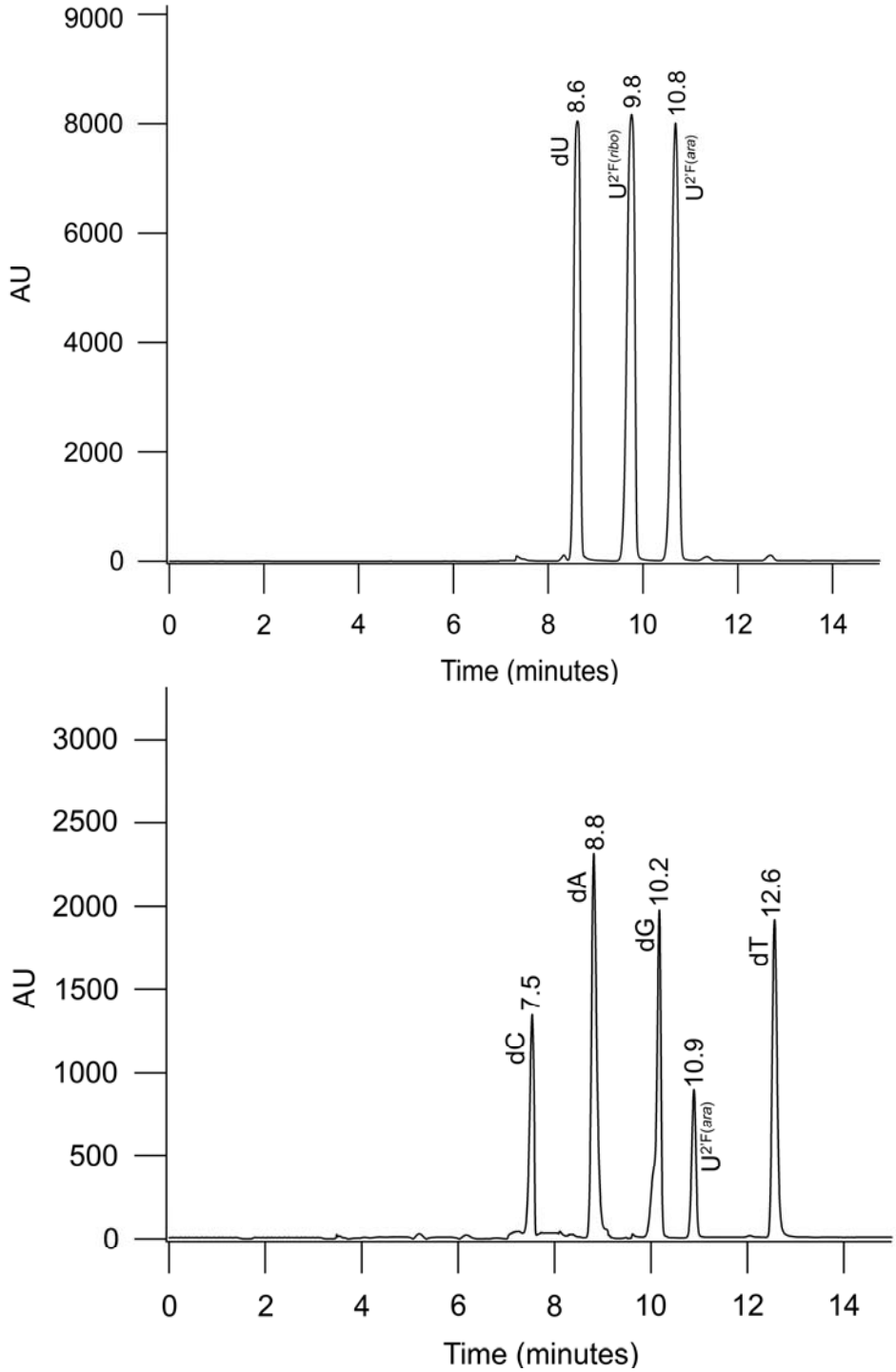

Figure 5. The composition of synthetic oligonucleotides were analyzed by HPLC following enzymatic digestion. A) HPLC was able to resolve the dU, $U^{2'F(ara)}$ and $U^{2'F(ribo)}$ nucleosides. B) The HPLC chromatogram confirming the composition of the oligonucleotide, 5'-CCGAA**X**GTTATT-3', where X is a $U^{2'F(ara)}$ residue.

DNA Ligase Activity

Oligonucleotides were assembled as shown in Figure 3C to create a ligase joint. The model ligase junction was incubated with human DNA ligase III and *E. coli* DNA ligase and the reaction products were examined by gel electrophoresis as shown in Figure 9. Human DNA ligase III and *E. coli* DNA ligase were able to ligate junctions containing all three analogs. Human DNA ligase III was found to ligate junctions containing dU, $U^{2'F(ara)}$ and $U^{2'F(ribo)}$ with k_{obs} values of $1.83 \pm 0.21 \times 10^{-2}$ s^{-1}, $4.70 \pm 0.43 \times 10^{-3}$ s^{-1} and $2.18 \pm 0.25 \times 10^{-2}$ s^{-1}, respectively. In addition, *E. coli* DNA ligase was found to ligate junctions containing dU, $U^{2'F(ara)}$ and $U^{2'F(ribo)}$ with k_{obs} values of $6.34 \pm 0.73 \times 10^{-3}$ s^{-1}, $8.64 \pm 1.33 \times 10^{-4}$ s^{-1} and $2.81 \pm 0.39 \times 10^{-2}$ s^{-1}, respectively.

Discussion

The experimental goal of this study was to examine the role of constrained sugar pucker on oligonucleotide stability for both a correct base pair and a wobble mispair in both internucleotide and 3'-terminal positions. These properties might help explain why polymerases initially insert correct nucleotides (insertion) and insert correct nucleotides following mispairs (extension) with such low efficiency. The impact of constrained sugar conformation on mispairs has not been previously examined. We considered the possibility that mispair geometry might be coupled with changes in sugar pucker at a duplex 3'-end which might help explain the inefficiency of mispair extension. Previous structural studies have suggested that aberrant base pair geometry could induce changes in sugar conformation (19-23), however, these effects have not been previously studied at a replication fork. The sugar-substituted nucleosides examined here are also members of an important class of nucleoside analogs with antitumor and antiviral properties (34-41),

and thus the data reported here might facilitate a greater understanding of the biological activity of this class of nucleoside analogs. Our experimental approach was to construct oligonucleotides containing dU and 2'-fluoro analogs constrained to either the 2'-endo (south, DNA-like) sugar pucker or the 3'-endo (north, RNA-like) sugar pucker and to measure thermodynamic stabilities of duplex oligonucleotides.

Melting temperatures for oligonucleotides containing standard and modified nucleotides were determined and measured values were consistent with expectations. In the studies reported here, uracil was selected as the pyrimidine rather than thymine so that the data set examined here could be used in future studies to compare a series of 5-substituted pyrimidines. The replacement of T by dU does not change base pairing geometry when paired with A (56) or mispaired with G (57) and results in only a modest decline in T_m due to reduced base stacking (58). Oligonucleotide duplexes were assembled as shown in Figure 3. Oligonucleotide melting temperatures were obtained from the temperature dependence of the UV absorbance as shown in Figure 5. Thermodynamic parameters were extracted from the melting curves and the corresponding data is presented in Table 1. The observed T_m of the duplex containing an internucleotide A:dU base pair was 43.8 ± 0.2 ^oC. The expected T_m for a duplex of the same sequence except dU would be replaced by thymine is 43.8 to 44.2 ^oC, depending upon which basis set and method of calculation is used (53). The observed T_m of the duplex in which the dU residue on the 3'-end was paired with A was observed to be 49.4 ± 0.3 ^oC, slightly below the 52.8 to 53.1 ^oC calculated range when dU is replaced by T (53).

Table 1: Experimental thermodynamic parameters of duplex formation. The values include measured free energy of duplex formation ($\Delta G°_{37}$), enthalpy ($\Delta H°$), entropy ($\Delta S°$) and melting temperature with a strand concentration of 28 μM ($T_{m\ 28\ \mu M}$). The thermodynamic parameters for the A:dU oligonucleotides were used as the references when calculating $\Delta\Delta G°_{37}$, $\Delta\Delta H°$, and $\Delta\Delta S°$ in the 3'-terminal (Figure 3A) or internucleotide positions (Figure 3B). Measured free energy, enthalpy and entropy differences that exceed experimental error are indicated in bold.

	$\Delta G°_{37}$ (kcal/mol)	$\Delta\Delta G°_{37}$ (kcal/mol)	$T_{m\ 28\mu M}$ (°C)	$\Delta T_{m\ 28\mu M}$ (°C)	$\Delta H°$ (kcal/mol)	$\Delta\Delta H°$ (kcal/mol)	$\Delta S°$ (cal/mol K)	$\Delta\Delta S°$ (cal/mol K)
				3'-Terminal				
A:dU	-9.5±0.2	-	49.4±0.3	-	-89.0±4.6	-	-251.2±14.2	-
G:dU	-9.0±0.2	**0.5±0.3**	48.1±0.2	-1.3±0.4	-86.0±5.4	3.0±7.1	-244.2±16.7	7.0±21.9
A:U$^{2'F(ara)}$	-9.5±0.2	0.0±0.3	50.3±0.1	0.9±0.3	-84.8±3.2	4.2±5.6	-238.4±9.7	12.8±17.2
G:U$^{2'F(ara)}$	-8.8±0.2	**0.7±0.3**	48.1±0.5	-1.3±0.6	-82.1±4.3	**6.9±6.3**	-232.0±13.4	19.2±19.5
A:U$^{2'F(ribo)}$	-9.0±0.2	**0.5±0.3**	49.2±0.2	-0.2±0.4	-79.9±3.9	**9.1±6.0**	-224.3±12.2	**26.9±18.7**
G:U$^{2'F(ribo)}$	-8.6±0.2	**0.9±0.3**	47.2±0.6	-2.2±0.7	-76.7±5.1	**12.3±6.9**	-215.7±15.8	**35.5±21.2**
				Internucleotide				
A:dU	-8.1±0.2	-	43.8±0.2	-	-93.2±5.1	-	-271.4±14.9	-
G:dU	-6.2±0.1	**1.9±0.2**	36.6±0.2	-7.2±0.3	-87.1±3.7	6.1±6.3	-257.6±12.4	13.8±19.4
A:U$^{2'F(ara)}$	-8.0±0.1	0.1±0.2	43.8±0.3	0.0±0.4	-85.4±3.0	**7.8±5.9**	-245.7±9.5	**25.7±17.6**
G:U$^{2'F(ara)}$	-6.5±0.1	**1.6±0.2**	37.5±0.2	-6.3±0.3	-81.7±3.7	**11.4±6.3**	-239.6±11.8	**31.9±19.0**
A:U$^{2'F(ribo)}$	-7.8±0.1	**0.3±0.2**	42.9±0.1	-0.9±0.2	-86.7±3.5	**6.4±6.2**	-250.7±11.1	**20.7±18.6**
G:U$^{2'F(ribo)}$	-6.4±0.1	**1.7±0.2**	36.7±0.5	-7.1±0.5	-81.9±2.9	**11.3±5.8**	-240.2±9.3	**31.2±17.5**

The conversion of a Watson-Crick base pair to a wobble mispair is known to significantly decrease melting temperatures (1,11,58). The formation of the internucleotide G:dU mispair results in a T_m of 36.6 ± 0.2 °C, 7.2 °C lower than the A:dU duplex. The calculated range for a duplex of the same sequence containing a G:dT mispair is 36.8 to 38.2 °C (54). When the G:dU mispair is moved from an internucleotide position to the 3'-end, the observed T_m is 48.1 ± 0.2 °C, only 1.3 °C lower than the T_m for the sequence containing a correct A:dU base pair. The expected T_m for an oligonucleotide of an otherwise same sequence, but with a G:dT rather than G:dU mispair at the 3'-end, is 50.2°C to 50.8°C (54). The data reported thus far is consistent with expectations based upon literature precedents and confirms that the impact of a mispair on T_m is substantially less when the mispair is located at the 3'end.

The T_m of the duplex containing the internucleotide A:U$^{2'F(ara)}$ base pair is observed to be 43.8 ± 0.3 °C, experimentally indistinguishable from that of the A:dU duplex. Previously, other investigators have observed that the placement of 2'-fluoroarabino analogs in duplex structures increases their melting temperatures by roughly 1°C per nucleotide, and this stabilizing effect has been attributed to constraining the sugar into the more DNA-like 2'-endo pucker (28,32). In most of the previous studies, however, the oligonucleotides included multiple substitutions. The observed T_m for the formation of the internucleotide G:U$^{2'F(ara)}$ mispaired duplex is 37.5 ± 0.2 °C, which is 0.9 °C higher than that of the G:dU duplex. The 3'-terminal A:U$^{2'F(ara)}$ base pair duplex exhibited a T_m 0.9°C higher than that of the 3'-terminal A:dU base pair duplex whereas the T_m of the terminal G:U$^{2'F(ara)}$ mispair duplex is indistinguishable from the T_m of the 3'-terminal G:dU duplex. These results demonstrate that incorporation of the

$U^{2'F(ara)}$ analog stabilizes duplexes in some cases; however, the observed effect on T_m is modest and substantially less than the impact of mispair formation.

Substitution of dU with the $U^{2'F(ribo)}$ analog at an internucleotide position has the opposing effect, slightly decreasing T_m's when paired with A or mispaired with G. Again, the impact of the sugar constraint on T_m is less than that of mispair formation at the internucleotide position. At the 3'-end, the effect of sugar constraint on T_m shows similar decreases. One of the initial hypotheses considered here is that mispair geometry might be related to sugar pucker at a duplex 3'-end, and therefore, a nucleotide with constrained sugar pucker might have an opposing impact on a mispair versus a normal pair. The evidence thus far on T_m's does not support this hypothesis in that mispairs with G are approximately 2 ^oC less stable than base pairs with A for both $U^{2'F(ara)}$ and $U^{2'F(ribo)}$ analogs.

Oligonucleotide duplexes with similar T_m's can have significantly different thermodynamic parameters if enthalpy and entropy changes are correlated. Although oligonucleotide duplexes might have similar T_m's, they can have different thermodynamic parameters. For this reason we examined the free energy changes at 37°C (ΔG^o_{37}), enthalpy (ΔH^o) and entropy (ΔS^o) changes for each of the duplex structures reported here (Table 1). In Figure 6B, the melting curves for oligonucleotides with A:dU and $A:U^{2'F(ara)}$ are shown. Although the midpoint for the temperature-dependent UV transition (T_m) is similar for each, the shapes of the curves, and corresponding thermodynamic parameters, are different. The magnitude of the experimental errors for ΔS^o, ΔH^o and ΔG^o observed here are in accord with previously reported studies (58,60).

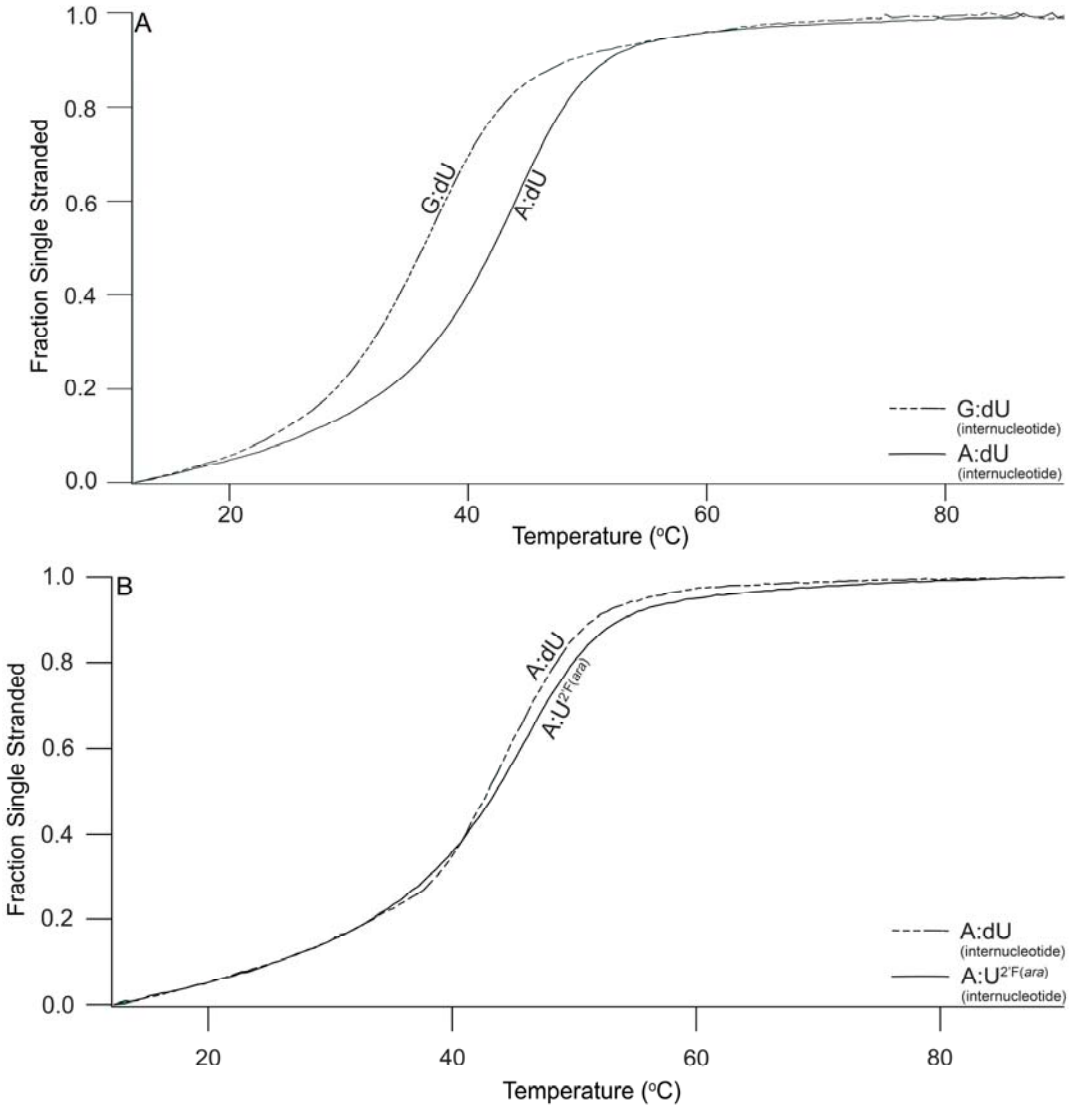

Figure 6. Ultraviolet melting curves of complexes at 28 μM (A) and 60 μM (B) in 100 mM NaCl, 0.1 mM EDTA and 10 mM phosphate buffer (pH 7.0).

In order to assess the impact of the substitution on the thermodynamic parameters, the free energy, enthalpy and entropy changes are expressed as the corresponding differences ($\Delta\Delta G^o$, $\Delta\Delta H^o$ and $\Delta\Delta S^o$) relative to the A:dU base pair for the internucleotide

or 3'-terminal series. In all cases, positive values are observed for $\Delta\Delta G^{o}_{37}$, $\Delta\Delta H^{o}$ and $\Delta\Delta S^{o}$, indicating that constraining the sugar pucker with either the $U^{2'F(ara)}$ or $U^{2'F(ribo)}$ analog has a destabilizing effect, as does mispair formation. Previously, positive values for $\Delta\Delta H^{o}$ and $\Delta\Delta S^{o}$ upon substitution with $U^{2'F(ara)}$ have been observed (25), and the magnitudes of these changes per substitution are similar to those reported here. The impact of the sugar constraint on $\Delta\Delta S^{o}$ has been attributed to a conformational preorganization, reducing the net conformational entropy change upon duplex formation (25). The impact on $\Delta\Delta H^{o}$ would be attributed to the constrained sugar preventing the formation of the most favorable base-stacking geometry.

In this study, we have assumed a two state equilibrium between 2'-endo and 3'-endo sugar puckers as supported by previous NMR studies with the $U^{2'F(ara)}$ and $U^{2'F(ribo)}$ analogs studied here (25-32). The reference nucleoside analog, dU, is in a rapid equilibrium between 2'-endo and 3'-endo conformations, with a preference (61%) for the 2'-endo conformation (32). The $U^{2'F(ara)}$ analog is 57% 2'-endo whereas the $U^{2'F(ribo)}$ analog is 69% 3'-endo (33). When located in oligonucleotides and constrained by internucleotide linkages, the conformational preference of dU and $U^{2'F(ara)}$ shifts more toward 2'-endo whereas $U^{2'F(ribo)}$ shifts more toward 3'-endo (26).

Enthalpy and entropy differences for the oligonucleotide duplexes examined here are shown to be proportional. In previous studies of oligonucleotide stability in which mispairs and constrained sugar pucker were considered separately, enthalpy and entropy contributions were shown to correlate (60). As shown in Figure 7, enthalpy and entropy are shown to correlate for the series examined here, as well. The relatively large size of the error bars when the values are presented as $\Delta\Delta S^{o}$ and $\Delta\Delta H^{o}$ are consistent with

previous studies as discussed by McTigue et al. (60). The slope of the line in Figure 7 is 2.9, and this plot includes normal base pairs, those with sugar constraints and unconstrained mispairs, and mispairs with sugar constraints in both internucleotide and 3'-terminal positions. This value compares favorably with the value of 2.8 from a previous study on mispairs with no sugar constraint (11) and with the value of 2.95 from a study that examined constrained sugars but no mispairs (60), suggesting that this value of $\Delta\Delta S^o$ / $\Delta\Delta H^o$ is broadly applicable to nucleic acids.

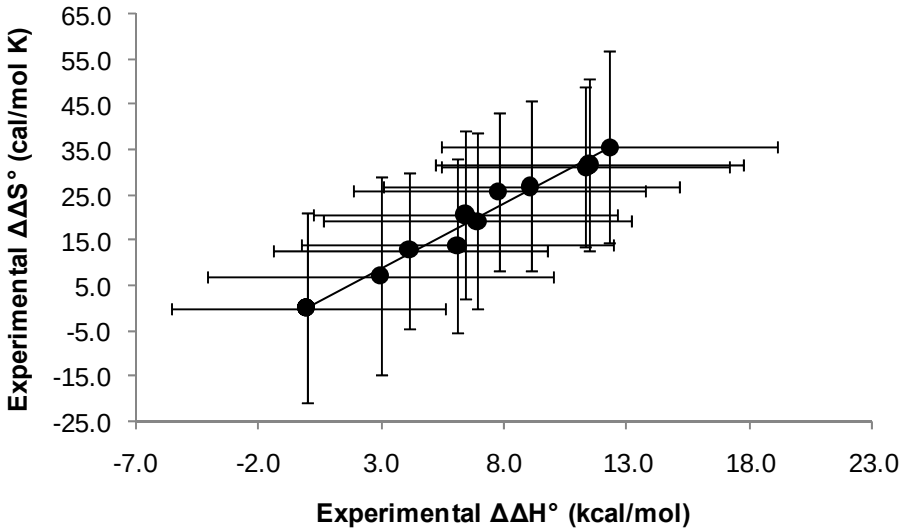

Figure 7: The thermodynamics of duplex formation display enthalpy-entropy compensation. The slope of the line is 2.9 and the R^2 value of the associated trend line is 0.98. Experimental ΔΔH° and ΔΔS° values are provided in Table 1.

Thermodynamic differences for 3'-end base pairs likely contribute to polymerase insertion kinetics. Previous studies have established that sugar pucker can also influence nucleotide insertion by DNA polymerases. DNA polymerases must distinguish between

NTP's with different sugars, and it is known that the discrimination is between one and three orders of magnitude depending upon the template and polymerase, and several apparent K_m values have been reported. Astatke et al. (9) demonstrated that the mechanism for *E. coli* DNA polymerase discrimination between deoxy and dideoxynucleotides involves a direct interaction with the 3'-OH present on the deoxy, but not dideoxynucleotide, accounting for several orders of magnitude higher K_m for the dideoxynucleotide. Richardson et al. (8) demonstrated that human polymerase α and polymerase γ accept $U^{2'F(ara)}$ nucleotides with K_m's similar to dUTP. However, both polymerases discriminate against ribonucleotides and 2'-deoxy-2'-fluororibonucleotides with K_m's that are increased between one and two orders of magnitude, although all of these nucleotides contain the necessary 3'-OH.

Previously, Goodman and coworkers (11) explained how polymerases could discriminate against mispairs by amplifying free energy differences ($\Delta\Delta G^o$) between correct and incorrect base pairs. Free energy differences are determined by the relative magnitude of the enthalpy and entropy contributions ($\Delta\Delta G^o = \Delta\Delta H^o - T\Delta\Delta S^o$). If $\Delta\Delta H^o$ and $\Delta\Delta S^o$ are proportional, large values of $\Delta\Delta H^o$ might be cancelled by large values of $\Delta\Delta S^o$, giving small values of $\Delta\Delta G^o$. On the other hand, if the polymerase active site accepts only nucleotides with sugar conformations that approximate the correct conformations, $\Delta\Delta G^o$ would approach $\Delta\Delta H^o$ providing sufficient energy for the observed discrimination. One of the surprising findings of this study is that, despite modest differences in T_m, (ΔT_m = -0.2 °C), the measured difference in free energy change between A:dU and $A:U^{2'F(ribo)}$ ($\Delta\Delta G^o$ = 0.5 kcal/mol) is as large as the corresponding difference in free energy change between a correct A:dU base pair and a G:dU mispair

($\Delta\Delta G^o$ = 0.5 kcal/mol) although the mispair has a substantially larger impact on the observed T_m (ΔT_m = -1.3 ^oC). These results are consistent with a thermodynamic contribution to sugar fidelity for polymerase insertion.

Thermodynamic differences resulting from mispair formation and sugar constraint appear to be additive in all cases suggesting that sugar conformation and mispair geometry are independent and not interacting. Our initial expectation was that constraining the sugar pucker to 2'-endo ($U^{2'F(ara)}$) would stabilize a correct base pair, but destabilize an incorrect base pair whereas the 3'-endo sugar ($U^{2'F(ribo)}$) would destabilize the correct base pair and stabilize the mispair. Our experimental results are inconsistent with this expectation. When examining the impact of mispair formation and sugar pucker on $\Delta\Delta G^o$, the contributions of each appear to be additive for both 3'-terminal and internucleotide positions. Neither constrained pucker appears to selectively stabilize or destabilize either the correct base pair or the mispair, in accord with observations of T_m discussed above. The contributions of mispair formation and constrained sugar pucker also appear to be additive for $\Delta\Delta H^o$ and $\Delta\Delta S^o$ in all cases presented here, as indicated in Figure 8. For example, for the internucleotide A:dU base pair, conversion to a G:dU mispair is associated with a $\Delta\Delta H^o$ of 6.1 kcal/mol. The energy penalty associated with constraining the sugar conformation of the mispairs by comparing G:dU and $G:U^{2'F(ara)}$ is associated with a $\Delta\Delta H^o$ of 5.3 kcal/mol. The combined effect of mispair formation and constraining the sugar with the $U^{2'F(ara)}$ analog would be expected to be 11.4 kcal/mol if they were additive and not interacting, which is the observed value obtained when comparing the thermodynamic properties of the A:dU and $G:U^{2'F(ara)}$ duplexes.

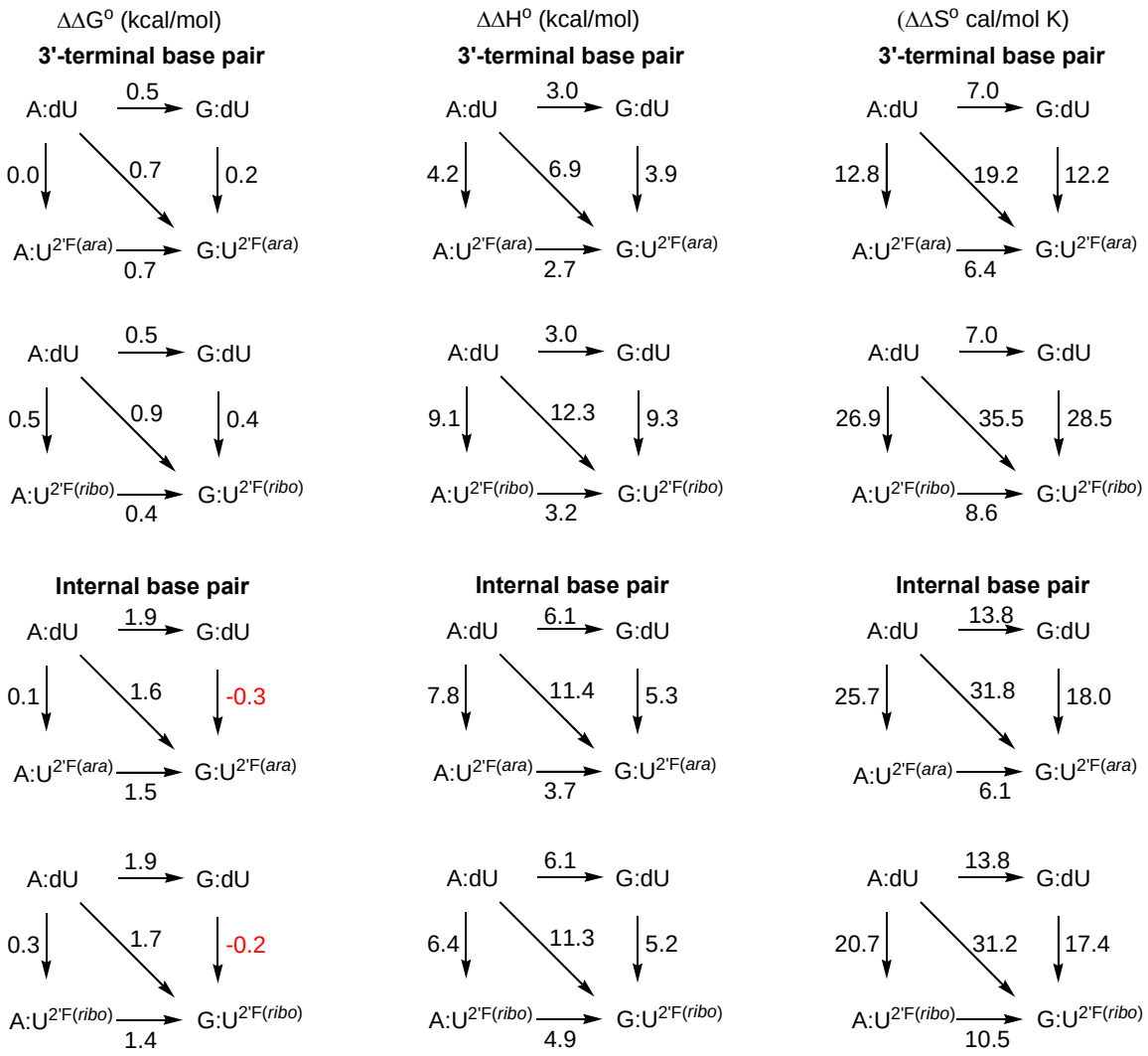

Figure 8. Comparison of differences in free energy ($\Delta\Delta G°_{37}$), enthalpy ($\Delta\Delta H°$) and entropy ($\Delta\Delta S°$) between substituted duplexes and the standard A:dU containing duplex. Numbers adjacent to arrows represent corresponding differences between duplexes. Values of $\Delta\Delta G°_{37}$, $\Delta\Delta H°$ and $\Delta\Delta S°$ for each duplex are presented in Table 1.

The observation that the influences of mispair geometry and sugar constraint are simply additive strengthens the proposal that aberrant base pair geometry and constrained sugar pucker are not linked. Therefore, it is unlikely that the altered base pairing geometry of a mispair induces a shift in equilibrium for the 3'-residue, placing the 3'-OH in a position inconsistent with insertion of the next nucleotide. The data presented thus

far suggests that polymerases are unlikely to exploit induced changes in sugar conformation to increase replication fidelity.

Net thermodynamic differences between 3'-end modified duplexes and internally modified duplexes might explain why polymerase extension beyond a mispair is so difficult. The magnitude of the observed $\Delta\Delta H^o$ and $\Delta\Delta S^o$ for the 3'-terminal G:dU mispairs are 3.0 kcal/mol and 7.0 cal/mol K, respectively, whereas for the internucleotide mispair, the values increase to 6.1 kcal/mol and 13.8 cal/mol K, respectively. Interestingly, the enthalpic and entropic destabilization approximately doubles when moving from a 3'-terminal mispair to an internucleotide mispair, and this observation likely has important implications for understanding why polymerases have substantial difficulty in extending beyond mispairs.

Previously, Goodman and coworkers (11) argued that polymerases can exploit differences in ΔG^o, ΔH^o and ΔS^o between correct and incorrect base pairs for nucleotide insertion, and the altered base pairing and stacking energy associated with mispair formation increases proportionately the apparent K_m for insertion of the incorrect nucleotide. A comparatively larger K_m for insertion of a modified nucleotide is associated with a higher tendency for a candidate nucleotide to dissociate from the enzyme-primer-template complex.

Extension past a mispair, however, involves inserting a correct nucleotide, yet the K_m is also substantially higher than when extending past a correct pair. When comparing the energetic penalty of mispair formation for the sequences examined here, it is apparent that an internucleotide mispair induces destabilization on both the 5'-side and on the 3'-side of the mispair. At the misinsertion step, an incorrect base pair does not stack as well

on the 5'-primer-template complex and is more likely to dissociate, resulting in an increased apparent K_m. At the extension step, an incoming correct nucleotide would stack - but only poorly - on the mispair. Thus, the destabilizing impact of the mispair is transmitted in the 3'-direction as well, perhaps explaining a significant component of polymerase extension fidelity.

Net thermodynamic differences between 3'-end base pairs and internal base pairs might be related to ligase efficiency. When comparing thermodynamic parameters for base pairs located at the 3'-terminal position with those obtained for the same base pair located in an internucleotide position, some trends are apparent that could be important for understanding the activities of enzymes that act upon nucleic acids including polymerases and ligases. The thermodynamic results presented here establish that the $U^{2'F(ribo)}$ substitution is more destabilizing, with larger magnitude ΔH^o and ΔS^o when on the 3'-end, relative to the internucleotide linkage. In contrast, $U^{2'F(ara)}$ is substantially less destabilizing than $U^{2'F(ribo)}$ on the 3'-end. However, when comparing the impact of $U^{2'F(ara)}$ substitution on the 3'-end to the internucleotide position, $U^{2'F(ara)}$ is more destabilizing in the internucleotide position than on the 3'-end. The conversion of the 3'-end modification to the internucleotide linkage could be accomplished by members of the DNA ligase family. Conversion of the 3'-end $U^{2'F(ara)}$ to an internucleotide linkage would increase the destabilizing impact of the substitution, however, conversion of the 3'-end $U^{2'F(ribo)}$ to an internucleotide linkage would substantially reduce the destabilizing impact of the substitution. We therefore predicted that the rate of ligation of the analog substrates examined here would be $A:U^{2'F(ribo)} > A:dU > A:U^{2'F(ara)}$.

Relative efficiency of DNA ligases is consistent with net thermodynamic differences on synthetic templates. Data obtained with *E. coli DNA ligase* and human DNA ligase III, as shown in Figure 9, is consistent with the above prediction, in that the order of ligase efficiency is $U^{2'F(ribo)} > dU > U^{2'F(ara)}$. As seen in the panel for the $U^{2'F(ara)}$ data, initial interaction of the ligase with the 5'-phosphate of the linker transfers an adenosine monophosphate group (App-5'-DNA). The same intermediate forms with both the $U^{2'F(ribo)}$ and dU substrates; however, with the $U^{2'F(ara)}$ substrate, the intermediate is less efficiently converted to the internucleotide linkage. Sugar pucker does impact ligase efficiency, however, the relative impact of the $U^{2'F(ara)}$ and $U^{2'F(ribo)}$ substitutions is opposite expectation based upon T_m's, but likely explained by the thermodynamic differences described here. We note that previously, Mikita and Beardsley (35) observed that an oligonucleotide containing araC is ligated by T4 ligase three times more slowly than one with dC, although both oligonucleotides had similar T_m's. It was suggested that the presence of the 2'-OH in the arabino configuration could directly interfere with the ligase. In the studies reported here, the $A:U^{2'F(ara)}$ containing oligonucleotide is ligated by human DNA ligase III approximately four times slower than the A:dU oligonucleotide. Likewise, the rate of ligation of the $A:U^{2'F(ara)}$ oligonucleotide by *E. coli* DNA ligase is approximately seven times slower than the A:dU oligonucleotide. Here, the difference in ligation rates is attributed to net thermodynamic differences between a 3'-end $A:U^{2'F(ara)}$ and the corresponding base pair in an internucleotide linkage.

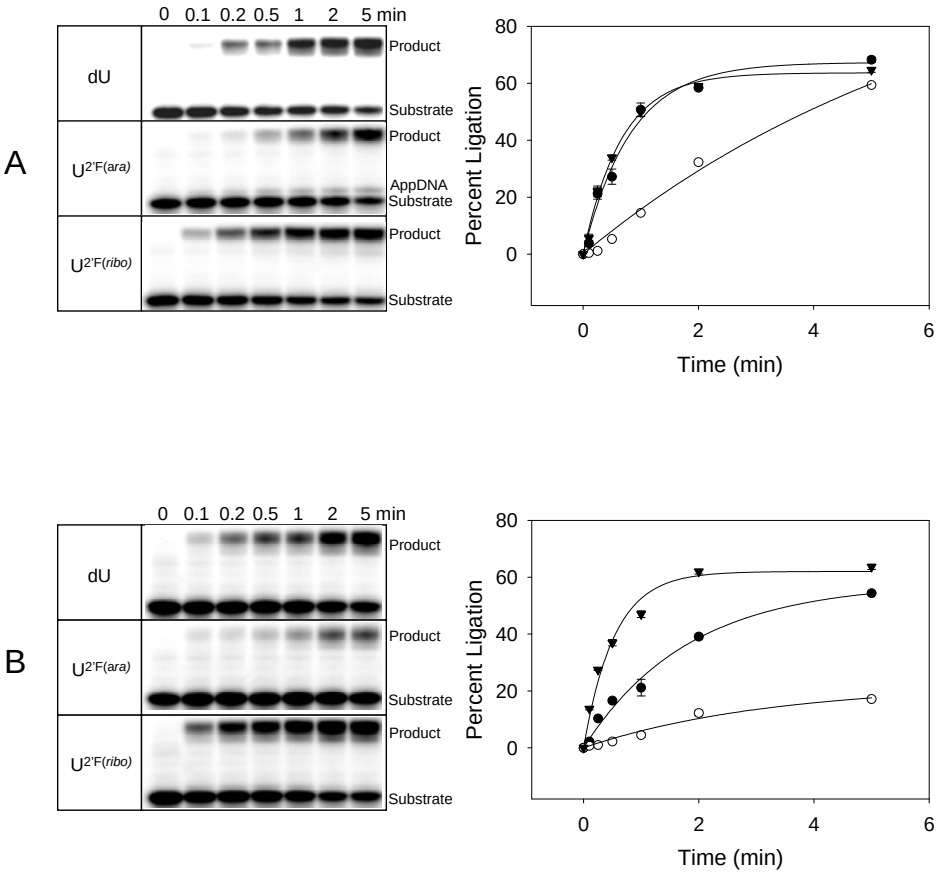

Figure 9. Ligase activities on 3'-terminal dU (●), $U^{2'F(ara)}$ (○), $U^{2'F(ribo)}$ (▼) residues paired with adenine. A) The experiments were performed at 26.5ºC with 50 nM substrate and 50 nM human DNA ligase III in a total volume of 10 µl. AppDNA indicates the 5'-AMP intermediate product of the ligation reaction. B) The experiments were performed at 16ºC with 50 nM substrate and 500 nM *E. coli* DNA ligase in a total volume of 10 µl.

Although $U^{2'F(ara)}$ is less disruptive thermodynamically when placed at a duplex 3'-end, it is more disruptive thermodynamically when in an internucleotide linkage, perhaps accounting for decreased ligase efficiency.

In the ligase studies reported here, it was assumed that the primary effect of the 2'F substitution was to constrain the sugar pucker equilibrium. It is important to note, however, that the larger fluorine substituent could induce additional steric effects as well

as electronic effects upon the nucleophilicity of the 3' OH, and these effects might be different for each isomer.

Net thermodynamic differences between 3'-end base pairs and internal base pairs might be related to polymerase extension efficiency. Multiple studies have been published on the impact of nucleotide analogs on polymerase incorporation and extension (7,8,34-41). The various studies examining different sets of analogs and polymerases make it difficult to draw specific conclusions. However, one of the consistent findings, and as yet unexplained paradoxes, with these nucleotide analogs is that some DNA polymerases strongly discriminate against ribonucleotides and 2'-deoxy-2'-fluororibo analogs at the insertion step, but incorporate arabino and 2'-deoxy-2'-fluoroarabino analogs with kinetics similar to normal dent's. Yet, once incorporated, the arabino and 2'-deoxy-2'-fluoroarabino analogs prevent further elongation and act as chain terminators. In contrast, some DNA polymerases discriminate against ribonucleotides at insertion, yet efficiently extend 3'-ribonucleotides. Indeed, DNA polymerase α preferentially adds dNTPs to ribonucleotide primers as part of the polymerase α/primase complex. Chain termination underlies the mechanism of toxicity for arabino analogs, yet the mechanism for the difference in polymerase preference between insertion and extension is as yet unknown.

Above, we discussed surprising results with DNA ligase which revealed that the $U^{2'F(ara)}$ analog was more thermodynamically destabilizing when in an internucleotide linkage as opposed to the 3'-end, and the net thermodynamic disadvantage with incorporating the 3'-OH of $U^{2'F(ara)}$ into an internucleotide linkage could provide an energetic barrier for polymerase extension. However, insufficient data currently exists to

resolve this issue. Further studies are currently in progress to understand the role of sugar constraint on thermodynamic properties, and the results of these studies might provide mechanistic insights into the mechanism of action of an important class of antitumor and antiviral compounds.

Acknowledgement

This work was supported by the National Institutes of Health.

References

(1) Petruska, J., Sowers, L.C. and Goodman, M.F. (1986). Comparison of nucleotide interactions in water, protein, and vacuum: Model for DNA polymerase fidelity. *Proc. Natl. Acad. Sci. USA. 83*, 1559-1562.

(2) Joyce, C.M., Sun, X.C. and Grindley, N.D.F. (1992). Reactions at the polymerase active site that contribute to the fidelity of *Escherichia coli* DNA polymerase I (Klenow Fragment). *J. Biol. Chem. 267*, 24485-24500.

(3) Johnson, K.A. (1993). Conformational coupling in DNA polymerase fidelity. *Annu. Rev. Biochem. 62*, 685-713.

(4) Goodman, M.F. and Fygenson, D.K. (1998). DNA polymerase fidelity: From genetics toward a biochemical understanding. *Genetics 148*, 1475-1482.

(5) Beard, W.A. and Wilson, S.H. (2003). Structural insights into the origins of DNA polymerase fidelity. *Structure 11*, 489-496.

(6) Joyce, C. M. and Benkovic, S.J. (2004). DNA polymerase fidelity: Kinetics, structure, and checkpoints. *Biochemistry 43*, 14318-14324.

(7) Thompson, H.T., Sheaff, R.J. and Kuchta, R.D. (1995). Interactions of calf thymus DNA polymerase α with primer/templates. *Nucleic Acids Res. 23*, 4109-4115.

(8) Richardson, F.C, Kuchta, R.D., Mazurkiewicz, A. and Richardson, K.A. (2000). Polymerization of 2'-Fluoro- and 2'-*O*-Methyl-dNTPs by human DNA polymerase α, polymerase γ, and primase. *Biochem. Pharm. 59*, 1045-1052.

(9) Astatke, M., Grindley, M.D.F. and Joyce, C.M. (1998). How *E. coli* DNA polymerase I (Klenow fragment) distinguishes between deoxy- and dideoxynucleotides. *J. Mol. Biol. 278*, 147-165.

(10) Marquez, V.E., Ben-Kasus, T., Barchi, J.J., Green, K.M., Nicklaus, M.C., Agbaria, R. (2004). Experimental and structural evidence that herpes 1 kinase and cellular DNA polymerase(s) discriminate on the basis of sugar pucker. *J. Am. Chem. Soc. 126*, 543-549.

(11) Petruska, J., Goodman, M.F., Boosalis, M.S., Sowers, L.S., Cheong, C. and Tinoco, I. (1988). Comparison between DNA melting thermodynamics and DNA polymerase fidelity. *Proc. Natl. Acad. Sci. USA. 85*, 6252-6256.

(12) Perrino, F.W., Preston, B.D., Sandell, L.L. and Loeb, L.A. (1989). Extension of mismatched 3' termini of DNA is a major determinant of the infidelity of human

immunodeficiency virus type 1 reverse transcriptase. *Proc. Natl. Acad. Sci. 86*, 8343-8347.

(13) Zinnen, S., Hsieh, J-C. and Modrich, P. (1994). Misincorporation and mispaired primer extension by human immunodeficiency virus reverse transcriptase. *J. Biol. Chem. 269*, 24195-24202.

(14) Mendelman, L.V., Petruska, J., and Goodman, M.F. (1990). Base pair extension kinetics. Comparision of DNA polymerase alpha and reverse transcriptase. *J. Biol. Chem. 265*, 2338-2346.

(15) Shah, A.M., Maitra, M. and Sweasy, J.B. (2003). Variants of DNA polymerase *β* extend mispaired DNA due to increased affinity for nucleotide substrate. *Biochemistry 42*, 10709-10717.

(16) Altona, C., and Sundaralingam, M. (1972) Conformational analysis of the sugar ring in nucleosides and nucleotides. A new description using the concept of pseudorotation. *J. Am. Chem. Soc. 94*, 8205-8212.

(17) Levitt, M. and Warshel, A. (1978). Extreme conformational flexibility of the furanose ring in DNA and RNA. *J. Am. Chem. Soc. 100*, 2607-2613.

(18) Ferrin, L. J. and Mildvan, A.S. (1985). Nuclear overhauser effect studies of the conformations and binding site environments of deoxynucleoside triphosphate substrates bound to DNA polymerase I and its large fragment. *Biochemistry 24*, 6904-6913.

(19) Harvey, S.C. and Prabhakaran, M. (1986). Ribose puckering: structure, dynamics, energetics, and the pseudorotation cycle. *J. Am. Chem. Soc. 108*, 6128-6136.

(20) Boulard, Y., Cognet, J.A., Gabarro-Arpa, J., Le Bret, M., Sowers, L.C. and Fazakerley, G.V. (1992). The pH dependent configurations of the C.A mispair in DNA. *Nucleic Acids Res. 20*, 1933-1941.

(21) Cullinan, D., Johnson, F., Grollman, A. P., Eisenberg, M. and De Los Santos, C. (1997). Solution structure of a DNA duplex containing the exocyclic lesion 3, N4-etheno-2'-deoxycytidine opposite 2'-deoxyguanosine. *Biochemistry 36*, 11933-11943.

(22) Allawi, H.T. and SantaLucia, J., Jr. (1998). NMR solution structure of a DNA dodecamer containing single G·T mismatches. *Nucleic Acids Res. 26*, 4925-4934.

(23) Tonelli, M. and James, T.L. (1998). Insights into the dynamic nature of DNA duplex structure via analysis of nuclear overhauser effect intensities. *Biochemistry 37*, 11478-11487.

(24) Berger, I., Tereshko, V., Ikeda, H., Marquez, V.E. and Egli, M. (1998). Crystal structure of B-DNA with incorporated 2'-deoxy-2'-fluoro-arabino-furanosyl thymines: implications of conformational preorganization for duplex stability. *Nucleic Acids Res. 26*, 2473-2480.

(25) Damha, M.J., Wilds, C.J., Noronha, A., Brukner, I., Borkow, G., Arion, D. and Parniak, M.A. (1998). Hybrids of RNA and arabinonucleic acids (ANA and 2'F-ANA) are substrates of Ribonuclease H. *J. Am. Chem. Soc. 120*, 12976-12977.

(26) Ikeda, H., Fernandez, R., Wilk, A., Barchi, J.J., Jr., Huang, X. and Marquez, V.E. (1998). The effect of two antipodal fluorine-induced sugar puckers on the conformation and stability of the Dickerson-Drew dodecamer duplex $[d(CGCGAATTCGCG)]_2$. *Nucleic Acids Res. 26*, 2237-2244.

(27) Wilds, C.J. and Damha, M.J. (1999). Duplex recognition by oligonucleotides containing 2'-Deoxy-2'-fluoro-D-arabinose and 2'-Deoxy-2'-fluoro-D-ribose. Intermolecular 2'-OH- phosphate contacts versus sugar puckering in the stabilization of triple-helical complexes. *Bioconjugate Chem. 10*, 299-305.

(28) Schultz, R. G. and Gryaznov, S.M. (2000). *Arabino*-fluorooligonucleotide N3' →P5' phosphoramidates: synthesis and properties. *Tetrahedron Lett. 41*, 1895-1899.

(29) Wilds, C.J. and Damha, M.J. (2000). 2'-Deoxy-2'-fluoro-β-D-arabinonucleosides and oligonucleotides (2'F-ANA): synthesis and physicochemical studies. *Nucleic Acids Res. 28*, 3625-3635.

(30) Trempe, J-F., Wilds, C.J., Denisov, A.Y., Pon, R.T., Damha, M.J. and Gehring, K. (2001). NMR solution structure of an oligonucleotide hairpin with a 2'F-ANA/RNA stem: Implications for RNase H specificity toward DNA/RNA hybrid duplexes. *J. Am. Chem. Soc. 123*, 4896-4903.

(31) Kalota, A., Karabon, L., Swider, C.R., Viazovkina, E., Elzagheid, E., Damha, M.J. and Gewirtz, A.M. (2006). 2'-Deoxy-2'-fluoro-β-D-arabinonucleic acid (2'F-ANA) modified oligonucleotides (ON) effect highly efficient, and persistent, gene silencing. *Nucleic Acids Res. 34*, 451-461.

(32) Peng, C.G. and Damha, M.J. (2007). G-quadruplex induced stabilization by 2'-deoxy-2'-fluoro-D-arabinonucleic acids (2'F-ANA). *Nucleic Acids Res. 35*, 4977-4988.

(33) Ziemkowski, P., Felczak, K., Poznanski, J., Kulikowski, T., Zielinski, Z., Ciesla, J. and Rode, W. (2007). Interactions of 2'-fluoro-substituted dUMP analogues with thymidylate synthase. *Biochem. Biophys. Res. Comm. 362*, 37-43.

(34) Pinto, D., Sarocchi-Landousy, M-T. and Guschlbauer, W. (1979). 2'-Deoxy-2'-fluorouridine-5'-triphosphates: a possible substrate for *E. coli* RNA polymerase. *Nucleic Acids Res. 6*, 1041-1048.

(35) Mikita, T. and Beardsley, G.P. (1988). Functional consequences of the arabinosylcytosine structural lesion in DNA. *Biochemistry 27*, 4698-4705.

(36) Kuchta, R.D., Ilsley, D., Kravig, K.D., Schubert, S., Harris, B. (1992). Inhibition of DNA primase and polymerase alpha by arabinofuranosylnucleoside triphosphates and related compounds. *Biochemistry 31*, 4720-4728.

(37) Perrino, F.W. and Mekosh, H.L. (1992). Incorporation of cytosine arabinoside monophosphate into DNA at internucleotide linkages by human DNA polymerase α. *J. Biol. Chem. 267*, 23043-23051.

(38) Lewis, W., Meyer, R.R., Simpson, J.F., Colacino, J.M., Perrino, F.W. (1994). Mammalian DNA polymerases alpha, beta, gamma, delta, and epsilon incorporate fialuridine (FIAU) monophosphate into DNA and are inhibited competitively by FIAU triphosphate. *Biochemistry 33*, 14620-14624.

(39) Ono, T., Scalf, M. and Smith, L.M. (1997). 2'-Fluoro modified nucleic acids: polymerase-directed synthesis, properties and stability to analysis by matrix-assisted laser desorption/ionization mass spectrometry. *Nucleic Acids Res. 25*, 4581-4588.

(40) Perrino, F.W., Mazur, D.J., Ward H. and Harvey, S. (1999). Exonucleases and the incorporation of aranucleotides into DNA. *Cell Biochem. Biophys. 30*, 331-352.

(41) Richardson, K.A., Vega, T.P., Richardson, F.C., Moore, C.L., Rohloff, J.C., Tomkinson, B., Bendele, R.A. and Kuchta, R.D. (2004). Polymerization of the triphosphates of AraC, 2', 2' –difluorodeoxycytidine (dFdC) and OSI-7836 (T-araC) by human DNA polymerase alpha and DNA primase. *Biochem. Pharmacol. 68*, 2644-3647.

(42) Tann, C.H., Brodfuehrer, P.R., Brundidge, S.P., Sapino, C., Jr. and Howell, H.G. (1985). Fluorocarbohydrates in synthesis. An efficient synthesis of 1-(2-deoxy-2-fluoro- *β*-D-arabinofuranosyl) thymine (*β*-FMAU). *J. Org. Chem. 50*, 3644-3647.

(43) Howell, H.G., Brodfuehrer, P.R., Brundidge, S.P., Benigni, D.A. and Sapino, C., Jr. (1988). Antiviral nucleosides. A stereospecific, total synthesis of 2'-fluoro-2'-deoxy- β-D-arabinofuranosyl nucleosides. *J. Org. Chem. 53*, 85-88.

(44) Martin, J.A., Bushnell, D.J., Duncan, I.B., Dunsdon, S.J., Hall, M.J., Machin, P.J., Merrett, J.H., Parkes, K.E.B., Roberts, N.A., Thomas, G.J., Galpin, S.A. and Kinchington, D. (1990). Synthesis and antiviral activity of monofluoro and difluoro analogues of pyrimidine deoxyribonucleosides against human immunodeficiency virus (HIV-1). *J. Med. Chem. 33*, 2137-2145.

(45) Vaidyanathan, G. and Zalutsky, M.R. (1998). Preparation of 5-[^{131}I] iodo- and 5-[^{211} At] astato-1-(2-deoxy-2-fluoro- β-D-arabinofuranosyl) uracil by a halodestannylation reaction. *Nucl. Med. & Biol. 25*, 487-496.

(46) Hamamoto, S. and Takaku, K. (1986). New approach to the synthesis of deoxyribonucleoside phosphoramidite derivatives. *Chem. Lett.*, 1401-1404.

(47) Gait, M.J. (1984). Oligonucleotide synthesis – a practical approach. Oxford, IRL Press, Washington, D.C.

(48) Cui, Z., Theruvathu, J.A., Farrel, A., Burdzy, A., Sowers, L.C. (2008). Characterization of synthetic oligonucleotides containing biologically important modified bases by matrix-assisted laser desorption/ionization time-of-flight mass spectrometry. *Anal. Biochem. 379*, 196-207.

(49) Connolly, B.A. and Newman, P.C. (1989). Synthesis and properties of oligonucleotides containing 4-thiothymidine, 5-methyl-2-pyrimidinone-1- β-D(2'-deoxyriboside) and 2-thiothymidine. *Nucleic Acids Res. 17,* 4957-4974.

(50) Pon, R.T. and Yu, R. (1997). Hydroquinone-*O*-*O*'-diacetic acid as a more labile replacement for succinic acid linkers in solid-phase oligonucleotide synthesis. *Tetrahedron Lett. 38*, 3327-3330.

(51) Azhayev, A.V. and Antopolsky, M.L. (2001). Amide group assisted 3'-dephosphorylation of oligonucleotides synthesized on universal A-supports. *Tetrahedron 57*, 4977-4986.

(52) Puglisi, J.D. and Tinoco, I., Jr. (1989). Absorbance melting curves of RNA. *Methods in Enzymology* (Dahlberg, J.E. and Abelson, E.N., Eds.) *180*, 304 – 325, Academic Press, Orlando, FL.

(53) SantaLucia, J., Jr., Allawi, H.T. and Seneviratne, P.A. (1996). Improved nearest-neighbor parameters for predicting DNA duplex stability. *Biochemistry 35*, 3555-3562.

(54) Allawi, H.T. and SantaLucia, J., Jr. (1997). Thermodynamics and NMR of internal G·T mismatches in DNA. *Biochemistry 36*, 10581-10594.

(55) Liu, P., Burdzy, A., and Sowers, L.C. (2004). DNA ligases ensure fidelity by interrogating minor groove contacts. *Nucleic Acids Res. 32*, 4503-11.

(56) Delort, A.M., Neumann, J.M., Molko, D., Herve, M., Teoule, R. and Tran, D.S. (1985). Influence of uracil defect on DNA structure: 1H NMR investigation at 500 MHz. Nucleic *Acids Res. 13*, 3343-3355.

(57) Carbonnaux, C., Fazakerley, G.V. and Sowers, L.C. (1990). An NMR structural study of deaminated base pairs in DNA. *Nucleic Acids Res. 18*, 4075-4081.

(58) Sowers, L.C., Shaw, B.R. and Sedwick, W.D. (1987). Base stacking and molecular polarizability: effect of a methyl group in the 5-position of pyrimidines. *Biochem. Biophys. Res. Commun. 148*, 790-794.

(59) Aboul-ela, F., Koh, D., Tinoco, I., Jr. and Martin, F.H. (1985). Base-base mismatches. Thermodynamics of double helix formation for dCA_3XA_3G + dCT_3YT_3G (X, Y = A,C,G,T). *Nucleic Acids Res. 13*, 4811-4824.

(60) McTigue, P.M., Peterson, R.J. and Kahn, J.D. (2004). Sequence-dependent thermodynamic parameters for locked nucleic acid (LNA)-DNA duplex formation. *Biochemistry 43*, 5388-5405.

CHAPTER THREE

THE IMPACT NUCLEOSIDE RIBOSE SUBSTITUTION ON POLYMERASE INCORPORATION

Adides A. Williams, Lawrence C. Sowers

Department of Basic Sciences, Loma Linda University School of Medicine

Loma Linda, CA 92350

Abstract

The accurate replication of DNA is critical for genomic integrity. During the insertion step, a DNA polymerase must select a nucleotide that is complimentary to the template base, has the correct deoxyribose sugar, and is able to bind to the primer-template complex with sufficient stability. While substantial work has revealed the structural and energetic factors that contribute to base-pairing fidelity, the role of sugar structure and conformation has received less attention. Sugar discrimination is especially challenging as DNA polymerases must accurately distinguish between deoxyribonucleoside 5'-triphosphates (dNTPs) and ribonucleoside 5'-triphosphates (rNTPs) even though rNTPs exist at higher intracellular concentrations. Apart from endogenously occurring NTPs, C2' (sugar) modified nucleoside analogues have been synthesized and shown to have potent toxicity. Although the underlying mechanism of cytotoxicity is incompletely understood, these therapeutic nucleoside analogues are used as primary agents for the treatment of human maladies including viral infections and tumors and their cytotoxicity depends on their ability to be phosphorylated and subsequently incorporated into DNA. Using stead-state kinetics, we investigated the ability of three different polymerases, human DNA polymerase β (pol β), avian myeloblastosis viral reverse transcriptase (AMVRT), and *Escherichia coli* Klenow fragment (exo-), to utilize sugar-modified NTP (modNTP) analogues. We found that pol β, AMVRT, and Klenow (exo-) readily incorporated arabinonucleotides (araNTPs) but incorporated rNTPs 2 – 5 orders of magnitude less efficiently than natural dNTPs. This observation led us to investigate the thermodynamic penalty associated with incorporating modNTPs onto the 3'-end of DNA. Interestingly, modNTP misinsertion

frequency increased proportionally with increasing melting temperatures (T_m) of 3'-end modified duplexes indicating that increased duplex thermal stability, as well as sugar conformation, contributed incorporation efficiency. These studies represent the first attempt to reconcile the thermodynamic consequence of misincorporating sugar-modified nucleoside analogues onto the 3'-end of a DNA strand and polymerase incorporation kinetics.

Abbreviations

dU, 2’-deoxyuridine; 5IdU, 5-iodo-2’-deoxyuridine; araU, 1-β-D-arabinofuranosyluracil; rU, Uridine; $U^{2'F(ribo)}$, 2’-deoxy-2’-fluorouridine; $U^{2'F(ara)}$, 1-(2’-deoxy-2’-fluoro-β-D-arabinofuranosyl) uracil; FIAU, 5-iodo-(2'-deoxy-2'-fluoro-β-D-arabinofuranosyl) uracil; dFdC, 2’-deoxy-2’,2’-difluorocytidine (Gemcitabine); dFdU, 2’-deoxy-2’,2’-difluorouridine (Gemcitabine metabolite); FIAU-P, 5’-*O*-dimethoxytrityl-5-iodo-2’-deoxy-2’-fluoroarabinosyluracil, 3’-*O*-[(2-cyanoethyl)(N,N,-diisopropyl)]-phosphoramidite; dFdU-P, 5’-*O*-dimethoxytrityl-2’-deoxy-2’,2’-difluorouridine, 3’-*O*-[(2-cyanoethyl)(N,N-diisopropyl)]-phosphoramidite.

Introduction

Fidelity of DNA synthesis is necessary to maintain genomic integrity, and errors made during replication and repair can lead to mutations and stalled replication forks [1]. Nucleotide insertion, exonucleolytic proofreading, and primer terminus extension are three distinct steps that contribute to overall replication fidelity [2]. During the insertion step a DNA polymerase selects a deoxyribonucleoside 5'-triphosphate (dNTP), whereas a RNA polymerase selects a ribonucleoside 5'-triphosphate (rNTP), that is complimentary to the template base and is able to bind to the primer-template complex with sufficient stability [3a]. During the extension step a correctly positioned terminal 3'-hydroxyl (3'-OH) is required to attack the α-phosphate (αP) of an incoming nucleoside triphosphate (NTP). While substantial work has revealed the structural and energetic factors that contribute to base-pairing fidelity [4 – 7], substantially less work has investigated the impact of nucleotide sugar structure and conformation on polymerase incorporation and extension.

Depending on the rNTP/dNTP pair, the cell-cycle phase, and organism, rNTPs have been shown to exist at intracellular concentrations that are 10 – 2000-fold greater than dNTP concentrations [8 – 10]. Remarkably, DNA polymerases efficiently distinguish dNTPs from rNTPs during the incorporation step despite this nucleotide pool imbalance. Depending on the DNA polymerase family, template sequence, and rNTP/dNTP pair, incorporation efficiency for dNMPs into DNA exceeds rNMP insertion efficiency by 10^2 – 10^6-fold [11, 12]. Though the basis for sugar discrimination is incompletely understood, the results of several structural and mutation studies has led to the proposed steric exclusion model in which the bulky side-chain [13 – 19] of amino

acid residues in the polymerase active site sterically clash with the C2'-OH of a rNTP. However, rNTP misincorporation is unavoidable. It has recently been demonstrated that DNA polymerases α (pol α), ε (pol ε), and δ (pol δ) from *Saccharomyces cerevisiae* misincorporate greater than 10000 rNMPs per round of nuclear genomic replication [10, 20] suggesting that ribonucleosides may be the most common contaminant in prokaryotic and eukaryotic genomic DNA. Misincorporation of a rNTP into DNA could target the resulting duplex for aberrant cleavage by enzyme activities including toposiomerase type I (Topo I), ribonuclease H type II (RNase H II), and flap endonuclease I (FEN I) [21, 22]. Together, these studies highlight the necessity and biological importance of the sugar selectivity mechanisms employed by DNA polymerases.

Apart from endogenously occurring NTPs, several nucleoside analogues, bearing C2' (sugar) and/or C5 (base) modifications, have been synthesized and shown to have significant toxicity [23 – 29]. Although the mechanism of action of these agents is incompletely understood, they are primary agents for the treatment of several human maladies including viral infections and tumors. This class of clinically significant nucleosides includes the thymidine analogues 5-iodo-2'-deoxyuridine (5IdU) and 5-iodo-(2'-deoxy-2'-fluoro-β-D-arabinosyl) uracil (Fialuridine, FIAU) (Figure 10) as well as the 2'-deoxycytidine analogues 2'-deoxy-2',2'-difluorocytidine (Gemcitabine, dFdC) and 1-β-D-arabinofuranosylcytosine (Cytarabine, araC). 5IdU is a C5-iodo-substituted analogue that has successfully been used in the treatment of vaccinia virus [30 – 32], herpes simplex virus type 1 [33] and herpes simplex keratitis [34]. FIAU, which bears both C5-iodo and C2'-fluoro substitutions, was used in the treatment of hepatitis B virus infection in NIH clinical trials where unexpected hepatotoxicity, progressive lactic acidosis and

pancreatitis resulted in the deaths of five patients [35]. Gemcitabine, in combination with platinum-containing drugs, is successfully used in the treatment of metastatic breast cancer [36], bladder cancer [37], and pancreatic adenocarcinoma [38]. Cytarabine, in combination with daunorubicin, is commonly used as a chemotherapeutic for treatment of acute myeloid leukemia (AML) and lymphomas [39] and has demonstrated activity against both herpes simplex and herpes zoster viruses [40, 41].

The mechanism of action of each nucleoside analogue is varied but ultimately involves inhibition of DNA synthesis following incorporation by a DNA polymerase. In general, the nucleoside analogues are transported across the cell membrane through the human nucleoside transporters (hNTs), including equilibrative (hENTs) and concentrative (hCNTs) nucleoside transporters and activated following intracellular phosphorylation to their respective monophosphate (MP), diphosphate (DP) and triphosphate (TP) forms which have multiple cellular targets [42 – 44]. For example, ribonucleotide reductase (RNR) is potently inhibited by dFdCDP ultimately leading to decreased dCTP pools [45] and dFdCTP has been implicated in the inhibition of both deoxycytidine monophosphate (dCMP) deaminase and CTP synthetase [46, 47]. In the triphosphate form, nucleoside analogues are incorporated into DNA and in the case of dFdC, araC and FIAU, act as chain terminators.

In addition to phosphorlyation, FIAU is further metabolized to 1-(2-deoxy-2-fluoro-β-D-arabinofuranosyl)uracil ($U^{2'F(ara)}$) (Figure 10).

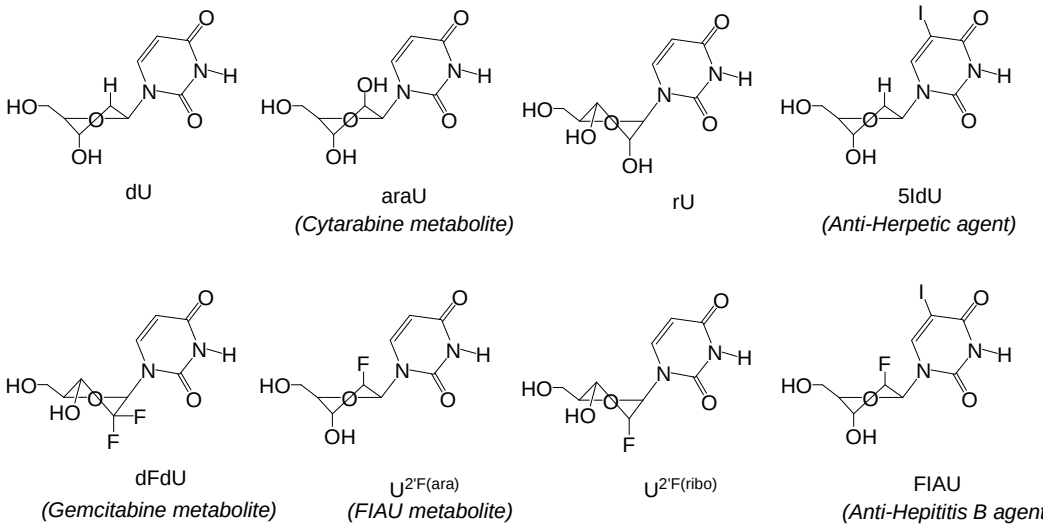

Figure 10: Chemical structures of an important class of antiviral and anticancer nucleoside analogues used in this study. The nucleoside analogues were either converted to 5'-triphosphates that were used in nucleotide incorporation experiments or converted to phosphoramidites which were then incorporated onto the 3'-end (primer terminus) of oligonucleotides which were used in primer extension experiments.

Interestingly, studies have shown that incubation of human hepatoma HepG2 cell lines with $U^{2'F(ara)}$ resulted in decreased mitochondrial DNA content [48a] suggesting that $U^{2'F(ara)}$ may contribute to the cytotoxic profile of FIAU. In addition, dFdC and araC are rapidly deaminated to the corresponding 2'-deoxy-2',2'-difluorouridine (dFdU) and 1-β-D-arabinofuranosyluracil (araU) metabolites (Figure 10), respectively, by the ubiquitously expressed enzyme cytidine deaminase [49, 50]. Studies have demonstrated that araU and dFdU exhibit especially long terminal half-lifes (14 – 89 h) relative to their cytidine cognates (8 – 16 min) [51 – 53]. Significantly, clinical studies have shown that dFdU nucleotides are formed and accumulate in the liver of mice and humans after multiple dosings of dFdC [51]. Moreover, Veltkamp and co-workers [54] demonstrated that dFdUTP was incorporated into the DNA and RNA of HepG2, A549 and hCNT1-

transfected MDCK cell lines and that the incorporation of dFdUTP correlated with dFdU cytotoxicity suggesting that liver accumulation of dFdU and subsequent misincorporation of dFdUTP might be associated with observed liver toxicity in patients following continuous oral and/or intravenous administration of dFdC. Plunkett and co-workers first demonstrated that araU accumulates in the cerebrospinal fluid of patients following intermittent infusion of high-dose araC [55] leading to the suggested role for araU accumulation in araC-associated neurotoxicity [50]. In all, these studies highlight the biological importance of these sugar modified nucleoside analogues and the contribution of their metabolites to observed cytotoxicity.

The underlying mechanism of cytotoxicity for the nucleoside analogues investigated in this report is believed to be chain termination following incorporation. Several *in vitro* incorporation and extension studies have demonstrated that pol α, pol ε, and pol δ exhibit greater than 10^3-fold reduction in catalytic efficiency when extending araC-, dFdC- and FIAU-terminated primers consistent with the chain termination model. However, araC and dFdC are often found in internucleotide linkages when studied in cell culture [56, 57] suggesting that additional polymerases may play a role in the incorporation of these nucleotide analogues into DNA. Indeed, Chou and co-workers have demonstrated that translesion DNA pol η efficiently extends araCMP- and dFdCMP-terminated primers [58]. Moreover, pol η-deficient fibroblast cells exhibited increased sensitivity to araC or dFdC treatment relative to normal human fibroblasts suggesting that the increased sensitivity was due to the inability of pol η-deficient fibroblasts to continue replication following polymerase pausing at araC and dFdC-terminated primers. In addition, DNA repair polymerases may participate in the

incorporation of nucleotide analogues into genomic DNA. Significantly, Plunkett and co-workers demonstrated that DNA repair synthesis was the primary route of incorporation of araC into the DNA of proliferating human leukemia cells [59]. When one takes into account the increased oxidative stress of the tumor [60] and that several tumor types exhibit increased expression of pol β [61], it is likely that pol β activity contributes to the cytotoxicity of these nucleoside analogues.

For this report we evaluated the ability of pol β, Klenow (exo-), and AMVRT to incorporate several modNTP analogues modified at either C2' (sugar) or C5 (nucleobase) onto the 3'-end of a DNA strand. We also constructed oligonucleotides with each of the modified nucleoside analogues (Figure 10) at the 3'-end position (Figure 11B). These 3'-end modified oligonucleotide duplexes were then used in thermal denaturation studies to probe the energetic penalty for misincorporation of the modified NTPs (modNTPs) on to the primer terminus of a DNA strand.

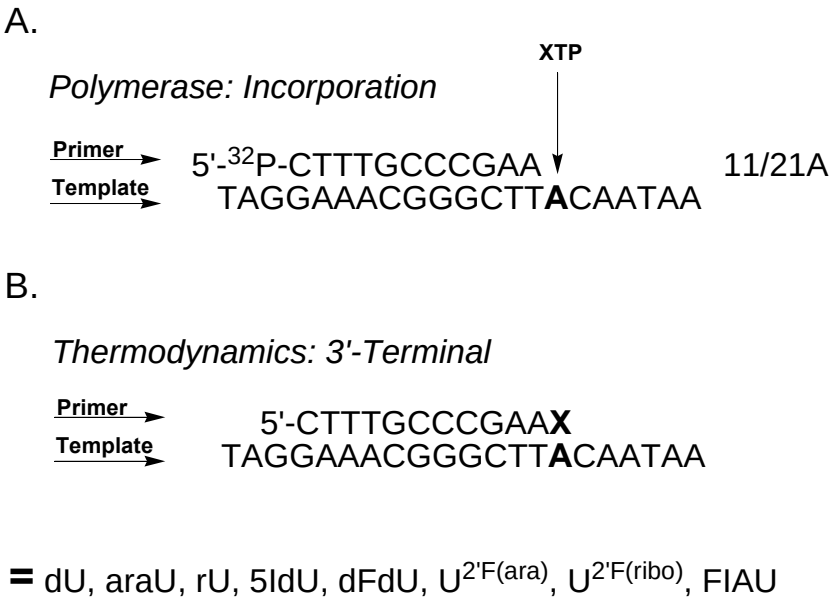

Figure 11: DNA substrates used in the present study for polymerase insertion kinetics and thermodynamic studies. For polymerase kinetics studies, a ^{32}P-labeled primer (11-mer) was annealed to a 21-mer template. The steady-state kinetic parameters for (A) the incorporation of modNTPs were measured and are presented in Table 2. For the thermodynamic studies, synthetic duplexes with sugar-modified residues at (B) the primer terminus (3'-terminal) were used.

Materials and Methods

Solvents and Reagents

All solvents were purchased from Sigma-Aldrich (St. Louis, MO). Thin layer chromatography (TLC) was performed on precoated silica gel 60 F_{254}, 5x20 cm, 250 μm thick plates purchased from EMD (Gibbstown, NJ). Universal support III PS and all normal (unmodified) phosphoramidites (dC, dG, dA, dT) were purchased from Glen Research (Sterling, VA).

Nucleotides and Nucleosides

The triphosphates dUTP, 5IdUTP, araUTP, and $U^{2'F(ribo)}TP$ were purchased from Trilink Biotechnologies (San Diego, CA), $U^{2'F(ara)}TP$ and FIAUTP were purchased from Moravek Biochemicals (Brea, CA), and rUTP was purchased from Promega (Madison, WI). The nucleoside dFdC (Gemcitabine) was purchased from Carbosynth Ltd. (Old Station Business Park, Compton Berkshire, UK) and FIAU was purchased from R.I. Chemical, Inc. (Orange, CA).

Synthesis and Purification of 2'-deoxy-2',2'-difluorouridine (dFdU)

Commercially available 2'-deoxy-2',2'-difluorocytidine (dFdC, Gemcitabine) was deaminated to the corresponding dFdU nucleoside analogue following [62, 63]. First, 100 mg of dFdC (0.38 mmol) and 700 mg of sodium nitrite ($NaNO_2$; 10.1 mmol) were combined in 20 mL of H_2O. The initial reaction mixture, pH of 7.2, was adjusted to a pH of 3.4 by the addition of hydrochloric acid (HCl). The reaction mixture temperature was adjusted to 57 °C and the reaction proceeded, with magnetic stirring, for 5 hr. The pH of the reaction mixture was monitored hourly and readjusted to a pH of 3.4 when necessary. Conversion of dFdC to dFdU was monitored by thin-layer chromatography (TLC) developed in a solvent system of dichloromethane (DCM) and methanol (MeOH) (90:10) at room temperature. The conversion of dFdC to dFdU was determined to be complete when the spot of R_F 0.11 (dFdC) was no longer visible and only the spot of R_F 0.39 (dFdU) was observed. The solvent (H_2O) was then removed under reduced pressure and the resulting white precipitate (ppt) was dissolved in MeOH. The methanolic solution was spiked with DCM and cooled, in an ice water bath, to 0 °C to precipitate out sodium salts (NaCl and unreacted $NaNO_2$). The sodium salts were then removed by vacuum

filtration, the filtrate (containing dFdU) was collected and the solvents were removed under reduced pressure. The resulting ppt was dissolved in DCM and purified by open silica gel column eluting the following gradient: 1) 0 – 10% MeOH in DCM for 10 min.; 2) 10 – 10% MeOH in DCM for 10 min.; 3) 10 – 20% MeOH in DCM for 10min for total run time of 30 min. Fractions containing dFdU, as determined by TLC, were combined and the solvents were removed under reduced pressure to afford 88.3 mg of dFdU (88 mmol), as a white foam, in 88% yield. The dFdU nucleoside analogue was characterized by electrospray ionization mass spectrometry (ESI-MS) in negative ion mode. The observed fragment ions were m/z = 111.27 ($C_4H_3N_2O_2$, uracil base); m/z = 220.19 ($C_8H_8F_2NO_4$, loss of CHNO from dFdU nucleoside); m/z = 263.13 ($C_9H_9F_2N_2O_5$, dFdU nucleoside); m/z = 527.18 ($C_{18}H_{19}F_4N_4O_{10}$, dFdU nucleoside dimer).

Synthesis of 2'-deoxy-2',2'-difluorouridine triphosphate (dFdUTP)

The 5'-triphosphate analogue of dFdU is not available and was synthesized using established procedures. Following Yoshikawa's monophosphorylation method [64], 10 mg of dFdU (37.9 μmol) was stirred in 97.4 μL of trimethylphosphate ($P(OCH_3)_3OH$; 116.6 mg, 833 μmol, 22 molar equiv. of nucleoside) at 0 °C. To this was added 14 μL of phosphorous (IV) oxychloride ($POCl_3$; 23 mg, 151 μmol, 4 molar equiv. of nucleoside) to generate the 5'-phosphodichloridate derivative of dFdU (dFdU-$POCl_2$, activated dFdU monophosphate). The reaction mixture was allowed to warm to room temperature during stirring. At 5 minute intervals 1-μL aliquots of the reaction mixture were treated with 19 μL of aqueous triethylammonium bicarbonate buffer (TEAb, pH 7.5) and assayed by anion exchange HPLC using a Mono Q HR 5/5 anion-exchange column eluting 0 – 2M ammonium acetate (NH_4OAc, pH 7). After maximum formation of dFdU-$POCl_2$ was

observed (40 – 50%), the reaction mixture was added drop-wise to a 0.5 M solution of 100 mg of tributylammonium pyrophosphate (TBA-PPi; 220 μmol) dissolved in 400 μL of dimethylformamide (DMF) and 40 μL of tributylamine (TBA) at -10 °C with stirring, according to the "one-pot, three-step" procedure [65, 66], to generate the corresponding 5'-triphosphate derivative (dFdUTP). The reaction mixture was then allowed to warm to room temperature and the reaction was checked for triphosphate formation by neutralizing 1-μL aliquots of the reaction mixture with 19 μL of TEAb (pH 7.5) which were then assayed by anion exchange HPLC using a Mono Q HR 5/5 anion-exchange column eluting a gradient of 0 – 2M ammonium acetate (NH_4OAc, pH 7). When formation of dFdUTP was maximal (10 – 20%), the reaction was quenched with excess cold aqueous TEAb (pH 7.5). The product was purified by open column chromatography on Sephadex DEAE A-25 eluting a gradient of 0 – 2M TEAb (pH 7.5). Fractions were collected and assayed for pyrophosphate content.

Assaying Triphosphate Fractions for Inorganic Pyrophosphate (PPi) Content

Typically the nucleoside phosphodichloridate intermediate (dN-$POCl_2$) is added to excess TBA-PPi to afford maximal conversion of dN-$POCl_2$ to dNTP [65 – 67]. However, it is known that polymerase activity is greatly reduced in the presence of excess PPi [68 – 72]. Thus, fractions obtained following the purification of the dFdUTP reaction by open column chromatography were assayed for PPi content using a molybdenum phosphate based reagent (MoPho-R) as previously described [73]. MoPho-R was prepared, fresh daily, by combining 1 volume (vol.) of 6N H_2SO_4, 1 vol. of a 2.5% aqueous solution of molybdenum phosphate (MoPho), 1 vol. of a 0.57 M aqueous

solution of ascorbic acid and 2 vol. of H_2O. The individual components of MoPho-R were prepared as follows: 6N H_2SO_4 was prepared by adding 18 mL of concentrated (conc.) H_2SO_4 to 108 mL of H_2O and stored at room temperature (rt). Aqueous 2.5% MoPho was prepared by dissolving 5 g of ammonium molybdate tetrahydrate ($(NH_4)_6Mo_7O_{24}\bullet 4H_2O$) in 200 mL of H_2O and stored at rt. Aqueous ascorbic acid (0.57 M) was prepared by dissolving 10 g of L-ascorbic acid in 100 mL of H_2O and stored at 4 °C.

Following open column purification of the dFdUTP reaction, 10-µL aliquots of each collected fraction were diluted into 990 µL of MoPho-R. The MoPho reaction mixtures were then vortexed and incubated at 37 °C for 1 h. Over time, the MoPho reaction mixtures became blue colored as a consequence of phosphomolybdate reduction product formation and the intensity of color development was proportional to phosphorous content as previously observed [73]. The UV absorption profile of each MoPho color reaction was monitored at 800 nm. Fractions containing appropriately pure dFdUTP (97 – 99% triphosphate and 1 – 3% diphosphate by HPLC) and acceptable PPi content were combined, lyophilized to dryness, relyophilized thoroughly from H_2O and MeOH (1:1, v/v) 5 times to remove excess buffer to afford dFdUTP in 25% yield which was then characterized by ESI-MS (negative-ion mode), HPLC and UV-vis spectral analyses (Figure 12).

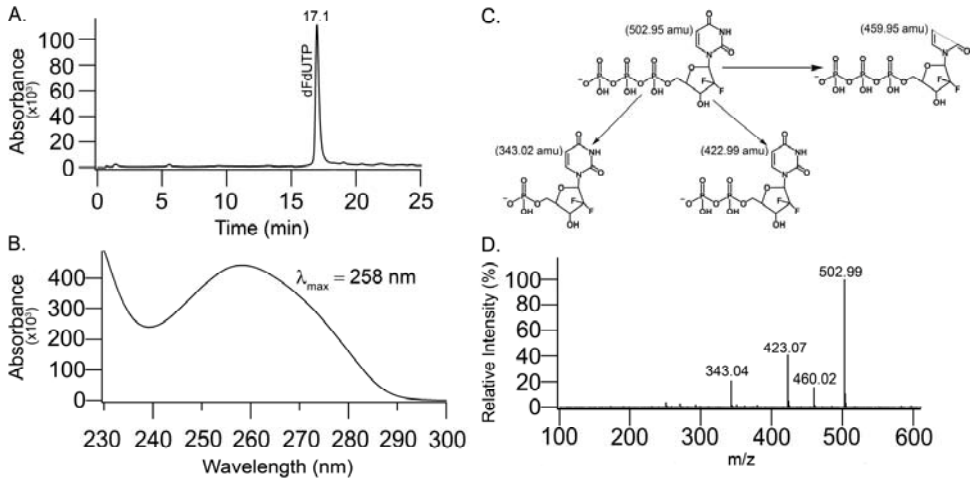

Figure 12: The HPLC, UV-vis and mass spectral analyses of dFdUTP. Panel A: HPLC chromatogram. Panel B: UV spectrum of the HPLC peak in Panel A. Panel C: The structure of dFdUTP and the proposed structures of its fragmentation products detected by mass spectrometry. The theoretical masses for each structure are in parentheses. Panel D: Mass spectrum obtained following direct inject onto a Thermo Finnigan Surveyor MSQ mass spectrometer using electrospray ionization (negative-ion mode).

Synthesis of FIAU and dFdU Phosphoramidites (FIAU-P and dFdU-P)

The phosphoramidite analogues of 5-iodo-(2'-deoxy-2'-fluoro-β-D-arabinofuranosyl) uracil (FIAU) and 2'-deoxy-2',2'-difluorouridine (dFdU) are not commercially available and were synthesized using established methods [74 – 76]. First, 250 mg of FIAU (0.67 mmol) was co-evaporated with anhydrous (anhyd.) pyridine (3 X 10 mL) and the resulting oily residue was re-dissolved in 10 mL anhyd. pyridine. To this was added 4.10 mg of 4-dimethylaminopyridine (DMAP; 0.034 mmol, 0.05 molar equiv. of nucleoside), 131 μL of TEA (0.94 mmol, 1.4 molar equiv. of nucleoside) and 276.4 mg of 4,4'-dimethoxytrityl chloride (DMT-Cl; 0.82 mmol, 1.2 molar equiv. of nucleoside). The reaction proceeded under an argon (Ar) atmosphere with magnetic stirring for 7 h. The conversion of FIAU to the corresponding 5'-dimethoxytrityl

protected derivative (5'-dimethoxytrityl-5-iodo-2'-deoxy-2'-fluoroarabinosyluracil, FIAU-DMT) was monitored by TLC developed in a solvent system of DCM and MeOH (95:5, v/v). The formation of FIAU-DMT was determined to be complete when the spot of R_F 0.11 (FIAU) was no longer visible and the spot of R_F 0.39 (FIAU-DMT) was observed. Upon completion of the reaction, pyridine was removed under reduced pressure and the resulting oily residue was dissolved in DCM and extracted with saturated aqueous sodium bicarbonate ($NaHCO_3$, pH 8). The organic layer was removed, washed with H_2O and dried over anhyd. sodium sulfate (Na_2SO_4). Evaporation of the solvent gave an oily residue that was then dissolved in DCM and purified by open silica gel column eluting a gradient of 0 – 3% MeOH in DCM for 50 min. Fractions containing FIAU-DMT, as determined by TLC, were combined and the solvents were removed under reduced pressure to afford 245 mg (0.36 mmol) of FIAU-DMT, as a white (slightly yellow) foam, in 53% yield. FIAU-DMT was characterized by ESI-MS in negative ion mode. The observed fragment ions were m/z = 673.18 ($C_{30}H_{27}FIN_2O_7$, FIAU-DMT); m/z = 303.07 ($C_{21}H_{19}O_2$, free DMT protecting group).

The FIAU phosphoramidite (5'-dimethoxytrityl-5-iodo-2'-deoxy-2'-fluoroarabinosyluracil, 3'-[(2-cyanoethyl)(N,N,-diisopropyl)]-phosphoramidite, FIAU-P) was prepared by combining 220 mg of FIAU-DMT (0.33 mmol) and 29.5 mg of diisopropylamine hydrotetrazolide (0.17 mmol, 0.5 molar equiv. of FIAU-DMT) in 5 mL of anhyd. acetonitrile (MeCN) under an Ar atmosphere. To this mixture was added 116.27 µL of 2-cyanoethyl-N,N,N',N'-tetraisopropylphosphoramidite (109 mg, 0.36 mmol, 1.1 molar equiv. of FIAU-DMT), dropwise, with continuous stirring for 3 h. The conversion of FIAU-DMT to FIAU-P was monitored by TLC developed in a solvent

system of DCM, ethyl acetate (EtOAc) and TEA (55:40:5, v/v). The conversion of FIAU-DMT to FIAU-P was determined to be complete when the spot of R_F 0.64 (FIAU-DMT) was no longer visible and the spot of R_F 0.89 (FIAU-P) was observed. Upon completion of the reaction, 2 mL of TEA was added to the reaction mixture which was then extracted with an aqueous solution of NaCl (3 X 10 mL). The organic (top) layer was recovered, dried over anhyd. Na_2SO_4 and evaporated in vacuo. The resulting colorless residue was dissolved in a solution of Hexanes, EtOAc and TEA (89:10:1, v/v) and purified by open silica gel column eluting a gradient of 10 – 100% solvent A (EtOAc, TEA; 99:1, v/v) in solvent B (Hexanes, TEA; 99:1, v/v) for 1 hr. Fractions containing FIAU-P, as determined by TLC, were combined and evaporated in vacuo to give 148.6 mg (0.17 mmol) of FIAU-P as a white (slightly yellow) foam, in 51% yield. The FIAU-P was characterized by ESI-MS (Figure 13).

Both the 5'-tritylated (dFdU-DMT) and phosphoramidite (5'-*O*-dimethoxytrityl-2'-deoxy-2',2'-difluorouridine, 3'-*O*-[(2-cyanoethyl)(N,N-diisopropyl)]-phosphoramidite, dFdU-P) analogues of dFdU were synthesized and purified exactly as FIAU-DMT and FIAU-P (previously described), respectively, to give dFdU-P, as a white foam, in 47% yield.

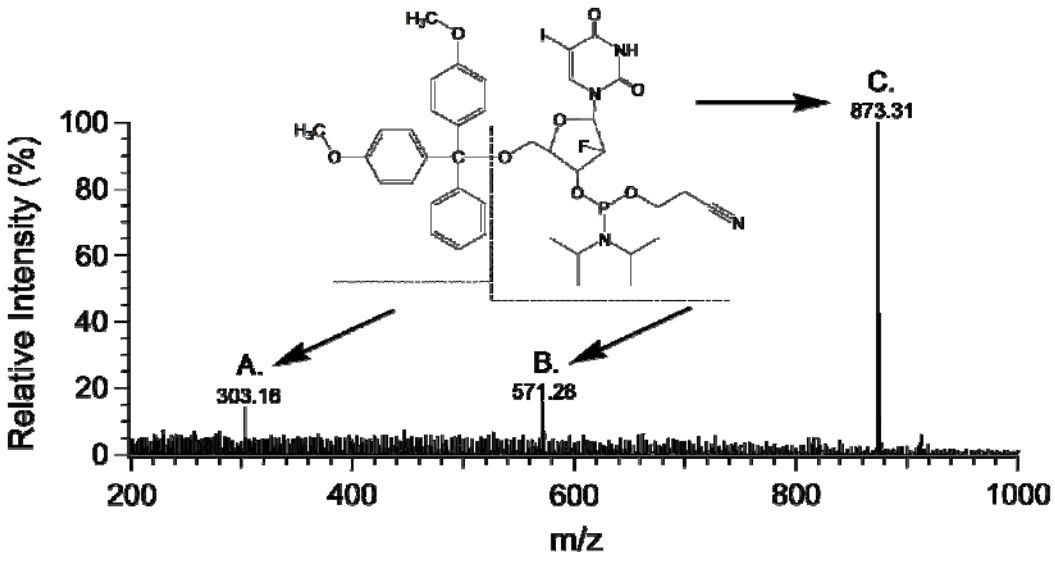

Figure 13: The FIAU phosphoramidite analogue (FIAU-P) was characterized by electrospray ionization mass spectrometry (ESI-MS) in negative ion mode. Fragments corresponding to free dimethoxytrityl (DMT) protecting group (A), loss of the DMT group from FIAU-P (B) and intact FIAU-P (C) were observed. Theoretical mass for fragment A. ($C_{21}H_{19}O_2$): (m/z) = 303.15 [M-H+]; observed: 303.16. Theoretical mass for fragment B. ($C_{18}H_{26}FIN_4O_6P$): (m/z) = 571.07 [M-H+]; observed: 571.28. Theoretical mass for C. ($C_{39}H_{44}FIN_4O_8P$): (m/z) = 873.20 [M-H+]; observed: 873.31.

Enzymes and DNA Preparation

Human DNA polymerase β (pol β) was obtained from Enzymax (Lexington, KY). Avian myeloblastosis virus reverse transcriptase (AMV-RT) and exonuclease-deficient Klenow fragment (exo-) polymerase were obtained from New England Biolabs (Ipswich, MA). For the polymerase incorporation assays, the primers were 5′-^{32}P-end labeled by T4 polynucleotide kinase (New England Biolabs) with [γ-^{32}P]adenosine triphosphate (MP Biomedicals, Costa Mesa, CA) under conditions recommended by the enzyme supplier. Labeled oligonucleotides were purified using G25 Sephadex columns (Roche Applied Science, Indianapolis, IN). A 2-fold excess of the complementary template strand was

then added to the labeled primer mixture, incubated at 95 °C for 5 min, and allowed to cool to room temperature gradually to create the oligo-primer duplex.

Steady-State Kinetic Experiments (Polymerase Incorporation Assays)

Polymerase β incorporation reactions were performed in pol β buffer (50 mM Tris-HCl, pH 7.5, 10 mM $MgCl_2$, 2mM dithiothreitol, 20 mM NaCl, 20 mM KCl, 200 μg/ml BSA, 1% glycerol) and increasing concentrations of dNTPs at 37°C. AMV-RT incorporation assays were performed in AMV-RT buffer (5 mM NaCl, 60 mM Tris-HCl, 8 mM $MgCl_2$, and 0.5 mM dithiothreitol, pH 7.5) and increasing concentrations of dNTPs at 37°C. Klenow (exo-) incorporation assays were performed in Klenow (exo-) buffer (50 mM NaCl, 10 mM Tris-HCl, 10 mM $MgCl_2$, and 1 mM dithiothreitol, pH 7.5) and increasing concentrations of dNTPs at 37°C. In general, the reactions were initiated by the addition of radiolabeled substrate to enzyme (pol β, AMVRT, or Klenow (exo-)) and dNTP. The radiolabeled DNA concentrations were 10-fold greater than polymerase concentrations and the dNTP concentrations ranged from 0.01 to 1000 μM. Reactions (20 μL) were quenched at various times using equal volumes of "STOP" solution (98% formamide, 0.01 M EDTA, 1 mg/mL xylene cyanole, and 1 mg/mL bromophenol blue) followed by heating at 95 °C for 2 min. The reaction products were electrophoresed on denaturing polyacrylamide gels containing 20% acrylamide (19:1 acrylamide:methylenediacrylamide) and 8 M urea. The size of the gel was 19.5 cm x 16 cm x 0.4 cm and was run at 519 V for 2.5 – 3 h using a Hoeter PS 500 XT DC Power Supply (Amersheim Pharmacia Biotech). The gel was visualized and quantified using a Storm 860 PhosphorImager (Molecular Dynamics, Sunnyvale, CA) and ImageQuant 5.2 software (GE Healthcare Bio-Sciences).

Determination of k_{cat} and K_m.

The previously described assays were used to measure the incorporation kinetics (k_{cat} and K_m) for the incorporation of a sugar modified NTP (modNTP) opposite template dA at pH 7.5 (Figure 11A). A series of reaction mixtures containing increasing concentrations of modNTP were incubated for 0, 15, 30, 60, 120 or 180 sec. The amount of product formed by nucleotide incorporation at the template target was determined by calculating the ratio of the band intensity of the extended primer (DNA_{n+1}) to the band intensity of the un-extended primer (DNA_n). Initial velocities (V_o) were determined by plotting product formation versus time (Figure 14B). The values of V_o were then plotted versus concentration (Figure 14C) and the data were fitted by nonlinear regression, using Prism version 5 (GraphPad Software, San Diego, CA; www.graphpad.com), to Equation 1,

$$v_o = \frac{(k_{cat})[E]_t[dNTP]}{K_m + [dNTP]} \qquad \text{Eq. 1}$$

where V_o is the initial velocity, k_{cat} is the catalytic turnover number, $[E]_t$ is the total enzyme concentration, [dNTP] is the concentration of nucleoside triphosphate and K_m is the Michaelis-Menten constant.

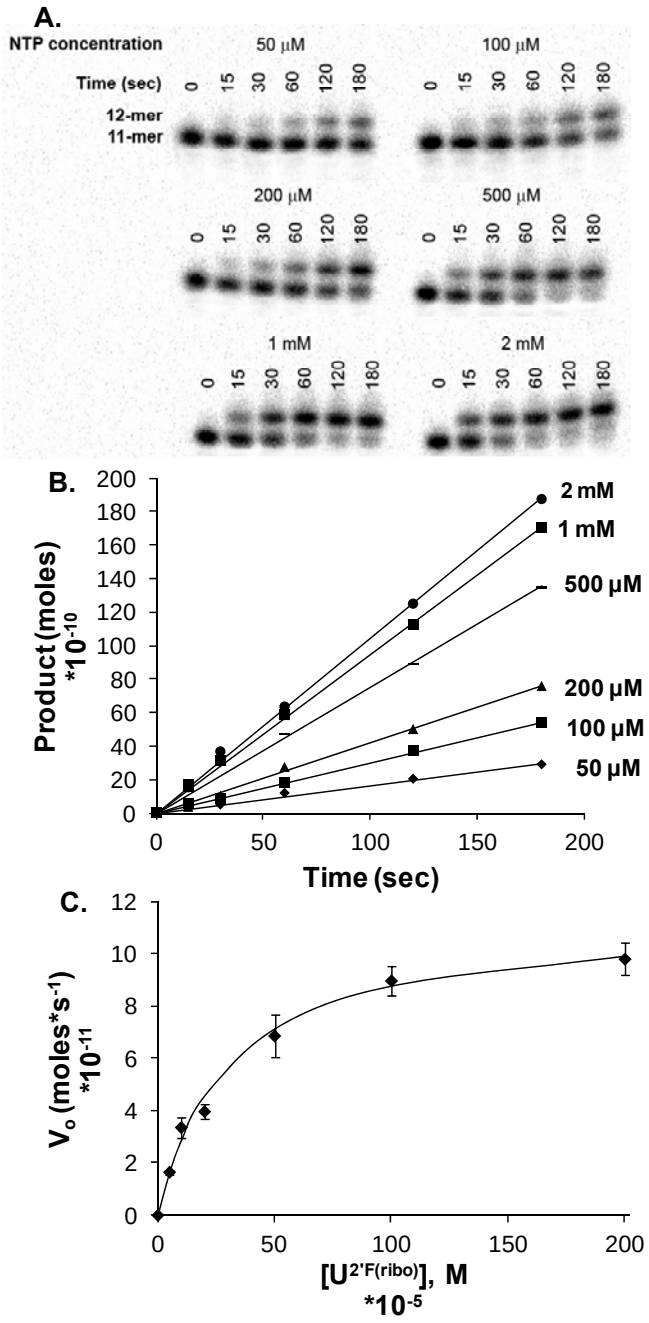

Figure 14: Representative gel (A), product formation plot (B) and saturation curve plot (C) to illustrate how Michaelis-Menten constants were determined from denaturing gel-based polymerase kinetics assays. The saturation curves (C) were fitted to Equation 1 to yield Km and kcat values for NTP incorporation. The plots are for the incorporation of $U^{2'F(ribo)}TP$ opposite template dA.

Thermal Denaturation Studies and Assessment of Duplex Melting Behavior

Samples containing non-self-complementary oligonucleotides were prepared in buffer containing 0.1 M NaCl, 0.01 M sodium phosphate, and 0.1 mM EDTA (pH 7.0). Complexes were prepared by mixing equimolar amounts primer and template strands (Figure 11B) , and concentration dependent melting temperature (T_m) measurements were conducted with a total strand concentration (C_T) between 2 and 60 μM in cuvettes with path lengths between 1 and 10 mm. Molar extinction coefficients of oligonucleotides were calculated [77] to determine single-strand concentrations. Oligonucleotide T_m's were determined using a Varian Cary 300 Bio UV-visible spectrophotometer (Varian, Walnut Creek, CA). Five temperature ramps were performed on each sample per run while the absorbance at 260 nm was observed: (1) from 12 to 90 °C at a rate of 0.5 °C/min, (2) from 90 to 12 °C at a rate of 0.5 °C/min, (3) from 12 to 90 °C at a rate of 0.5 °C/min, (4) from 90 to 12 °C at a rate of 0.5 °C/min, and (5) from 12 to 90 °C at a rate of 0.5 °C/min. The sample was held for 3 min when the temperature reached 90 °C and for 10min when it reached 12 °C, and then the next cycle was started. Data were collected at 0.5 °C intervals while the temperature was monitored with a probe inserted into a cuvette containing only buffer. The Tm of each duplex was determined using Cary WinUV Thermal software (Varian). Theoretical T_m values for the control duplexes (A:dU) were determined [78, 79] and compared against values obtained using Cary WinUV Thermal. Thermodynamic parameters for non-self-complementary duplexes were calculated in two ways: (1) averages from fits of individual melting curves at different concentrations using the van't Hoff calculation in Cary WinUV Thermal and (2) $1/T_m$ versus $\ln(C_T/4)$ plots fitted to Equation 2 for the non-self-complementary sequences examined here:

$$\frac{1}{T_m} = \frac{R}{\Delta H^\circ} \ln\left(\frac{C_T}{4}\right) + \frac{\Delta S^\circ}{\Delta H^\circ} \qquad \text{Eq. 2}$$

Both methods assume a two-state model, and ΔCp = 0 for the transition equilibrium. The two-state approximation was assumed to be valid for sequences in which the ΔH° values derived from the two methods agreed within 15% [79]. The ΔH° values derived from the two methods agree within 15%, indicating that the two-state approximation is valid for all other sequences employed in this study.

Analysis of Thermodynamic Data

Thermal and thermodynamic data obtained for the ensemble of oligonucleotides examined here were expressed as the corresponding differences by comparing the measured value for the substituted duplexes with the standard A:dU containing duplex for the 3'-end and internucleotide series. The corresponding values of ΔT_m, $\Delta\Delta G^o_{37}$, $\Delta\Delta H^o$ and $\Delta\Delta S^o$ are presented in Table 3.

Results

Characterization of Phosphoramidites by Electrospray Ionization Mass Spectrometry (ESI-MS)

The phosphoramidite derivatives of FIAU and dFdU are not commercially available and were synthesized using established methods [74, 75]. Traditionally, phosphoramidites have been characterized using several techniques including ^{1}H, ^{13}C and ^{31}P NMR and IR. In general, phosphoramidites contain both 5'-*O*-dimethoxytrityl (acid labile) and 3'-*O*-β-cyanoethyl-N,N-diisopropyl (base labile) groups making

characterization by mass spectrometric techniques problematic. Indeed, even mild ionization methods including matrix assisted laser desorption ionization (MALDI), fast atom bombardment (FAB) and liquid secondary ion mass spectrometry (LSIMS) employ acidic media and matrices that are not compatible with the acid-labile substituents [80, 81].

Conventionally, ESI methods employ mixtures of aqueous organic solvents (MeOH or MeCN) and weak organic acid for mass spectrometric analysis in positive ion mode. However, in the present study, a method using ESI-MS was used with MeCN and H_2O (1:1, v/v) to characterize phosphoramidites in negative ion mode. The FIAU phosphoramidite analogue was characterized by ESI-MS and a representative spectrum is shown in Figure 13. All mass spectrometric measurements were performed on a Thermo Finnigan Surveyor MSQ mass spectrometer (Finnigan MAT, San Jose, CA). We found that it was possible to generate mass spectra in negative ion mode using only aqueous MeCN without the use of organic acids. In general we observed fragments corresponding to the free DMT protecting group (Figure 13A), loss of the DMT group from FIAU-P (Figure 13B), and intact FIAU-P (Figure 13C).

Oligonucleotide Synthesis and Characterization

Oligonucleotide resins and phosphoramidites of the normal DNA bases were obtained from Glen Research (Sterling, VA). Oligonucleotide synthesis was conducted with a Pharmacia gene assembler (GE Healthcare Bio-Sciences, Piscataway, NJ). In general, oligonucleotides containing sugar-modified residues were deprotected with concentrated aqueous ammonia (33% as NH_3) at 60 °C for approximately 12 – 15 h,

purified by HPLC, and characterized by MALDI-TOF-MS, as previously described [82, 83]. However, oligonucleotides containing C5-iodo-substituted residues (i.e. 5IdU and FIAU) were instead deprotected at room temperature for 24 h to prevent the formation of C5-amino side products as previously described [84, 85]. A synthetic approach [82], using Universal Support III PS [86, 87] available from Glen Research was used to insert dU, 5IdU, araU, rU, $U^{2'F(ara)}$, $U^{2'F(ribo)}$ FIAU and dFdU at the 3'-end (primer terminus) of synthetic duplexes. For each of the C2'-fluorine-substituted residues (i.e. FIAU, $U^{2'F(ara)}$, $U^{2'F(ribo)}$ and dFdU) it was necessary to increase the coupling times to 10 min.

Determination of Steady-State Kinetic Parameters for Polymerase Incorporation of Modified NTPs (modNTPs)

The incorporation of modNTPs onto the 3'-end of an 11-mer primer annealed to a 21-mer template (termed 11/21A, Figure 11A) was examined under steady-state standing-start conditions. The steady-state kinetic parameters (Km and kcat) and the catalytic efficiencies (kcat/Km) for pol β, AMVRT or Klenow (exo-) incorporation of each modNTP opposite template dA are summarized in Table 2. To measure the stead-state kinetic parameters for modNTP incorporation, a solution of enzyme (pol β, AMVRT or Klenow (exo-)), 5'-^{32}P-labeled 11/21A, and the appropriate enzyme buffer (see Materials and Methods) was mixed and reacted with increasing concentrations of modNTPs at 37 °C for various times. Gel electrophoresis followed by autoradiographic image analysis revealed that the enzyme gradually incorporated the modNTP substrate; as primer 11-mer was elongated to a 12-mer (Figure 15A – H). Product (elongated primer) formation was plotted as a function of time to determine initial velocities (Figure 14B).

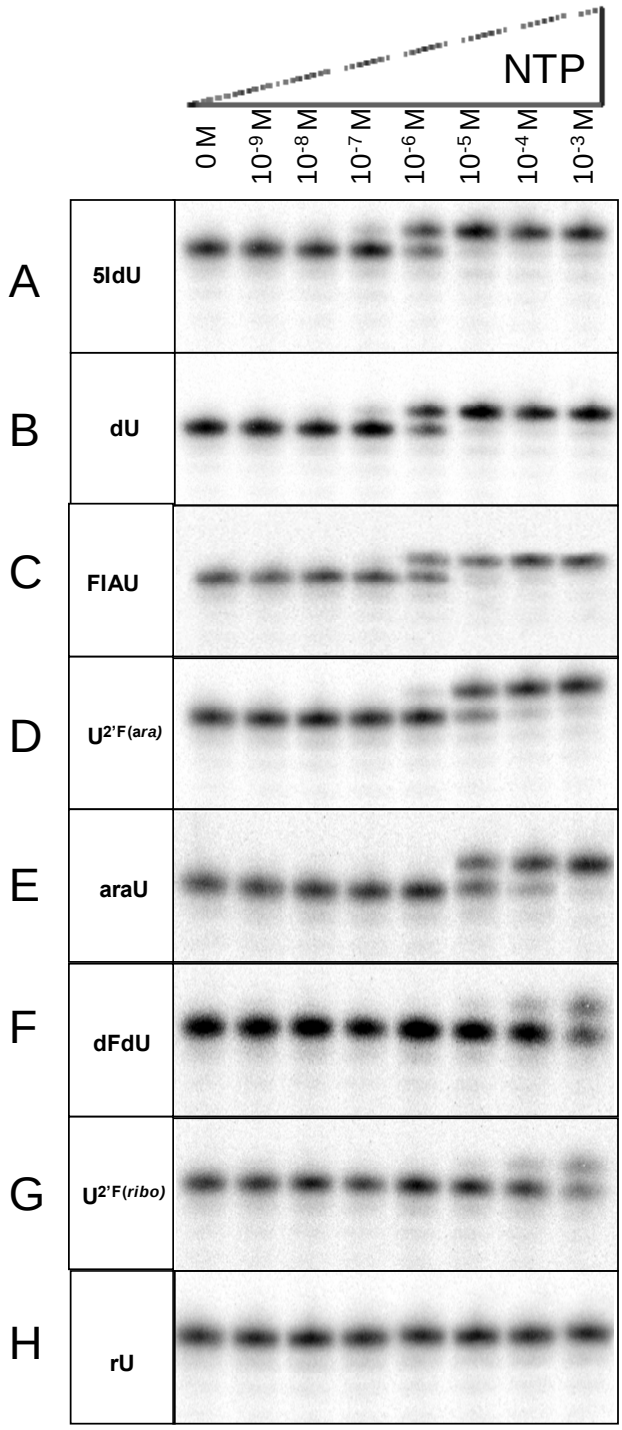

Figure 15: Polymerase β incorporation of modified NTPs opposite template A. Gel showing band intensities as a function of increasing concentrations of A) 5IdUTP, B) dUTP, C) FIAUTP, D) $U^{2'F(ara)}TP$, E) araUTP, F) dFdUTP, G) $U^{2'F(ribo)}TP$ and H) rUTP.

The initial velocities were then plotted as a function of increasing NTP concentration (Figure 14C) and a nonlinear least-squares fit of the data to the Michaelis-Menten rectangular hyperbola (equation 1), as previously described [88], was performed to obtain Km and kcat. The relative insertion efficiencies for pol β, AMVRT, or Klenow(exo-) incorporation of modNTPs were determined by $(kcat/Km)_{dNTP}$ $/(kcat/Km)_{dUTP}$, where $(kcat/Km)_{dUTP}$ is the catalytic efficiency for incorporation of the reference nucleotide dUTP, and are summarized in Table 2.

Ribonucleotide (rNTP) Insertion Kinetics

When compared with the reference nucleotide dUTP, we observed that rUTP, $U^{2'F(ribo)}TP$, and dFdUTP (Gemcitabine metabolite) were poor substrates for each of the polymerases examined (Table 2, Figure 16). When using pol β, the catalytic efficiency for $U^{2'F(ribo)}TP$ and dFdUTP incorporation was reduced by 100 – 300-fold and the catalytic efficiency for rU incorporation was reduced by more than 3000-fold consistent with previous results [18]. When using AMV-RT, the catalytic efficiencies for dFdUTP and $U^{2'F(ribo)}TP$ incorporation were reduced by 400 and 1,100-fold, respectively, and the catalytic efficiency for rUTP incorporation was reduced by more than 30,000-fold (Table 2, Figure 16). When using Klenow (exo-), incorporation efficiencies for dFdUTP and $U^{2'F(ribo)}TP$ were reduced by 7,000- and 26,000-fold, respectively, and the incorporation efficiency for rUTP was reduced by 80,000-fold (Table 2, Figure 16). Thus, pol β, Klenow (exo-) and AMV-RT strongly discriminate against rNTPs. We found that the loss in incorporation efficiency for ribonucleotides (rNTPs) was due to an increase in Km

values and a decrease in catalytic turnover (kcat) rates, although, discrimination against rNTPs appears to be based more on Km.

Arabinonucleotide (araNTP) Insertion Kinetics

Arabinonucleotides (araNTPs) differ structurally from rNTPs by having their C2'-substituents on opposite ends of the sugar plane. Thus, the C2'-substituent of an araNTP might avoid the steric gate mechanisms used by DNA polymerases to exclude rNTPs. In addition, araNTPs represent an important class of anticancer and antiviral compounds. Therefore, we probed the ability of pol β, AMVRT, and Klenow (exo-) to efficiently incorporate these modNTP analogues into DNA. We found that the araNTPs, namely, $U^{2'F(ara)}TP$ (FIAU metabolite), araUTP (Cytarabine metabolite), and FIAUTP (anti-Hepatitis B agent) were good substrates for each of the polymerases examined. When using pol β incorporation efficiencies for araUTP and $U^{2'F(ara)}TP$ were modestly reduced by 1.1 – 2.5-fold. Significantly, the catalytic efficiency for FIAUTP incorporation was 3-fold greater than for dUTP, indicating that pol β will readily incorporate FIAUTP into genomic DNA (Table 2, Figure 16). When using AMV-RT, the insertion efficiency for FIAUTP and was modestly reduced by 3-fold. AMV-RT, however, exhibited greater discrimination against $U^{2'F(ara)}TP$ and araUTP as their catalytic efficiencies were reduced by 32- and 75-fold, respectively. Interestingly, when using Klenow (exo-), araNTP incorporation efficiencies were reduced 70 – 600-fold (Table 2, Figure 16). These data indicate that both araNTPs and rNTPs distort the active site of Klenow (exo-), although, an araNTP appears to be better tolerated.

When considering that araNTP/rNTP pairs we found that conversion of $U^{2'F(ribo)}TP$ to $U^{2'F(ara)}TP$ resulted in a 243-fold increase in incorporation efficiency for pol β, a 34-fold increase in the kcat/Km value with AMV-RT and a 68-fold increase with Klenow (exo-). Moreover conversion of rUTP to araUTP resulted in an increase in catalytic efficiency that was ≥1200-fold for pol β, a 137-fold increase in the kcat/Km value when using Klenow (exo-), and an increase in catalytic efficiency that was ≥250-fold when using AMV-RT.

Discussion

The experimental goal of this study was to examine the role of constrained ribose geometry on polymerase incorporation kinetics. These properties might help to explain how the configuration of the nucleoside sugar affects polymerase mediated processes including nucleotide incorporation and primer extension. The nucleoside analogues analyzed here represent an important class of compounds with demonstrated anticancer and antiviral properties. Our experimental approach was to incubate an enzyme (pol β, AMVRT, Klenow (exo-)) with several base- and sugar-modified NTP analogues, including 2'-fluoro- and 2'-OH-modified triphosphates, constrained to the either the C2'-endo (DNA-like) configuration or C3'-endo (RNA-like) configuration (Figure 10), and examine how efficiently each polymerase inserted them opposite template dA. The data reported here might facilitate an improved understanding of the actions of this class of nucleoside analogues.

Kinetic parameters (Km, kcat, kcat/Km) for Klenow (exo-), AMV-RT and pol β incorporation of standard triphosphate analogues (dTTP, dUTP) opposite template dA were determined and observed values were consistent with expectations. In the present

study uracil was chosen rather than thymine so that the data set examined here could be used to compare a series of C5-substituted pyrimidines. In general, during the polymerase incorporation experiments a DNA polymerase (Klenow (exo-) or AMV-RT) was incubated with radiolabeled primer/template substrate and a modNTP in buffer containing $MgCl_2$ (see Materials and Methods). The kinetic parameters Km, kcat and kcat/Km were determined from non-linear regression analysis of saturation curves and the corresponding data are presented in Table 2. Though our focus is on the incorporation of dUTP and its analogues, we investigated the incorporation of dTTP to validate our incorporation assays.

Using Klenow (exo-) and the appropriate incorporation assay conditions (Materials and Methods), we report a Km value of 1.39±0.14 X 10^{-8} M and a kcat value of 2.15±0.11 X 10^{-3} s^{-1} leading to a kcat/Km value of 1.55±0.18 X 10^{5} M^{-1} s^{-1} for the insertion of dTTP opposite template dA. Our Km value is in agreement with previously reported Km values for Klenow (exo-) incorporation of dTTP opposite template dA [2, 3b]. Using Klenow (exo-), we report an apparent Km value of 2.07±0.07 X 10^{-8} M for the insertion of dUTP opposite template dA; a value that is approximately 1.5-fold higher than the observed Km for dTTP insertion (1.39 X 10^{-8} M). Previously, Loeb L. A. and co-workers demonstrated that Klenow (exo-) incorporation efficiency of dUTP is modestly reduced by 1.75-fold compared to dTTP [3b]. Consistent with the literature, we report a kcat/Km value of 9.47±0.43 X 10^{4} M^{-1} s^{-1} for dUTP incorporation (Table 2); a value that is 1.63-fold less than dTTP (1.55±0.18 X 10^{5} M^{-1} s^{-1}).

Using AMV-RT and the appropriate incorporation assay conditions (Materials and Methods), we report a Km value of 2.10±0.15 X 10^{-7} M and a kcat value of

3.15±0.30 X 10^{-3} s^{-1} leading to a kcat/Km value of 1.50±0.18 X 10^{4} M^{-1} s^{-1} for the insertion of dTTP opposite template dA. Previously Goodman, M.F. and co-workers [4] investigated the ability of AMV-RT to extend various base pairs and mispairs at the primer terminus and observed that AMV-RT incorporated dTTP against a 3'-A●T base pair with a Km value of 1.5 X 10^{-7} M; a value that is merely 1.4-fold lower than the Km value reported here (2.10±0.15 X 10^{-7} M) with similar sequence context.

Using pol β, under the assay conditions described (Materials and Methods), we report a Km value of 1.76±0.08 X 10^{-6} M and a kcat value of 2.27±0.12 X 10^{-3} s^{-1} leading to a kcat/Km value of 1.29±0.81 X 10^{3} M^{-1} s^{-1} for the insertion of dTTP opposite template dA. Our Km value is in agreement with previously reported Km values for pol β insertion of dTTP opposite template dA whether using single-gapped DNA substrates [90] or DNA substrates with a 3'-overhang [91]. We report an apparent Km value of 3.66±0.59 X 10^{-6} M for the incorporation of dUTP opposite template dA; a value that is approximately 2-fold higher than the observed Km value for dTTP insertion (1.76 X 10^{-6} M). We note that researchers have previously investigated the ability of DNA polymerases to incorporate dUTP into a nascent DNA chain. Depending on the polymerase preparation and primer/template sequence, pol β has been shown to incorporate dUTP with Km values that are approximately 2 – 3-fold higher than dTTP [92, 93]. Similar observations have also been made using human pol α [94] and, interestingly, feline immunodeficiency viral (FIV) reverse transcriptase and murine leukemia virus (MuLV) reverse transcriptase [95], implying that dUTP can serve as an alternative substrate to dTTP for polymerases of both human and viral origins. The data reported thus far is consistent with literature precedence and indicates that our incorporation assays are appropriate.

Table 2: Kinetic parameters (k_{cat}, K_m and k_{cat}/K_m) for insertion of sugar-modified NTPs opposite template A using pol β, AMV-RT and Klenow (exo-) at pH 7.5

[a.] Insertion efficiency is defined as $(kcat/Km)_{NTP}$ /$(kcat/Km)_{dUTP}$, where NTP is the incoming sugar-modified triphosphate.
[b.] NDA – **N**o **D**etectable **A**ctivity. The reaction was too inefficient to independently determine Km and kcat values.

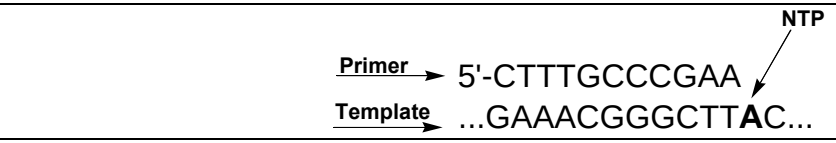

Polymerase	Template	NTP	Km (M)	kcat (s^{-1})	kcat/Km (M^{-1} s^{-1})	Insertion frequency
Pol β	A	dU	$3.66\pm0.59 \times 10^{-6}$	$1.69\pm0.12 \times 10^{-3}$	$4.61\pm0.81 \times 10^{2}$	1.00
		FIAU	$5.01\pm0.48 \times 10^{-6}$	$6.31\pm0.28 \times 10^{-3}$	$1.26\pm0.13 \times 10^{3}$	2.73
		5IdU	$3.06\pm0.29 \times 10^{-6}$	$1.40\pm0.06 \times 10^{-3}$	$4.57\pm0.47 \times 10^{2}$	9.91×10^{-1}
		$U^{2'F(ara)}$	$5.91\pm0.73 \times 10^{-6}$	$2.59\pm0.16 \times 10^{-3}$	$4.38\pm0.61 \times 10^{2}$	9.50×10^{-1}
		araU	$8.15\pm0.86 \times 10^{-6}$	$1.52\pm0.09 \times 10^{-3}$	$1.87\pm0.22 \times 10^{2}$	4.06×10^{-1}
		dFdU	$7.14\pm0.61 \times 10^{-5}$	$2.33\pm0.08 \times 10^{-4}$	$0.32\pm0.03 \times 10^{1}$	6.94×10^{-3}
		$U^{2'F(ribo)}$	$3.12\pm0.43 \times 10^{-4}$	$5.60\pm0.20 \times 10^{-4}$	$0.18\pm0.03 \times 10^{1}$	3.90×10^{-3}
		rU	NDA[b]	NDA	$<0.015 \times 10^{1}$	$\geq 3.25 \times 10^{-4}$
AMV-RT	A	dU	$4.83\pm0.32 \times 10^{-7}$	$2.45\pm0.19 \times 10^{-3}$	$5.07\pm0.52 \times 10^{3}$	1.00
		5IdU	$7.87\pm0.45 \times 10^{-7}$	$2.59\pm0.15 \times 10^{-3}$	$3.29\pm0.27 \times 10^{3}$	6.49×10^{-1}
		FIAU	$5.97\pm0.75 \times 10^{-7}$	$9.86\pm0.45 \times 10^{-4}$	$1.65\pm0.21 \times 10^{3}$	3.25×10^{-1}
		$U^{2'F(ara)}$	$3.85\pm0.03 \times 10^{-6}$	$6.16\pm0.18 \times 10^{-4}$	$1.60\pm0.05 \times 10^{2}$	3.16×10^{-2}
		araU	$7.26\pm0.05 \times 10^{-6}$	$4.91\pm0.28 \times 10^{-4}$	$6.76\pm0.39 \times 10^{1}$	1.33×10^{-2}
		dFdU	$1.37\pm0.09 \times 10^{-5}$	$1.75\pm0.08 \times 10^{-4}$	$1.28\pm0.10 \times 10^{1}$	2.52×10^{-3}
		$U^{2'F(ribo)}$	$3.50\pm0.12 \times 10^{-5}$	$1.60\pm0.30 \times 10^{-4}$	$0.46\pm0.08 \times 10^{1}$	9.07×10^{-4}
		rU	NDA[b]	NDA	$<0.015 \times 10^{1}$	$\geq 2.96 \times 10^{-5}$
Klenow (exo-)	A	dU	$2.07\pm0.07 \times 10^{-8}$	$1.96\pm0.06 \times 10^{-3}$	$9.74\pm0.43 \times 10^{4}$	1.00
		FIAU	$7.57\pm0.56 \times 10^{-7}$	$1.07\pm0.26 \times 10^{-3}$	$1.41\pm0.36 \times 10^{3}$	1.45×10^{-2}
		5IdU	$3.85\pm0.60 \times 10^{-6}$	$1.30\pm0.06 \times 10^{-3}$	$3.38\pm0.70 \times 10^{2}$	3.47×10^{-3}
		$U^{2'F(ara)}$	$4.63\pm0.53 \times 10^{-6}$	$1.20\pm0.18 \times 10^{-3}$	$2.59\pm0.30 \times 10^{2}$	2.66×10^{-3}
		araU	$4.45\pm0.84 \times 10^{-6}$	$7.30\pm0.33 \times 10^{-4}$	$1.64\pm0.32 \times 10^{2}$	1.68×10^{-3}
		dFdU	$1.40\pm0.11 \times 10^{-5}$	$1.59\pm0.26 \times 10^{-4}$	$1.41\pm0.21 \times 10^{1}$	1.45×10^{-4}
		$U^{2'F(ribo)}$	$6.71\pm0.05 \times 10^{-5}$	$2.55\pm0.07 \times 10^{-4}$	$0.38\pm0.01 \times 10^{1}$	3.90×10^{-5}
		rU	$1.13\pm0.04 \times 10^{-4}$	$1.36\pm0.28 \times 10^{-4}$	$0.12\pm0.03 \times 10^{1}$	1.23×10^{-5}

DNA polymerase β, Klenow (exo-), and AMVRT efficiently select against ribonucleoside triphosphates (rNTPs). The furanose ring of a NTP is not planar an can adopt several conformations [96 – 98]. However, substitution of electronegative groups at the C2' position greatly influences conformational equilibria and population. For example, chemical addition of hydroxyl (OH) and fluorine (F) groups at the C2' position in the ribo (down, "below the sugar plane") configuration constrain nucleoside furanose geometry to a C3'-endo (RNA-like) geometry [99]. Indeed, it has been observed that the conformation of the nucleoside furanose moiety can be predicted by the electronegativity of the C2' substituent and that the most electronegative groups will pull the sugar pucker toward its side of the sugar plane [100 – 102]. Likewise, if those same electronegative groups are substituted at the C2' position in the arabino (up, "above the sugar plane") configuration, the nucleoside furanose will predominately adopt a C2'-endo (DNA-like) conformation [103 – 105]. Further, modNTP analogues constrained to a C3'-endo conformation (e.g. rNTPs) are activated as substrates for RNA polymerases [106], whereas, modNTP analogues constrained to the C2'-endo conformation (e.g. dNTPs) are activated as substrates for DNA polymerases [27]. Therefore, we hypothesized that ribo configured modNTP analogues would be poor substrates for each of the DNA polymerases examined (pol β, AMVRT, and Klenow (exo-)) regardless of the C2' substituent.

During DNA synthesis and repair a DNA polymerase must efficiently select against rNTPs which are present in higher cellular concentrations than dNTPs [8]. Depending on the rNTP/dNTP pair, pol β, Klenow (exo-) and reverse transcriptases (RTs) have been shown to select against ribonucleotides by 10^3 – 10^6-fold [11, 13, 17, 18,

107]. Under the experimental conditions used (see Materials and Methods), we observed that the insertion efficiency of rUTP (Figure 10) was reduced by 80,000-fold when using Klenow (exo-), by greater than 3,000-fold when using pol β and by greater than 30,000-fold when using AMVRT (Table 2, Figure 15, Figure 16).

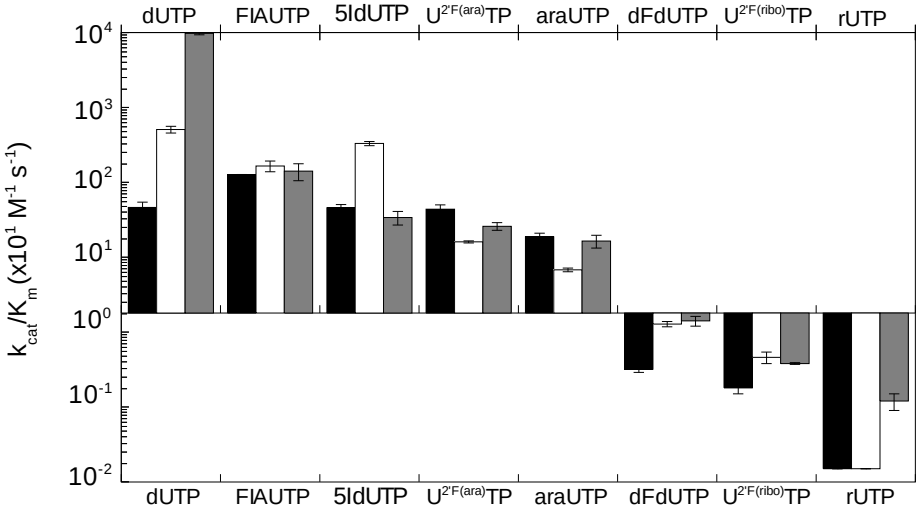

Figure 16: A log plot comparing the incorporation efficiencies for sugar-modified triphosphate analogues using the following polymerases: polymerase β (*black-filled bars*), AMV reverse transcriptase (*open-bars*), and Klenow (exo-) (*gray-filled bars*). The base line represents a catalytic efficiency of 10^1 M^{-1} s^{-1}. The catalytic efficiencies are tabulated in Table 2.

X-ray crystallographic studies and mutation studies imply that this strong selection against rUTP is afforded by a "steric gate" mechanism whereby the side chain or backbone of an active site residue sterically interacts with the 2'-OH of rUTP. The steric gate mechanism varies slightly depending on the polymerase family. For example, pol β selects against a rNTP using a protein-backbone segment spanning Tyrosine residue 271 (Tyr271) to Glycine residue 274 (Gly274) that sterically interacts with the C2'-OH of an incoming rNTP, thus preventing rNTP binding and misinsertion [19, 108], Klenow

(exo-) utilizes glutamic acid residue 710 (Glu 710) to prevent rNTP misincorporation [13], and AMVRT (like other RTs) employs either a Tyr or phenylalanine (Phe) residue to exclude rNTPs from its active site [17]. Our observation that rUTP insertion is reduced by $10^3 – 10^5$-fold relative to dUTP is consistent with this steric model.

DNA polymerase selection against rNTPs could be attributed to the sugar conformation or the steric challenge presented by the C2'-OH. We hypothesized that reducing the size of the C2' substituent would recover incorporation efficiency. This led us to investigate the ability of DNA polymerases to incorporate $U^{F(ribo)}TP$. $U^{2'F(ribo)}TP$ differs from rUTP through replacement of the C2'-OH with a C2'-F (Figure 10). In addition the steric size of fluorine (1.47 Å) as predicted by van der Waals radius is intermediate between the steric sizes of a proton (1.2 Å) and a hydroxyl (2.8 Å) [**7**]. Previously, researchers have investigated the ability of $U^{2'F(ribo)}TP$ to act as a substrate for several polymerases including Deep Vent (exo-) and 9 degrees North (modified) (9° N_m) DNA polymerases [28, 110]; human immunodeficiency virus-1 (HIV-1) and Moloney Murine Leukemia Virus (MMLV) reverse transcriptases [28, 106, 110, 111]. In general, $U^{2'F(ribo)}TP$ was readily incorporated by RNA polymerases yet was a poor substrate for DNA polymerases. Indeed, Richardson, F.C. et al observed that catalytic efficiency for incorporation of $U^{2'F(ribo)}TP$, opposite template dA, was reduced by 19-fold for polymerase alpha (α) and 137-fold for polymerase gamma (γ) relative to dUTP incorporation [94].Consistent with these observations, the steady-state kinetic data revealed that, relative to dUTP, insertion efficiency for $U^{2'F(ribo)}TP$ was reduced 256-fold when using pol β, by 26,000-fold when using Klenow (exo-), and by 1,100-fold when using AMVRT (Table 2, Figure 16).

Guschlbauer and Jankowski [101] have solved the solution-phase structure for the $U^{2'F(ribo)}$ nucleoside analogue using NMR and found $U^{2'F(ribo)}$ to be preferentially in the C3'-endo form (~82 - 88%). During the incorporation step, it is likely that $U^{2'F(ribo)}$TP remains in the C3'-endo conformation when initially bound to the enzyme-primer/template complex. However, during the phosphoryl transfer step DNA pol β is expected to convert $U^{2'F(ribo)}$TP from its initial C3'-endo conformation to the more suitable C2'-endo-like conformation to allow proper alignment of the αP of $U^{2'F(ribo)}$TP with the primer terminus 3'-OH. Therefore, the energetic penalty incurred during this process is likely to reduce the incorporation efficiency of $U^{2'F(ribo)}$TP. Moreover, the C2'-F group is predicted to increase the electron density at the C2' position and consequently, the size of the furanose ring at the site of substitution [112]. The increased size likely results in unfavorable steric interactions with the steric gate residues of pol β, AMVRT, and Klenow (exo-) resulting in reduced incorporation efficiency. Although, conversion of the C2'-OH (rUTP) to a C2'-F ($U^{2'F(ribo)}$TP) resulted in 31-fold recovery in catalytic efficiency for AMVRT but only a modest 11-fold recovery for pol β and a 3-fold recovery for Klenow (exo-) (Table 2, Figure 16). Together, these data indicate that the active sites of Klenow (exo-) and pol β are more sensitive to rNTP sugar conformation relative to the AMVRT active site. An alternative explanation would be that the fluorine atom is still large enough to interact with the Glu710 residue in the Klenow (exo-) active site or the carbonyl backbone of Tyr271 in the pol β active site.

Gemcitabine (dFdC), a 2',2'-difluoro-substituted nucleoside analogue has been shown to adopt a C3'-endo configuration as the free nucleoside hydrochloride salt [113] and when substituted into the DNA duplex region (DDR) of a model Okazaki fragment

[114]. Previously, researchers have investigated the incorporation of 2',2'-difluoro-substituted nucleoside analogues (including dFdCTP and dFdGTP) into DNA and found that they were poor substrates for DNA polymerases. Depending on the sequence context and the kinetics approach (i.e. steady-state or pre-steady state kinetics) it has been observed that the catalytic efficiency for dFdCTP incorporation is reduced by 20-fold for pol ε [116], ~50 – 3000-fold for pol β [117], 80-fold for pol α [118], 150-fold for pol λ [119], and 432-fold for pol γ [120] relative to dCTP incorporation. It has been reasoned that one of the contributing factors to poor misincorporation of dFdUTP is that its sugar is constrained to a C3'-endo geometry that is amenable to RNA polymerase incorporation [117, 120]. Interestingly, the deaminated metabolite, dFdU, investigated in the present study has been shown to prefer the C2'-endo conformation (58%) in solution [115]. One might then predict, on the basis of conformation, that dFdUTP should be a good substrate for DNA polymerases. Yet, despite its apparent preference for the C2'-endo geometry, dFdUTP was strongly selected against by each of the polymerases as if it were a rNTP.

We observed that incorporation efficiency for the dFdUTP analogue was reduced by 144-fold when using pol β, by 400-fold when using AMVRT, and by 7,000-fold when using Klenow (exo-) (Table 2, Figure 16). There are several structural properties of dFdU that likely render it a poor substrate for DNA pol β incorporation: 1) The C2'-difluoro group increases the electron density and size of dFdUTP which may cause steric clash with polymerase active site residues and/or 2) a combination of increased electron density (in the vicinity of the difluoro group), increased physical size and altered sugar geometry, likely weaken the interactions between dFdUTP and the template base dA rendering it more likely to dissociate from the enzyme-primer/template complex resulting in

relatively larger apparent Km values. In addition, the C2' geminal difluoro group alters the electrostatic surface potential of the dFdC nucleoside [114] and this altered electrostatic potential is predicted to affect the rate and stability of complex formation between dFdU and the polymerase. Therefore, when considering C2'-difluoro-substituted nucleotide analogues additional features, including the electrostatic potential of the geminal difluoro group, may be more important determinants of incorporation efficiency.

In all, each of the polymerases (Klenow (exo-), AMVRT, and pol β) efficiently selected against rUTP, $U^{2'F(ribo)}TP$, and dFdUTP. We observed that kinetic discrimination was based more on Km than kcat and that when compared to the reference dUTP incorporation efficiencies were reduced by $10^2 – 10^5$-fold. Previously, Branscomb, Galas, and co-workers reasoned that relative NTP insertion frequencies were directly proportional to NTP residence times within the polymerase active site and that the NTP residence times were a reflection of the stability of the ternary ground-state enzyme-DNA-NTP complex [121, 122]. Therefore, these data imply that, rUTP, $U^{2'F(ribo)}TP$, and dFdUTP analogues form comparatively unfavorable enzyme-DNA-NTP complexes and, consequently, exhibit a greater tendency to dissociate from the enzyme-primer-template complex as reflected in the increased Km values.

DNA polymerase β, Klenow (exo-), and AMVRT readily inserted arabinonucleoside triphosphates (ararNTPs). The Arabinonucleotides (araNTPs) represent an important class of anticancer and antiviral agents [48a] and their sugar moieties preferentially adopt a C2'-endo conformation [103 – 105]. AraNTPs and rNTPs differ structurally by having their respective C2’ substituents on opposite ends of the

sugar plane (Figure 10). DNA polymerases are known to incorporate araNTPs with Km values similar to their unmodified dNTP cognates [25 – 27, 29, 48a, 123, 124]. Fialuridine (FIAU) is an antiviral agent that was developed for the treatment of chronic Hepatitis-B infection. During clinical trials, 5 of the 15 enrolled patients succumbed to unexpected liver failure resulting from progressive lactic acidosis and acute mitochondrial toxicity [35]. For a nucleoside analogue to be effective it must be transported across the cell membrane, phosphorylated and incorporated into DNA. It has been demonstrated that FIAU is phosphorylated to FIAUTP by herpes simplex virus thymidine kinase (HSV-TK) and human thymidine kinase 2 (TK2) [27]. FIAU is an antimetabolite and two products of its metabolic activation, 1-(2-deoxy-2-fluoro-β-D-arabinofuranosyl)-5-methyluracil (FMAU), 1-(2-deoxy-2-fluoro-β-D-arabinofuranosyl)uracil ($U^{2'F(ara)}$), are considered to contribute to its cytotoxicity [48a].

In addition, NMR studies of 5-methyl-(2'-deoxy-2'-fluoro-β-D-arabinofuranosyl) uracil (FMAU) reveal that FMAU prefers the 2'-endo conformation (64%) [48b]. FIAU and FMAU are structurally similar and differ only by their C5 (base) substituent. It is assumed, therefore, that the sugar portion of FIAU will prefer the 2'-endo conformation as well. Significantly, we found that the incorporation efficiency for FIAUTP (1.26×10^3 $M^{-1} s^{-1}$) was similar to dTTP (1.29×10^3 $M^{-1} s^{-1}$) implying that FIAUTP can serve as an alternative substrate to dTTP and that in addition to being readily incorporated into mitochondrial DNA by pol γ [125, 126], FIAUTP is predicted to be readily incorporated into genomic DNA, by pol β, through the BER pathway. Moreover, AMVRT incorporation efficiency of FIAUTP was modestly reduced by 3-fold and Klenow (exo-) incorporation efficiency was reduced by 75-fold (Table 2). In an effort to resolve the

structural features that likely render FIAUTP a high affinity substrate for all polymerases examined, we investigated the incorporation of $U^{2'F(ara)}TP$, which differs structurally from FIAUTP only in that it lacks the C5-iodo substituent, and 5IdUTP, which differs structurally from FIAUTP in that it lacks the C2'-F substituent (Figure 10). Each of these analogues allows isolation of the contribution of the C2'-F ($U^{2'F(ara)}TP$) or the C5-Iodo group (5IUdUTP) to FIAUTP's kinetic profile.

The solution-phase structure for the $U^{2'F(ara)}$ nucleoside analogue has been solved using NMR and has revealed that $U^{2'F(ara)}$ is preferentially in the C2'-endo conformation [115, 127]. We found that, relative to dUTP, pol β incorporated $U^{2'F(ara)}TP$ with near identical catalytic efficiency. Moreover, when compared with FIAUTP, pol β incorporated $U^{2'F(ara)}TP$ with a similar Km value but a kcat value that was approximately 2.4-fold lower, resulting in a kcat/Km value that was approximately 3-fold lower (Table 2). Previously, Goodman and co-workers [128] reasoned that the Km value reflects base pairing free energy differences which, in turn, are influenced by two interactions: 1) *hydrogen bonding interactions* between the base of the incoming dNTP and the templated base and 2) *base stacking interactions* between the base of the incoming dNTP and the primer terminus base. Therefore, it would appear that the presence of the C5-iodo group does not influence the ability of FIAUTP to either hydrogen bond with template dA or stack properly on the primer terminated by 3'-dAMP during the incorporation step (Figure 11A) since $U^{2'F(ara)}TP$ (FIAUTP minus the C5-iodo) was incorporated with an identical Km to FIAUTP (Table 2). The same is observed with 5IdUTP as well in that pol β incorporated 5IdUTP with Km and kcat/Km values that were nearly identical to dUTP (Table 2). However, we note that, when compared with FIAUTP, pol β incorporated

5IdUTP with a Km value that was reduced by 1.6-fold and a kcat value that was reduced by 4.5-fold. Thus, whereas the C5-iodo does not appear to significantly alter base stacking interactions, the C2'-F group appears to contribute to the rate at which FIAUTP is bound by pol β and subsequently incorporated into the DNA strand as conversion of 5IdU to FIAU (addition of arabino C2'-F) resulted in 4-fold increase in the catalytic turnover rate (kcat) (Table 2). We also note that pol β and AMVRT (a viral reverse transcriptase) incorporated FIAUTP with near identical incorporation efficiencies (Figure 16), further strengthening the argument that pol β, via the BER pathway, provides a major route for FIAUTP incorporation misincorporation.

Cytarabine (araC) is rapidly deaminated to araU and has been shown to accumulate in the cerebrospinal fluid of patients following intermittent infusion of high-dose araC [55] leading to the suggested role for araU accumulation in araC-associated neurotoxicity [50]. We were therefore interested in the ability of DNA polymerases to utilize araUTP as a substrate. The sugar moiety of araU (cytarabine metabolite) has been shown to adopt a C2'-endo conformation as the free nucleoside [104, 129] and araUTP is presumed to adopt the same conformation in solution and when bound to the enzyme-primer-template complex . Relative to dUTP, we observed that pol β incorporation efficiency was modestly reduced by 2.4-fold (Table 2). While the backbone carbonyl of Tyr271 of α-helix M within the pol β active site is predicted to sterically clash with the C2'-OH of an incoming rNTP, Aspartate residue 276 (Asp276) of α-helix N is predicted to block the C2'-OH of an incoming araNTP [11]. The modest reduction in incorporation efficiency, however, suggests that Asp276 can adjust to permit incorporation of a C2'-OH of an araNTP. Interestingly, we observed that pol β incorporated $U^{2'F(ara)}TP$ with a Km

that was 1.4-fold lower and a kcat/Km value that was 2.3-fold higher than araUTP. Moreover, dUTP was incorporated with Km that was 2.2-fold lower and a kcat/Km value that was 2.5-fold higher than araUTP (Table 2). These data imply that incorporation efficiency was recovered as the araNTP C2' substituent size was decreased. As such, it would appear that pol β possesses two steric gate-like mechanisms: 1) a "rigid", intolerable gate protruding from α-helix M to block bulky rNTP C2' substituents and 2) a "soft", relatively tolerable gate protruding from α-helix N to block bulky araNTP C2' substituents. Interestingly, a similar trend is observed for Klenow (exo-) and AMVRT (Figure 16). Thus, it would appear that steric gate mechanisms interact with the C2' substituent whether it exists above or below the sugar plane.

Thermodynamic differences for 3'-end modified duplexes appear to contribute to polymerase insertion kinetics. A combination of stacking interactions between adjacent bases and hydrogen bonding interactions between complementary strands is primarily responsible for duplex stability. Past comparisons of polymerase kinetics and DNA stability [4] have revealed that polymerases likely exploit differences in free energy (ΔG°), enthalpy (ΔH°), entropy (ΔS°), and melting temperature (T_m) between correct and incorrect base pairs at the insertion step; and, the altered base pairing and stacking energy associated with mispair formation reduces duplex thermodynamic and thermal stability resulting in larger observed Km values for incorporation of the incorrect nucleotide. Thus, the stability of the DNA-primer/template-dNTP complex is reflected in the Km and catalytic efficiency (kcat/Km). In order to estimate the impact of sugar conformation on duplex stability and incorporation kinetics the misinsertion frequency, *fins*, was determined by Equation 3

$$fins = (kcat / Km)_{dNTP} / (kcat / Km)_{dUTP} \quad \text{Eq. 3}$$

The magnitude of *fins* was observed to increase continuously with increasing Tm of 3'-end modified duplexes (Figure 17), suggesting that the increased duplex thermal stability was contributing to nucleotide incorporation. The araNTPs were the most frequently incorporated but also formed the most stable duplexes when incorporated onto the 3'-end. Conversely, the rNTPs were not readily incorporated and misincorporation onto the 3'-end resulted in reduced duplex Tms.

The impact of 3' aranucleoside. Previously, we discussed the rigid geometrical constraints and steric blocking mechanisms of the polymerase active site that likely deter rNTP incorporation and that these unfavorable interactions are largely avoided by araNTPs. Here, we show that in addition to steric constraints there possibly exists a thermodynamic component of Km discrimination on the basis of sugar conformation. The data presented in Table 3 and Figure 17 imply that pol β will most frequently incorporate NTPs in a manner that maintains or increases the stability of the primer-template complex and the resulting duplex. Significantly, FIAUTP was the most readily incorporated of the NTPs investigated and a FIAU-terminated primer formed the most stable duplex. We note that 5IdU (FIAU minus C2'-F) and $U^{2'F(ara)}$ (FIAU minus C5-I) terminated primers increased duplex Tms by 0.8 °C and 0.9 °C, respectively (Table 3). Interestingly, the impact of 3'-FIAU on duplex Tm (ΔTm = 1.9 °C) is approximately the result of adding the thermal stabilizing contribution of 5IdU and $U^{2'F(ara)}$. Thus, it would appear that the C5-I of FIAU contributes as much to its thermodynamic profile as its C2'-F.

Table 3: Experimental thermodynamic parameters of duplex formation. The values include measured free energy of duplex formation ($\Delta G°_{37}$), enthalpy ($\Delta H°$), entropy ($\Delta S°$) and melting temperature with a strand concentration of 28 μM ($T_{m\ 28\ \mu M}$). The thermodynamic parameters for the A:dU oligonucleotide was used as the reference when calculating $\Delta\Delta G°_{37}$, $\Delta\Delta H°$, and $\Delta\Delta S°$ in the 3'-terminal position. Measured free energy, enthalpy and entropy differences that exceed experimental error are indicated in bold.

	$\Delta G°_{37}$ (kcal/mol)	$\Delta\Delta G°_{37}$ (kcal/mol)	$T_{m\ 28\mu M}$ (°C)	$\Delta T_{m\ 28\mu M}$ (°C)	$\Delta H°$ (kcal/mol)	$\Delta\Delta H°$ (kcal/mol)	$\Delta S°$ (cal mol^{-1} K^{-1})	$\Delta\Delta S°$ (cal mol^{-1} K^{-1})
				3'-Terminal				
A:dU	-9.5±0.2	-	49.4±0.3	-	-89.0±4.6	-	-251.2±14.2	-
A:U$^{2'F(ara)}$	-9.5±0.2	0.0±0.3	50.3±0.1	0.9±0.3	-84.8±3.2	4.2±5.6	-238.4±9.7	12.8±17.2
A:U$^{2'F(ribo)}$	-9.0±0.2	**0.5±0.3**	49.2±0.2	-0.2±0.4	-79.9±3.9	**9.1±6.0**	-224.3±12.2	**26.9±18.7**
A:dFdU	-9.5±0.2	0.0±0.3	51.0±0.4	1.6±0.5	-85.5±3.3	3.5±5.7	-240.4±10.1	10.8±17.4
A:araU	-9.4±0.1	0.1±0.2	49.8±0.4	0.4±0.5	-85.9±2.6	3.1±5.3	-242.1±7.8	9.1±16.2
A:rU	-9.2±0.1	**0.3±0.1**	49.2±0.2	-0.2±0.4	-83.7±2.2	**5.3±5.1**	-235.7±6.5	15.5±15.6
A:5IdU	-9.4±0.2	0.1±0.3	50.2±0.2	0.8±0.4	-80.3±3.9	**8.7±6.1**	-224.5±12.2	**26.7±18.7**
A:FIAU	-9.7±0.1	-0.2±0.2	51.3±0.2	1.9±0.4	-85.3±3.6	3.7±5.8	-238.9±11.2	12.3±18.1

Surprisingly, dFdU (dFdC metabolite) terminated primers increase the duplex thermal stability (ΔTm = 1.6 °C) nearly as much as FIAU terminated primers (ΔTm = 1.9 °C). The source of dFdU-induced stability is not understood, however, these observations likely have broader applications. For example, 5'→3' NTP insertion, extension of primer termini, and 3'→5' exonucleolytic activity are three distinct steps that contribute to the overall fidelity of DNA replication [2]. Butlag and Kornberg first demonstrated that the exonucleolytic activity of DNA pol I removed terminal mispairs more efficiently than correct terminal base pairs [130]. A "melting capacity" model was defined as the likely mechanism for exonucleolytic activity. In the melting model an exonuclease is intrinsically a single-stranded nuclease that preferentially recognizes a duplex with a terminal mispair because it is more likely to be in the single-stranded state due to its lower Tm. In the same report it was demonstrated that the exonuclease of DNA pol I exhibited specificity for single-stranded DNA and that its activity on double-stranded DNA increased proportionally with increasing temperature. Here, we report that terminally located FIAU and, surprisingly, terminally located dFdU form the most stable of the 3'-modified duplexes investigated in this report (Table 3, Figure 17). It is likely that the increased thermal stability resulting from the incorporation of FIAU and dFdU onto the 3'-end of a growing strand precludes exonuclease editing and may explain, in part, why DNA polymerases with highly efficient exonuclease activities such as pol γ and pol ε exhibit difficulty removing FIAU and dFdC from primer termini [57, 114, 120].

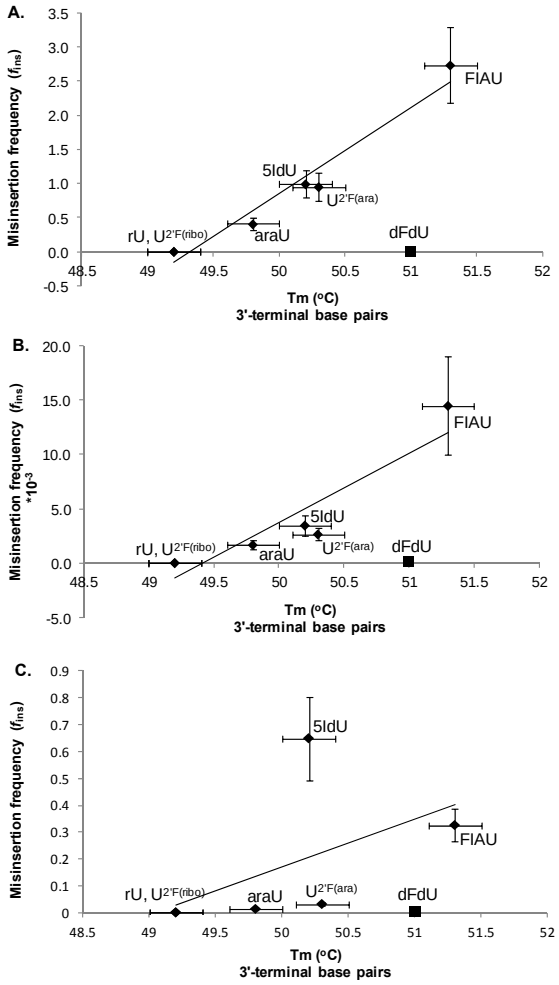

Figure 17: Relationship between polymerase insertion of modified NTPs onto the 3'-end of a DNA strand and melting temperatures of 3'-end modified duplexes (Table 3). A *line* is drawn through all of the points except dFdU. A) When using human DNA pol β, the slope of the line is 1.26, the intercept of the line is -62.09 and the R^2 value is 0.95. B) When using Klenow (exo-), the slope of the line is 6.35, the intercept of the line is -313.69 and the R^2 value is 0.85. C) When using AMVRT, the slope of the line is 0.178, the intercept of the line is -8.73 and the R^2 value is 0.28.

Impact of 3' ribonucleoside. Goodman and co-workers reasoned [4b] that a polymerase could achieve observed Km discrimination against base mispairs by amplifying free energy differences (ΔΔG°) between correct and incorrect base pair formation. Free energy differences are derived from the relative magnitude of enthalpy

and entropy contributions ($\Delta\Delta G° = \Delta\Delta H° - T\Delta\Delta S°$). When enthalpy and entropy changes for duplex formation are proportional, as observed in aqueous media, values of $\Delta\Delta H°$ are nearly offset by values of $\Delta\Delta S°$ to give small values of $\Delta\Delta G°$. If, however, rigid geometrical constraints at the polymerase active site only allowed those NTPs whose sugar conformations approximated the correct conformations, then $\Delta\Delta S°$ would reduce to 0 and the polymerase could achieve Km discrimination that would approach $\Delta\Delta G° = \Delta\Delta H°$. Although $\Delta\Delta G°$ values in solution are expected to be negligible due to entropy-enthalpy compensation, we note that the ribonucleotides exhibit relatively large positive free energy changes ($\Delta\Delta G° = 0.3 – 0.5$ kcal/mol) that exceed error (Table 3). In a previous study [82] we evaluated the impact of sugar geometry on base pair and mispair stability. We observed that, surprisingly, the measured difference in free energy change between the correct terminal A:dU base pair and the terminal A:$U^{2'F(ribo)}$ base pair ($\Delta\Delta G° = 0.5$ kcal/mol) was as large as the corresponding difference in free energy change between the reference A:dU terminal base pair and a G:dU terminal base mispair ($\Delta\Delta G° = 0.5$ kcal/mol). We've extended this finding by investigating the impact of a terminal A:rU base pair on DNA duplex stability. We found that a A:rU base pair on the 3'-end destabilizes DNA duplexes ($\Delta\Delta G° = 0.3$ kcal/mol) nearly as much as the A:$U^{2'F(ribo)}$ (Table 3) and G:dU [82] terminal base pairs. Although $\Delta\Delta G°$ values in solution are expected to be negligible due to entropy-enthalpy compensation we note that previously, Goodman and co-workers [4b] observed that the difference in free energy change between a correct terminal base pair (A:T) and terminal mispairs (G:T, C:T, and T:T) was $\Delta\Delta G° = 0.25 – 0.41$ kcal/mol. It is interesting that the ribonucleosides, examined in this report, exhibit a range of relatively large positive free energy changes ($\Delta\Delta G° = 0.3 – 0.5$

kcal/mol) (Table 3) that are consistent with the observations made by Goodman and co-workers for terminal mispairs. These results are consistent with a thermodynamic contribution to sugar fidelity for polymerase incorporation.

It is known, however, that misincorporation of a single ribonucleotide into DNA influences DNA structure and conformation. For example, Sundaralingam and co-workers have solved the crystal structures for self-complementary DNA decamers containing a ribonucleoside at both 5' and 3' termini [131], at an internucleotide position [132, and at the 3'-end [133]. Surprisingly, each of the ribonucleoside-containing decamers investigated crystallized as A-form DNA with all residues adopting a C3'-endo-like conformation despite the all DNA decamers crystallizing in the B-form. These observations likely have implications for the ribonucleoside-containing duplexes studied here. Bresslauer K et al demonstrated that conformationally ordered single strands exhibit intramolecular interactions that enthalpically prepare them for duplex formation [134]. Therefore, one would predict that pairing between strands that are conformationally preorganized for DNA duplex formation is entropically more favorable than pairing between strands whose conformations differ from the duplex [135]. During thermal denaturation studies a duplex is "melted" into single strands that are then allowed to pair again. A strand containing a ribonucleoside (in our case the primer, Figure 11B) would have a different conformation than the all DNA strand (the template) and the pairing between the two would be entropically unfavorable resulting in relatively less stable duplexes (Figure 17, Table 3).

Concluding Remarks

We found that Klenow (exo-), AMVRT, and pol β inefficiently incorporated a rNTP yet readily inserted an araNTP opposite template dA. Though rigid geometrical constraints of the polymerase active site (i.e. steric gate mechanism) may be the primary contributor to rNTP exclusion, we present a basic thermodynamic model for sugar discrimination. Consistent with expectations based on kinetic data, arabinonucleoside analogues formed the most stable duplexes when incorporated onto the primer terminus (3'-end). Consequently, misincorporation efficiency increased proportionally with increasing melting temperature of 3'-end duplexes indicating that DNA polymerases will incorporate modNTPs in a manner that maintains or increases duplex thermal stability. Thus, results from our polymerase incorporation and thermal denaturation studies implies that sugar substitution impacts polymerase incorporation. Whereas araNTPs are stabilizing on the 3'-end and readily incorporated, rNTPs are not. In addition, we also reported that FIAU- and, surprisingly, dFdU-terminated primers increase duplex stability by ~2 °C. The increased duplex thermal stability resulting from misincorporation of FIAU and dFdU (or the parent compound dFdC) onto the 3'-end likely allows these analogues to elude exonuclease editing mechanisms.

References

(1) Kunkel, T. A. (2004) DNA replication fidelity. *J. Biol. Chem.* 279, 16895-16898.

(2) Goodman, M. F., Creighton, S., Bloom, L. B., and Petruska J. (1993) Biochemical basis of DNA replication fidelity. *Crit. Rev. Biochem. Mol. Biol.* 28, 1559-1562.

(3) **a.** Joyce, C. M., Sun, X. C., and Grindley, N. D. F. (1992) Reactions at the polymerase active site that contribute to the fidelity of Escherichia coli DNA polymerase I (Klenow Fragment). *J. Biol. Chem.* 267, 24485–24500. **b.** Patel, P. H. and Loeb, L. A. (2000) Multiple amino acid substitutions allow DNA polymerases to synthesize RNA. *J. Biol. Chem.* 275, 40266-40272

(4) **a)** Loeb, L.A., Kunkel T.A. (1982) Fidelity of DNA synthesis. *Annu. Rev. Biochem.* 51, 429-457; **b)** Petruska, J., Goodman, M.F., Boosalis, M.S., Sowers, L.C., Cheong, C., Tinoco, I Jr. (1988) Comparison between DNA melting thermodynamics and DNA polymerase fidelity. Proc. Natl. Acad. Sci. USA 85, 6252-6256.

(5) Topal M.D., Fresco, J.R. (1976) Complementary base pairing and the origin of substitution mutations. *Nature* 263, 285-289.

(6) Beard, W.A., Wilson S.H. (2003) Structural insights into the origins of DNA polymerase fidelity. *Structure* 11, 489-496.

(7) Joyce, C.M., Benkovic, S.J. (2004) DNA polymerase fidelity: kinetics, structure, and checkpoints. *Biochemistry* 43, 14317-14324.

(8) Traut, T.W. (1994) Physiological concentrations of purines and pyrimidines. *Mol. Cell. Biochem.* 140, 1-22.

(9) Ferraro, P., Franzolin, E., Pontarin, G., Reichard, P., Bianchi, V. (2010) Quantitation of cellular deoxynucleoside triphosphates. *Nucleic Acids Res.* 38, e85, 1-7.

(10) Nick McElhinney, S.A., Watts, B.E., Kumar, D., Watt, D.L., Lundstrom, E.-B., Burgers, P.M.J., Johansson, E., Chabes, A., Kunkel, T.A., (2010) Abundant incorporation into DNA by yeast replicative polymerases. *Proc. Natl. Acad. Sci. USA.* 107, 4949-4954.

(11) Cavanaugh, N.A., Beard, W.A., Wilson, S.H. (2010) DNA polymerase β ribonucleotide discrimination: insertion, misinsertion, extension, and coding. *J. Biol. Chem.* 285, 24457-24465.

(12) Brown, J.A., Suo, Z. (2011) Unlocking the sugar "steric gate" of DNA polymerases. *Biochemistry* 50, 1135-1142.

(13) Astatke, M., Grindley, N.D., and Joyce, C.M. (1998) A single side chain prevents *Escherichia coli* DNA polymerase I (Klenow fragment) from incorporating ribonucleotides. *J. Mol. Biol.* 278, 147–165.

(14) Yang, G., Franklin, M., Li, J., Lin, T.C., Konigsberg, W. (2002) A conserved Tyr residue is required for sugar selectivity in a Pol α DNA Polymerase. *Biochemistry* 41, 10256–10261.

(15) Bonnin, A., Lazaro, J.M., Blanco, L., Salas, M. (1999) A single tyrosine prevents insertion of ribonucleotides in the Eukaryotic-type Φ29 DNA polymerase. *J. Mol. Biol.* 290, 241–251.

(16) Boyer, P.L., Sarafianos, S.G., Arnold, E., Hughes, S.H. (2000) Analysis of mutations at positions 115 and 116 in the dNTP binding site of HIV-1 reverse transcriptase. *Proc. Natl. Acad. Sci. U.S.A.* 97, 3056–3061.

(17) Cases-Gonzalez, C.E., Gutierrez-Rivas, M., and Menendez-Arias, L. (2000) Coupling ribose selection to fidelity of DNA synthesis. The role of Tyr-115 of human immunodeficiency virus type 1 reverse transcriptase. *J. Biol. Chem.* 275, 19759–19767.

(18) Brown, J.A., Fiala, K.A., Fowler, J.D., Sherrer, S.M., Newmister, S.A., Duym, W.W., Suo, Z. (2010) A novel mechanism of sugar selection utilized by a human X-family DNA polymerase. *J. Mol. Biol.* 395, 282–290.

(19) Pelletier, H., Sawaya, M.R., Kumar, A., Wilson, S.H., Kraut, J. (1994) Structures of ternary complexes of rat DNA polymerase beta, a DNA template-primer, and ddCTP. *Science* 264, 1891–1903.

(20) Nick McElhinny S.A., Kumar, D., Clark, B.A., Watt, D.L., Watts, B.E., Lundstrom, E.-B., Johansson, E., Chabes, A., Kunkel, T.A. (2010) Genome instability due to ribonucleotide incorporation into DNA. *Nat. Chem. Biol.* 6, 774-781.

(21) Sekiguchi, J., and Shuman, S. (1997) Site-specific ribonuclease activity of eukaryotic DNA topoisomerase I. *Mol. Cell.* 1, 89–97.

(22) Rydberg, B., and Game, J. (2002) Excision of misincorporated ribonucleotides in DNA by RNase H (type 2) and FEN-1 in cell-free extracts. *Proc. Natl. Acad. Sci. U.S.A.* 99, 16654–16659.

(23) Pankiewicz K.W. (2000) Fluorinated nucleosides. *Carbohyd. Res.* 327, 87-105.

(24) Mikita, T., and Beardsley, G.P. (1988) Functional consequences of the arabinosylcytosine structural lesion in DNA. *Biochemistry* 27, 4698–4705.

(25) Kuchta, R. D., Ilsley, D., Kravig, K. D., Schubert, S., and Harris, B. (1992) Inhibition of DNA primase and polymerase α by arabinofuranosylnucleoside triphosphates and related compounds. *Biochemistry* 31, 4720–4728.

(26) Perrino, F.W., and Mekosh, H.L. (1992) Incorporation of cytosine arabinoside monophosphate into DNA at internucleotide linkages by human DNA polymerase α. J. Biol. Chem. 267, 23043-23051.

(27) Lewis, W., Meyer, R.R., Simpson, J.F., Colacino, J.M., and Perrino, F.W. (1994) Mammalian DNA polymerases α, β, γ, δ, and ε incorporate fialuridine (FIAU) monophosphate into DNA and are inhibited competitively by FIAU triphosphate. Biochemistry 33, 14620–14624.

(28) Ono, T., Scalf, M., and Smith, L.M. (1997) 2'-Fluoro modified nucleic acids: Polymerase-directed synthesis, properties and stability to analysis by matrix-assisted laser desorption/ionization mass spectrometry. Nucleic Acids Res. 25, 4581–4588.

(29) Kuchta, R.D. and Willhelm, L. (1991) Inhibition of DNA primase by 9-beta-D-arabinofuranosyladenosine triphosphate. Biochemistry 30, 797-803.

(30) Prusoff, W.H., Bakhle, Y.S., McCrea, J.F. (1963) Incorporation of 5-iodo-2'-deoxyuridine in the deoxyribonucleic acid of vaccinia virus. *Nature* 199, 1310-1311.

(31) Prusoff, W.H., Mancini, W.R., Lin, T.S., Lee, J.J., Siegel, S.A., Otto, M.J. (1984) Physical and biological consequences of incorporation of antiviral agents into virus DNA. *Antiviral Res.* 4, 303-315.

(32) Neyts, J., Verbeken, E., Clercq, E.D. (2002) Effect of 5-iodo-2'-deoxyuridine on vaccinia virus (orthopoxvirus) infections in mice. *Antimicrob. Agents Chemother.* 46, 2842-2847.

(33) Fischer, P.H., Chen, M.S., Prusoff, W.H. (1980) The incorporation of 5-iodo-5'-amino-2',5-dideoxyuridine and 5-iodo-2'-deoxyuridine into herpes simplex virus DNA. Relationship between antiviral activity and effects on DNA structure. *Biochim Biophys Acta*, 606, 236-245.

(34) Davidson, S.I., Evans, P.J. (1964) IDU and the treatment of herpes simplex keratitis. *Br. J. Ophthalmol.* 48, 678-683.

(35) McKenzie R., Fried M.W., Sallie R., et al. (1985) Hepatic failure and lactic acidosis due to Fialuridine (FIAU), an investigational nucleoside analogue for chronic hepatitis B. *N Engl. J. Med.* 333, 1099–1105.

(36) Heinemann V. (2002) Gemcitabine plus cisplatin for the treatment of metastatic breast cancer. Clin. Breast Cancer 3, Suppl. 1, S24-s29.

(37) von der Maase, H., Hansen, S.W., Roberts, J.W., Dogliotti, L., Oliver, T., Moore, M.J., Bodrogi, I., Albers, P., Knuth A., Lippert, C.M., Kerbrat, P., Sanchez Rovira, P., Wershall, P., Cleall, S.P., Roychowdhury, D.F., Tomlin, I., Visseren-Grul, C.M., and Conte, P.F. (2000) Gemcitabine and cisplatin versus methotrexate, vinblastine, doxorubicin, and cisplatin in advanced or metastatic bladder cancer: Results of a large, randomized, multinational, multicenter, phase III study. J. Clin. Oncol. 17, 3068-3077.

(38) Colucci, G., Giuliani, F., Gebbia, V., Biglietto, M., Rabitti, P., Uomo, G., Cigolari, S., Testa, A., Maiello, E., and Lopez, M. (2002) Gemcitabine alone or with cisplatin for the treatment of patients with locally advanced and/or metastatic pancreatic carcinoma: A prospective, randomized phase III study of the Gruppo Oncologico dell'Italia Meridonale. Cancer 94, 902-910.

(39) Frei, E 3rd, Bickers, J.N., Hewlett, J.S., Lane, M., Leary, W.V., Talley, R.W. (1969) Dose schedule and antitumor studies of arabinosyl cytosine (NSC 63878). *Cancer Res.* 29, 1325-1332.

(40) Leopold, I.H. (1965) Clinical experience with nucleosides in herpes simplex eye infections in man and animals. *Ann. N.Y. Acad. Sci.* 130, 181-191; Renis, H.E. (1973) Antiviral activity of cytarabine in herpesvirus-infected rats. Antimicrob. Agents Chemother. 4, 439-444.

(41) Rapp, F. (1964) Inhibition by metabolic analogues of plaque formation by herpes zoster and herpes simplex viruses. *J.Iimmunol.* 93, 643-648.

(42) Lai, Y., Tse, C.M., Unadkat, J.D. (2004) Mitochondrial expression of the human equilibrative nucleoside transporter 1 (hENT1) results in enhanced mitochondrial toxicity of antiviral drugs. *J. Biol. Chem. 279*, 4490-4497.

(43) Pastor-Anglada, M., Molina-Arcas, M., Casado, F.J., Bellosillo, B., Colomer, D., and Gil, J. (2004) Nucleoside transporters in chronic lymphocytic leukaemia. Leukemia 18, 385-393.

(44) Zhang, J., Visser, F., King, K.M., Baldwin S.A., Young, J.D., Cass, C.E. (2007) The role of nucleoside transporters in cancer chemotherapy with nucleoside drugs. Cancer Metastasis Rev. 26, 85-110.

(45) Heinemann, V., Xu, Y.-Z., Chubb, S., Sen, A., Hertel, L.W., Grindey, G.B., and Plunkett, W. (1990) Inhibition of ribonucleotide reduction in CCRF-CEM cells by 2',2'-difluorocytidine. Mol. Pharmacol. 38, 567-572.

(46) Heinemann, V., Schulz, L., Issels, R.D., and Plunkett, W. (1995) Gemcitabine: a modulator of intracellular nucleotide and deoxynucleotide metabolism. Semin Oncol. 4, Suppl. 11, 11-18.

(47) Bergman, A.m., Pinedo, H.M., and Peters, G.J. (2002) Determinants of resistance to 2',2'-difluorodeoxycytidine (gemcitabine). Drug Resist. Update 5, 19-33.

(48) **(a)** Lewis, W., Levine, E.S., Griniuviene, B., Tankersley, K.O., Colacino, J.M., Sommadossi, J.P., Watanabe, K.A., Perrino, F.W. Fialuridine and its metabolites inhibit DNA polymerase gamma at sites of multiple adjacent analog incorporation, decrease mtDNA abundance, and cause mitochondrial structural defects in cultured hepatoblasts. *Proc. Natl. Acad. Sci. USA* 93, 3592-3597. **(b)** Hicks, N., Howarth, O.W., Hutchinson, D.W. N.m.r. studies of the flexibility of the glycosyl ring in thymidine and uridine nucleosides. Carbohyd. Res. 216, 1-9.

(49) Abbruzzese, J.L., Grunewald, R., Weeks, E.A., Gravel, D., Adams, T., Nowak, B., Mineishi, S., Tarassoff, P., Satterlee, W., Raber, M.N., and Plunkett, W. (1991) A phase I clinical, plasma, and cellular pharmacology study of gemcitabine. J. Clin. Oncol. 9, 491-498.

(50) Lindner, L.H., Ostermann, H., Hiddemann, W., Kiani, A., Wurfel, M., Illmer, T., Karsch, C., Platzbecker, U., Ehninger, G., Schleyer, E. (2008) AraU accumulation in patients with renal insufficiency as a potential mechanism for cytarabine neurotoxicity. Int. J. Hematol. 88, 381-386.

(51) Veltkamp, S.A., Jansen, R.S., Callies, S., Pluim, D., Visseren-Grul, C.M., Rosing, H., Kloeker-Rhoades, S., Andre, V.A.M., Beijnen, J.H., Slapak, C.A., and Schellens, J.H.M. (2008) Oral administration of gemcitabine in patients with refactory tumors: A clinical and pharmacologic study. Clin. Cancer Res. 14, 3477-3485.

(52) Veltkamp, S., Pluim, D., van Tellingen, O., Beijen, J.H., and Schellens, J.H.M. (2008) Extensive metabolism and hepatic accumulation of gemcitabine after multiple oral and intravenous administration in mice. Drug. Metab. Dispos. 36, 1606-1615.

(53) Capizzi, R.L., Yang, J.L., Cheng, E., Bjornsson, T., Sahasrabudhe, D., Tan, R.S., Cheng, Y.C. (1983) Alteration of the pharmacokinetics of high-dose ara-C by its metabolite, high ara-U patients with acute leukemia. J. Clin. Oncol. 12, 763-771.

(54) Veltkamp, S.A., Pluim, D., van Eijndhoven, M.A.J., Bolijn, M.J, Ong, F.H.G., Govindarajan, R., Unadkat, J.D. Beijnen, J.H., and Schellens, J.H.M., (2008) New

insights into the pharmacology and cytotoxicity of gemcitabine and 2',2'-difluorodeoxyuridine. Mol. Cancer Ther. 7, 2415-2425.

(55) Damon, L.E., Plunkett, W., Linker, C.A. (1991) Plasma and cerebrospinal fluid pharmacokinetics of 1-β-d-arabinofuranosylcytosine and 1-β-d-arabinofuranosyluracil following the repeated intravenous administration of high- and intermediate-dose of 1-β-d-arabinofuranosylcytosine. *Cancer Res.* 51, 4141-4145.

(56) Graham, F.L., Whitmore, G.F. (1970) Studies of mouse L-cells on the incorporation of 1-beta-D-arabinofuranosylcytosine into DNA and on inhibition of DNA polymerase by 1-beta-D-arabinofuranosylcytosine 5'-triphosphate. Cancer Res. 30, 2636-2644.

(57) Huang, P., Chubb, S., Hertel, L.W., Grindey, G.B., Plunkett, W. (1991) Action of 2',2'-difluorodeoxycytidine on DNA synthesis. *Cancer Res.* 51, 6110-6117.

(58) Chen, Y.-W., Cleaver, J.E., Hanaoka, F., Chang, C.-F., Chou K.-M. (2006) A novel role of DNA polymerase η in modulating cellular sensitivity to chemotherapeutic agents. *Mol. Cancer Res.* 4, 257-265.

(59) Iwasaki, H., Huang, P., Keating, M.J., Plunkett, W. (1997) Differential incorporation of ara-c, gemcitabine, and fludarabine into replicating and repairing DNA in proliferating human leukemia cells. Blood 90, 270-278.

(60) Pelicano, H., Carney, D., and Huang, P. (2004) ROS stress in cancer cells and therapeutic implications. Drug Resist. Updates 7, 97–110.

(61) Albertella, M.R., Lau, A., O'Connor, M.J. (2005) The overexpression of specialized DNA polymerases in cancer. DNA Repair 4, 583–593.

(62) Shapiro, R. and Pohl S.H. (1968) The reaction of ribonucleosides with nitrous acid. Side products and kinetics. Biochemistry 7, 448-455.

(63) Shapiro, S.H. and Chargaff E. (1966) Studies on the nucleotide arrangement in deoxyribonucleic acids. XI. Selective removal of cytosine as a tool for the study of the nucleotide arrangement in deoxyribonucleic acid. Biochemistry 9, 3012-3018.

(64) Yoshikawa, M., Kato, T., Takenishi, T. (1969) Studies of phsophorylation. III. Selective phosphorylation of unprotected nucleosides. Bull. Chem. Soc. Jpn. 42, 3505-3508.

(65) Ludwig, J. (1981) A new route to nucleoside 5'-triphosphates. *Acta. Biochim. et Biophys. Acad. Sci. Hung.* 16, 131-133.

(66) Ruth, J.L. and Cheng, Y.-C. (1981) Nucleoside analogues with clinical potential in antivirus chemotherapy. The effect of several thymidine and 2'-deoxycytidine analogue 5'-triphosphates on purified human (α, β) and herpes simplex virus (types 1, 2) DNA polymerases. Mol. Pharmacol. 20, 415-422.

(67) Burgess, K. and Cook, D. (2000) Syntheses of nucleoside triphosphates. Chem. Rev. 100, 2047-2059.

(68) Modak, M.J. and Marcus, S.L. (1977) Purification and properties of Rauscher leukemia virus DNA polymerase and selective inhibition of mammalian viral reverse transcriptase by inorganic phosphate. J. Biol. Chem. 252, 11-19.

(69) Modak, M.J., Rao, K., Marcus, S.L. (1982) The mechanism of inorganic phosphate-mediated inhibition of calf thymus DNA polymerase β and Raucher leukemia virus DNA polymerase Biochem. Bioph. Res. Co. 107, 811-819.

(70) Chang, L.M.S. and Bollum, F.J. (1972) A comparison of associated enzyme activities in various deoxyribonucleic acid polymerases. J. Biol. Chem. 248, 3398-3404.

(71) Knopf K.-W., Yamada, M., Weissbach, A. (1976) HeLa cell DNA polymerase γ: further purification and properties of the enzyme. Biochemstry 15, 4540-4548.

(72) Yamaguchi, M., Tanabe, K., Taguchi, Y.N., Nishizawa, M., Takahashi, T., Matsukage, A. (1980) Chick embryo DNA polymerase β: purified enzyme consists of a single M_r = 40,000 polypeptide. J. Biol. Chem. 255, 9942-9948.

(73) Chen Jr, P.S., Toribara, T.Y., Warner, H. (1956) Microdetermination of phosphorous. Anal. Chem. 28, 1756-1758.

(74) Hamamoto, S and Takaku, K. (1986) New approach to the synthesis of deoxyribonucleoside phosphoramidite derivatives. Chem. Lett., 1401-1404.

(75) Barone, A.D., Yang, J.-Y. Caruthers, M.H. (1984) *In situ* activation of bis-dialkylaminophosphines - a new method for synthesizing deoxyoligonucleotides on polymer supports.

(76) Gait, M.J. (1984) Oligonucleotide synthesis: a practical approach, Oxford, IRL Press, Washington, DC.

(77) Puglisi, J. D., and Tinoco, I., Jr. (1989) Absorbance melting curves of RNA. Methods in Enzymology (Dahlberg, J. E., and Abelson, E. N., Eds.) Vol. 180, pp 304-325, Academic Press, Orlando, FL.

(78) SantaLucia, J., Jr., Allawi, H. T., and Seneviratne, P. A. (1996) Improved nearest-neighbor parameters for predicting DNA duplex stability. Biochemistry 35, 3555–3562.

(79) Allawi, H. T., and SantaLucia, J., Jr. (1997) Thermodynamics and NMR of internal G●T mismatches in DNA. Biochemistry 36, 10581–10594.

(80) 8Kupihar, Z., Timar, Z., Darula, Z., Dellinger, D.J., Caruthers, M.H. (2008) An electrospray mass spectrometric method for accurate mass determination of highly acid-sensitive phosphoramidites. Rapid Commun. Mass Sp. 22, 533-540.

(81) Kele, Z., Kupihar, Z., Kovacs, L., Janaky, T., Szabo, P.T. (1999) Electrospray mass spectrometry of phosphoramidites, a group of acid-labile compounds. J. Mass Spectrom. 34, 1317-1321.

(82) Williams, A.A., Darwanto, A., Theruvathu, J.A., Burdzy, A., Neidigh, J.W., Sowers, L.C. (2009) Impact of sugar pucker on base pair and mispair stability. Biochemistry 48, 11994-12004.

(83) Cui, Z., Theruvathu, J.A., Farrel, A., Burdzy, A., Sowers, L.C. (2008) Characterization of synthetic oligonucleotides containing biologically important modified bases by matrix-assisted laser desorption/ionization time-of-flight mass spectrometry. Anal. Biochem. 379, 196-207.

(84) Ferrer, E., Wiersma, M., Kazimierczak, B., Muller, C.W., Eritja, R. (1997) Preparation and properties of oligodeoxynucleotides containing 5-iodouracil and 5-bromo- and 5-iodocytosine. Bioconjugate Chem. 8, 757-761.

(85) Sheardy, R.D., and Seeman, N.C. (1986) Synthesis of a deoxyoligonucleotide incorporating 5-iododeoxyuridine. J. Org. Chem. 51, 4301-4303.

(86) Pon, R. T., and Yu, R. (1997) Hydroquinone-O,O-diacetic acid as a more labile replacement for succinic acid linkers in solid-phase oligonucleotide synthesis. Tetrahedron Lett. 38, 3327–3330.

(87) Azhayev, A. V., and Antopolsky, M. L. (2001) Amide group assisted 3'-dephosphorylation of oligonucleotides synthesized on universal A-supports. Tetrahedron 57, 4977–4986.

(88) Boosalis, M.S., Petruska, J., Goodman, M.F. (1987) DNA polymerase insertion fidelity: gel assay for site-specific kinetics. J. Biol. Chem. 262, 14689-14696.

(89) Beard, W.A., and Wilson, S.H. (2006) Structure and mechanism of DNA polymerase Beta. Chem. Rev 106, 361-362.

(90) .Beard, W.A., Shock, D.D., Vande Berg, B.J., Wilson, S.H. (2002) Efficiency of correct nucleotide insertion governs DNA polymerase fidelity. J. Biol. Chem. 277, 47393-47398.

(91) Bassett E., Vaisman, A., Havener, J.M., Masutani, C., Hanaoka, F., Chaney, S.G. (2003) Efficiency of extension of mismatched primer termini across from cisplatin and oxaliplatin adducts by human DNA polymerase β and η in vitro. Biochemistry 42, 14197-14206.

(92) Dube, D.K., Kunkel, T.A., Seal, G., Loeb, L.A. (1979) Distinctive properties of mammalian DNA polymerases. Biochim Biophys Acta. 561, 369-382.

(93) Yashida, S. and Masaki, S. (1979) Utilization *in vitro* of deoxyuridine triphosphate in DNA synthesis by DNA polymerases α and β from calf thymus Biochim Biophys Acta. 561, 396-402.

(94) Richardson, F.C., Kuchta, R.D., Mazurkiewicz, A., Richardson, K.A. (2002) Polymerization of 2'-fluoro- and 2'-O-methyl-dNTPs by human DNA polymerase α, polymerase γ, and primase. Biochem. Pharmacol. 59, 1045-1052.

(95) Kennedy, E.M., Daddacha, W., Slater, R., Gavegnano, C., Fromentin, E., Schinazi, R.F., Kim, B. (2011) Abundant non-canonical dUTP found in primary human macrophages drives its frequent incorporation by HIV-1 reverse transcriptase. J. Biol. Chem. 286, 25047-25055.

(96) Altona, C., and Sundaralingam, M. (1972) Conformational analysis of the sugar ring in nucleosides and nucleotides. A new description using the concept of pseudorotation. J. Am. Chem. Soc. 94, 8205–8212.

(97) Levitt, M., and Warshel, A. (1978) Extreme conformational flexibility of the furanose ring in DNA and RNA. J. Am. Chem. Soc. 100, 2607–2613.

(98) Ferrin, L.J., and Mildvan, A.S. (1985) Nuclear overhauser effect studies of the conformations and binding site environments of deoxynucleoside triphosphate substrates bound to DNA polymerase I and its large fragment. Biochemistry 24, 6904–6913.

(99) Ikeda, H., Fernandez, R., Wilk, A., Barchi, J.J., Jr., Huang, X., and Marquez, V.E. (1998) The effect of two antipodal fluorine-induced sugar puckers on the conformation and stability of the Dickerson-Drew dodecamer duplex $[d(CGCGAATTCGCG)]_2$. Nucleic Acids Res. 26, 2237–2244.

(100) Uesugi, S., Miki, H., Ikehara, M., Iwahashi, H., Kyogoku, Y. (1979) A linear relationship between electronegativity of 2'-substituents and conformation of adenine nucleosides. Tetrahedron Lett. 42, 4073-4076.

(101) Guschlbauer, W. and Jankowski, K. (1980) Nucleoside conformation is determined by the electronegativity of the sugar substituent. Nucleic Acids Res. 8, 1421-1433.

(102) Blandin, M., Son, T.-D., Catlin, J.C., Guschlbauer, W. (1974) Nucleoside conformations 16. Nuclear magnetic resonance and circular dichroism studies on pyrimidine-2'-fluoro-2'-deoxyribonucleosides. Biochim. Biophys. Acta 361, 249-256.

(103) Berger, I., Tareshko, V., Ikeda, H., Marquez, V.E., Egli, M. (1998) Crystal structures of B-DNA with incorporated 2'-deoxy-2'-fluoro-arabino-furanosyl thymines: implications of conformational preorganization for duplex stability. Nucleic Acids Res. 26, 2473-2480.

(104) . Sundaralingam,, M. (1975) Structure and conformation of nucleosides and nucleotides and their analogs as determined by x-ray diffraction. Ann N. Y. Acad. Sci. 255, 3-42.

(105) Cushley, R.J., Codington, J.F., Fox, J.J. (1967) Nucleosides. XLIX. Nuclear magnetic resonance studies of 2'- and 3'-halogeno nucleosides. The conformations of 2'-deoxy-β-D-arabinofuranosyluracil. Can. J. Chem. 46, 1131-1140.

(106) Pinto, D., Landousy-Sarocchi, M.-T., Guschlbauer, W. (1979) 2'-deoxy-2'-fluorouridine-5'-triphosphates: a possible substrate for *E. coli* RNA polymerase. *Nucleic Acids Res. 6*, 1041-1048.

(107) Nick McElhinny, S.A. and Ramsden, D.A. (2003) Polymerase mu is a DNA-directed DNA/RNA polymerase. Mol. Cell. Biol. 23, 2309-2315.

(108) Pelletier, H., Sawaya, M.R., Wolfe, W., Wilson, S.H., Kraut, J. (1996) Crystal structures of human DNA polymerase β complexed with DNA: implications for catalytic mechanism, processivity, and fidelity. Biochemistry 35, 12742-12761.

(109) Darwanto, A., Theruvathu, J.A., Sowers, J.L., Rogstad, D.K., Pascal, T., Goddard 3rd, W.A., Sowers, L.C. (2009) Mechanisms of base selection by human single-stranded selective monofunctional uracil-DNA glycosylase. J. Biol. Chem. 284, 15835-15846.

(110) Peng, C.G. and Damha, M.J. (2008) Probing DNA polymerase activity with stereoisomeric 2'-fluoro-β-D-arabinose (2'F-araNTPs) and 2'-fluoro-β-D-ribose (2'F-rNTPs) nucleoside 5'-triphosphate. Can. J. Chem. 86, 881-891.

(111) Aurup, H., Williams, D., Eckstein, F. (1992) 2'-Fluoro- and 2'-amino-2'-deoxynucleoside 5'-triphosphates as substrates for T7 RNA polymerase. Biochemistry 31, 9636-9641.

(112) Smart, B.E., (2001) Fluorine substituent effects (on bioactivity). J. Fluorine Chem. 109, 3-11.

(113) Sivalakshmidevi, A., Vyas, K., Om Reddy, G., Sivaram, S.D.V.N., Swamy, P.V., Puranik, R., and Sairam, P (2003) 2'-deoxy-2',2'-difluorocytidine monohydrochloride (Gemcitabine hydrochloride). Acta Crystallography E59, 1435-1437.

(114) Konerding, D., James, T.L., Trump, E., Soto, A.M., Marky, L.A., and Gmeiner, W.H. (2002) NMR structure of a Gemcitabine-substituted model Okazaki fragment. Biochemistry 41, 839-846.

(115) Ziemkowski, P., Felczak, K., Poznanski, J., Kulikowski, T., Zielinski, Z., Ciesla, J., and Rode, W. (2007) Interactions of 2'-fluoro-substituted dUMP analogues with thymidylate synthase. Biochem. Bioph. Res. Co. 362, 37-43.

(116) Plunkett, W. (1991) Action of 2',2'-difluorodeoxycytidine on DNA synthesis. Cancer Res. 51, 6110-6117.

(117) Prakasha Gowda, A.S., Polizzi, J.M., Eckert, K.A., and Spratt T.E. (2010) Incorporation of Gemcitabine and Cytarabine into DNA by DNA Polymerase Beta and Ligase III/XRCC1. Biochemistry 49, 4833-4840.

(118) Richardson K.A., Vega, T.P., Richardson, F.C., Moore, C.L., Rohloff, J.C., Tomkinson, B., Bendele, R.A., and Kuchta, R.D. (2004). Polymerization of the triphosphates of AraC, 2',2'-difluorocytidine (dFdC) and OSI-7836 (T-araC) by human DNA polymerase Alpha and DNA primase. Biochemical Pharm. 68, 2337-2346.

(119) Garcia-Diaz, M., Murray, M.S., Kunkel, T.A., and Chou K-.M. (2010) Interaction between DNA polymerase Lambda and anticancer nucleoside analogs. J. Biol. Chem. 285 16874-16879.

(120) Fowler, J.D., Brown, J.A., Johnson, K.A., and Suo, Z. (2008) Kinetic investigation of the inhibitory effect of Gemcitabine on DNA polymerization catalyzed by human mitochondrial DNA polymerase. J. Biol. Chem. 283, 15339-15348.

(121) Clayton, L.K., Goodman, M.F., Branscomb, E.W., Galas, D.J. (1979) Error induction and correction by mutant and wild type T4 DNA polymerases. Kinetic error discrimination mechanisms. *J. Biol. Chem.* 254, 1902-1912.

(122) Galas, D. J. and Branscomb, E. W. (1978) Enzymatic determinants of DNA polymerase accuracy. Theory of coliphage T4 polymerase mechanisms. *J. Mol. Biol.* 124, 653-687.

(123) Reid, R., Mar, E.-C, Huang, E.-S., Topal, M.D. (1988) Insertion and extension of acyclic, dideoxy, and ara nucleotides by herpesviridae, human α and human β polymerases: a unique inhibition mechanism for 9-(1,3-dihydroxy-2-propoxymethyl)guanine triphosphate. J. Biol. Chem. 263, 3898-3904.

(124) Keller, K.E., Cavanaugh, N., Kutcha, R.D. (2008) Interaction of herpes primase with the sugar of a NTP. Biochemistry 47, 8977-8984.

(125) Johnson, A.A., Tsai, Y., Graves, S.W., Johnson, K. A. (2000) Human mitochondrial DNA polymerase holoenzyme: reconstitution and characterization. *Biochemistry* 39, 1702–1708.

(126) Johnson, A.A., Ray, A.S., Hanes, J., Suo, Z., Colacino, J.M., Anderson, K.S., Johnson, K. A. (2001) Toxicity of antiviral nucleoside analogs and the human mitochondrial DNA polymerase. *J. Biol. Chem.* 276, 40847–40857.

(127) Wilds, C.J. and Damha, M.J. (2000) 2'-Deoxy-2'-fluoro-β-D-arabinonucleosides and oligonucleotides (2'F-ANA): synthesis and physiochemical studies. Nucleic Acids Res 28, 3625-3635.

(128) Mendelman, L.V., Boosalis, M.S., Petruska, J., Goodman, M.F. (1989) Nearest neighbor influences on DNA polymerase insertion fidelity. J. Biol. Chem 264, 14415-14423.

(129) Tollin, P., Wilson, H.R., Young, D.W. (1973) The crystal and molecular structure of uracil-β-D-arabinofuranoside. Acta Cryst B29, 1641-1647.

(130) Brutlag, D. and Kornberg, A. (1972) Enzymatic synthesis of deoxyribonucleic acid. 36. A proofreading function for the 3' leads to 5' exonuclease activity in deoxyribonucleic acid polymerases. *J. Biol. Chem.* 247, 241-248.

(131) Ban, C., Ramakrishnan, B., Sundaralingam, M. (1994) Crystal structure of the highly distorted chimeric decamer r(C)d(CGGCGCCG)r(G)●spermine complex – spermine binding to phosphate only and minor groove tertiary base-pairing. Nucleic Acids Res. 22, 5466-5476.

(132) Ban, C., Ramakrishnan, B. and Sundaralingam, M. (1994) A single 2'-hydroxyl group converts B-DNA to A-DNA. Crystal structures of the DNA-RNA chimeric decamer duplex d(CCGGC)r(G)d(CCGG) with a novel intermolecular G●C base-pair quadruplet. J. Mol. Biol. 236, 275-285.

(133) Wahl, M.C. and Sundaralingam, M. (2000) B-form to A-form conversion by 3'-terminal ribose: crystal structure of the chimera d(CCACTAGTG)r(G). Nucleic Acids Res. 28, 4356-4363.

(134) Vesnaver, G. and Breslauer, K. (1991) The contribution of DNA single-stranded order to the thermodynamics of duplex formation. Proc. Natl. Acad. Sci. USA 88, 3569-3573.

(135) Egli, M. (1998) Conformational preorganization, hydration, and nucleic acid duplex stability. Antisense Nucleic Acid Drug Dev. 8, 123-128.

CHAPTER FOUR

THE IMPACT OF NUCLEOSIDE RIBOSE SUBSTITUTION POLYMERASE EXTENSION

Adides A. Williams and Lawrence C. Sowers

Department of Basic Sciences, Loma Linda University School of Medicine

Loma Linda, CA 92350

Abstract

Nucleotide insertion, exonucleolytic proofreading, and primer terminus extension are three distinct steps that contribute to overall replication fidelity. Multiple factors appear to influence both incorporation and extension efficiency including the relative thermal and thermodynamic stability of a given base pair, base pair geometry, furanose conformation and geometry and the interaction of the incoming or terminal 3' nucleotide with DNA polymerase. Numerous studies have examined the role of base pair formation on both incorporation and elongation, however substantially less is known about the properties of the nucleoside sugar that determine incorporation or elongation efficiency. It is known, however, that during the extension step a correctly positioned terminal 3'-hydroxyl (3'-OH) is required to attack the α-phosphate (αP) of an incoming nucleoside triphosphate (NTP). The furanose ring of a nucleoside is not planar an can adopt several conformations. However, substitution of electronegative groups at the C2' position greatly influences conformational equilibria and population. For example, chemical addition of hydroxyl (OH) and fluorine (F) groups at the C2' position in the ribo (down, "below the sugar plane") configuration constrain nucleoside furanose geometry to a C3'-endo (RNA-like) geometry. Likewise, if those same electronegative groups are substituted at the C2' position in the arabino (up, "above the sugar plane") configuration, the nucleoside furanose will predominately adopt a C2'-endo (DNA-like) conformation. The terminal 3'-OH is directly tethered to the furanose ring. As such, its position relative to the αP of the incoming triphosphate is predicted to be influenced by the conformation of the nucleoside sugar to which it is attached. Therefore, we predicted that nucleoside sugar substitution would impact primer extension efficiency of DNA polymerases. For

this report, we have synthesized oligonucleotides containing modified nucleoside analogues at the 3'-end in a model replication fork. Using stead-state kinetics, we investigated the ability of three different polymerases, human DNA polymerase β (pol β), avian myeloblastosis viral reverse transcriptase (AMVRT), and *Escherichia coli* Klenow fragment (exo-), to extend modified primer termini. Surprisingly, we found that all polymerases investigated readily extended primers terminated by the ribonucleosides rU, dFdU, and $U^{2'F(ribo)}$ and that extension efficiencies were reduced by no greater than 13-fold. Conversely, the arabinonucleosides araU, FIAU and $U^{2'F(ara)}$ were inefficiently extended with extension efficiencies being reduced by as much as 570-fold.

Abbreviations

dU, 2'-deoxyuridine; 5IdU, 5-iodo-2'-deoxyuridine; araU, 1-β-D-arabinofuranosyluracil; rU, Uridine; $U^{2'F(ribo)}$, 2'-deoxy-2'-fluorouridine; $U^{2'F(ara)}$, 1-(2'-deoxy-2'-fluoro-β-D-arabinofuranosyl) uracil; FIAU, 5-iodo-(2'-deoxy-2'-fluoro-β-D-arabinofuranosyl) uracil; dFdC, 2'-deoxy-2',2'-difluorocytidine (Gemcitabine); dFdU, 2'-deoxy-2',2'-difluorouridine (Gemcitabine metabolite); FIAU-P, 5'-*O*-dimethoxytrityl-5-iodo-2'-deoxy-2'-fluoroarabinosyluracil, 3'-*O*-[(2-cyanoethyl)(N,N,-diisopropyl)]-phosphoramidite; dFdU-P, 5'-*O*-dimethoxytrityl-2'-deoxy-2',2'-difluorouridine, 3'-*O*-[(2-cyanoethyl)(N,N-diisopropyl)]-phosphoramidite.

Introduction

The accurate replication of nucleic acids requires that polymerases select the correct nucleotide at each successive step of replication [1]. DNA polymerases ensure the fidelity of DNA replication in both eukaryotes and prokaryotes. Nucleotide insertion, exonucleolytic proofreading and extension of primer termini are three distinct steps that contribute to overall replication fidelity [2]. During the insertion step a DNA polymerase selects from the deoxynucleoside triphosphate (dNTP) pool a dNTP that is complimentary to the template base and is able to bind to the primer-template complex with sufficient stability [3]. During extension, a polymerase commits to further rounds of dNTP addition by selecting and adding the next correct nucleotide to the primer termini. Interestingly, polymerase extension beyond a mispair is very difficult, even for the insertion of a correct dNTP and even though base-pairing and geometry conditions are met [4-8]. For reasons that have not yet been revealed, extension fidelity contributes nearly as much to the overall replication fidelity as the initial insertion step. Although polymerase pausing at the extension step following a nucleotide misinsertion event would reduce overall mutation frequency by facilitating proofreading or other repair, the mechanistic basis for extension fidelity has not yet been established.

Both the insertion and extension steps require a correctly positioned terminal 3'-hydroxyl (3'-OH) is required to attack the α-phosphate (αP) of an incoming nucleoside triphosphate (NTP). In the case of geometrically aberrant base pairs, such as a purine-purine mispair, the 3’-OH would be shifted several angstroms from the correct position, potentially preventing polymerase extension. With purine-pyrimidine mispairs, however, the geometry is closer to that of a normal Watson-Crick base pair, so that more subtle

differences, such as sugar conformation, might become important. In addition to mispair geometry, nucleoside sugar conformation can also be biased by the presence of substituents in the furanose ring. The conformational difference between deoxyribose and ribose sugars is attributed primarily to the presence of the 2'-OH in the ribonucleosides. Other substituents, in particular, electron-withdrawing substituents including fluorine, are known to profoundly influence sugar conformation [9-18]. Evidence exists that sugar pucker can influence both nucleotide incorporation and extension by polymerases [19-27]. Nucleotides that are constrained to a 3'-endo conformation - for example, 2'-deoxy-2'-fluororibo nucleotides - are preferentially incorporated by RNA polymerases [19]. Conversely, 2'-deoxy-2'-fluoroarabino nucleotides that prefer the 2'-endo conformation are preferentially incorporated by DNA polymerases, yet surprisingly, are very difficult to extend [23]. The physical basis for this selectivity has not as yet been established.

Nucleoside analogues with chemically modified sugars (Figure 18) comprise an important class antitumor and antiviral agents [21-22, 25, 27], and existing evidence indicates that the activity of these analogues results largely from interfering with DNA synthesis following misincorporation. In general, the nucleoside analogues are transported across the cell membrane through the human nucleoside transporters (hNTs), including equilibrative (hENTs) and concentrative (hCNTs) nucleoside transporters and activated following intracellular phosphorylation to their respective monophosphate (MP), diphosphate (DP) and triphosphate (TP) forms which have multiple cellular targets [28-30]. In the triphosphate form, nucleoside analogues are incorporated into DNA and in the case of dFdC, araC and FIAU, act as chain terminators.

Several *in vitro* incorporation and extension studies have demonstrated that pol α, pol ε, and pol δ exhibit greater than 10^3-fold reduction in catalytic efficiency when extending araC-, dFdC- and FIAU-terminated primers consistent with the chain termination model [31-33]. In addition, thermal denaturation studies of araC- and dFdC-substituted synthetic oligonucleotides revealed that these analogues reduce DNA duplex melting temperatures by 4 – 5 °C [34, 35]. As such, reduced DNA thermal or thermodynamic stability following misincorporation of these nucleoside analogues might explain, in part, why polymerase extension of araC-, dFdC-, and FIAU-terminated primers is difficult.

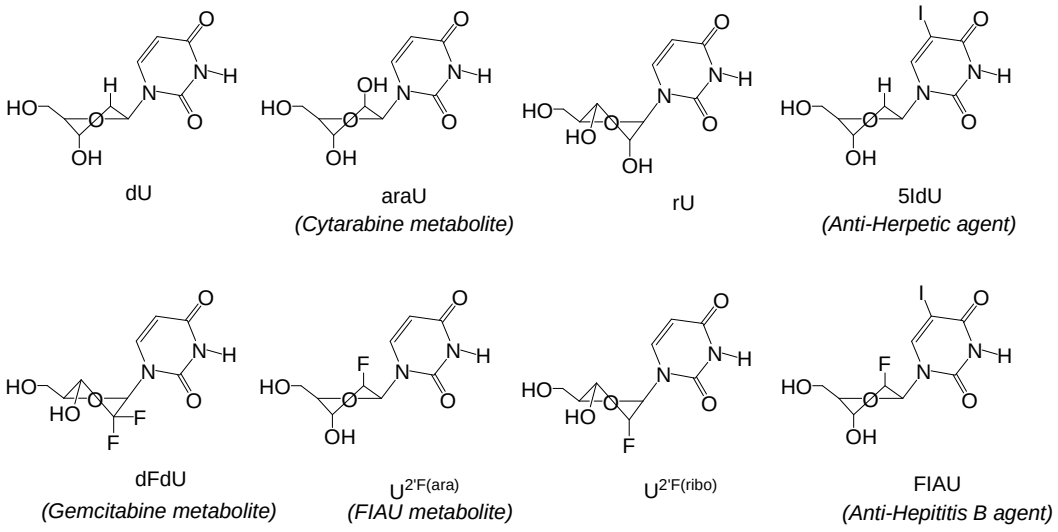

Figure 18: Chemical structures of an important class of antiviral and anticancer nucleoside analogues used in this study. The nucleoside analogues were either converted to 5'-triphosphates that were used in nucleotide incorporation experiments or converted to phosphoramidites which were then incorporated onto the 3'-end (primer terminus) of oligonucleotides which were used in primer extension experiments.

For this study, we constructed oligonucleotide primers containing modified nucleosides at the 3'-end and also at an internucleotide position. These primers were then coupled with complementary sequences to form replication forks in which the modified nucleosides were correctly paired with template dA. With the series of 3'-end modified duplexes we were able to study the ability of Klenow (exo-), AMVRT and pol β to extend sugar-modified termini. In addition, the series of primers with modifications at an internucleotide position were used in thermal denaturation studies to investigate the thermodynamic consequence of extending a sugar-modified terminus. Overall, the studies performed here represent the first systematic study of the impact of sugar modifications on primer extension.

Materials and Methods

Solvents and Reagents

All solvents were purchased from Sigma-Aldrich (St. Louis, MO). Thin layer chromatography (TLC) was performed on precoated silica gel 60 F_{254}, 5x20 cm, 250 μm thick plates purchased from EMD (Gibbstown, NJ). Universal support III PS and all normal (unmodified) phosphoramidites (dC, dG, dA, dT) were purchased from Glen Research (Sterling, VA). The sugar-modified phosphoramidites, $U^{2'F(ribo)}$, araU, rU, and dU, are commercially available and were purchased from Glen Research (Sterling, VA). The remaining nucleoside analogues, $U^{2'F(ara)}$, 5IdU, dFdU, and FIAU, were synthesized according to established procedures as discussed below.

Synthesis of FIAU and dFdU Phosphoramidites (FIAU-P and dFdU-P)

The phosphoramidite analogues of 5-iodo-(2'-deoxy-2'-fluoro-β-D-arabinofuranosyl) uracil (FIAU) and 2'-deoxy-2',2'-difluorouridine (dFdU) are not commercially available and were synthesized using established methods [36-38]. First, 250 mg of FIAU (0.67 mmol) was co-evaporated with anhydrous (anhyd.) pyridine (3 X 10 mL) and the resulting oily residue was re-dissolved in 10 mL anhyd. pyridine. To this was added 4.10 mg of 4-dimethylaminopyridine (DMAP; 0.034 mmol, 0.05 molar equiv. of nucleoside), 131 μL of TEA (0.94 mmol, 1.4 molar equiv. of nucleoside) and 276.4 mg of 4,4'-dimethoxytrityl chloride (DMT-Cl; 0.82 mmol, 1.2 molar equiv. of nucleoside). The reaction proceeded under an argon (Ar) atmosphere with magnetic stirring for 7 h. The conversion of FIAU to the corresponding 5'-dimethoxytrityl protected derivative (5'-dimethoxytrityl-5-iodo-2'-deoxy-2'-fluoroarabinosyluracil, FIAU-DMT) was monitored by TLC developed in a solvent system of DCM and MeOH (95:5, v/v). The formation of FIAU-DMT was determined to be complete when the spot of R_F 0.11 (FIAU) was no longer visible and the spot of R_F 0.39 (FIAU-DMT) was observed. Upon completion of the reaction, pyridine was removed under reduced pressure and the resulting oily residue was dissolved in DCM and extracted with saturated aqueous sodium bicarbonate ($NaHCO_3$, pH 8). The organic layer was removed, washed with H_2O and dried over anhyd. sodium sulfate (Na_2SO_4). Evaporation of the solvent gave an oily residue that was then dissolved in DCM and purified by open silica gel column eluting a gradient of 0 – 3% MeOH in DCM for 50 min. Fractions containing FIAU-DMT, as determined by TLC, were combined and the solvents were removed under reduced pressure to afford 245 mg (0.36 mmol) of FIAU-DMT, as a white (slightly yellow) foam, in 53% yield. FIAU-DMT was characterized by ESI-MS in negative ion

mode. The observed fragment ions were m/z = 673.18 ($C_{30}H_{27}FIN_2O_7$, FIAU-DMT); m/z = 303.07 ($C_{21}H_{19}O_2$, free DMT protecting group).

The FIAU phosphoramidite (5'-dimethoxytrityl-5-iodo-2'-deoxy-2'-fluoroarabinosyluracil, 3'-[(2-cyanoethyl)(N,N,-diisopropyl)]-phosphoramidite, FIAU-P) was prepared by combining 220 mg of FIAU-DMT (0.33 mmol) and 29.5 mg of diisopropylamine hydrotetrazolide (0.17 mmol, 0.5 molar equiv. of FIAU-DMT) in 5 mL of anhyd. acetonitrile (MeCN) under an Ar atmosphere. To this mixture was added 116.27 μL of 2-cyanoethyl-N,N,N',N'-tetraisopropylphosphoramidite (109 mg, 0.36 mmol, 1.1 molar equiv. of FIAU-DMT), dropwise, with continuous stirring for 3 h. The conversion of FIAU-DMT to FIAU-P was monitored by TLC developed in a solvent system of DCM, ethyl acetate (EtOAc) and TEA (55:40:5, v/v). The conversion of FIAU-DMT to FIAU-P was determined to be complete when the spot of R_F 0.64 (FIAU-DMT) was no longer visible and the spot of R_F 0.89 (FIAU-P) was observed. Upon completion of the reaction, 2 mL of TEA was added to the reaction mixture which was then extracted with an aqueous solution of NaCl (3 X 10 mL). The organic (top) layer was recovered, dried over anhyd. Na_2SO_4 and evaporated in vacuo. The resulting colorless residue was dissolved in a solution of Hexanes, EtOAc and TEA (89:10:1, v/v) and purified by open silica gel column eluting a gradient of 10 – 100% solvent A (EtOAc, TEA; 99:1, v/v) in solvent B (Hexanes, TEA; 99:1, v/v) for 1 hr. Fractions containing FIAU-P, as determined by TLC, were combined and evaporated in vacuo to give 148.6 mg (0.17 mmol) of FIAU-P as a white (slightly yellow) foam, in 51% yield. The FIAU-P was characterized by ESI-MS.

Both the 5'-tritylated (dFdU-DMT) and phosphoramidite (5'-*O*-dimethoxytrityl-2'-deoxy-2',2'-difluorouridine, 3'-*O*-[(2-cyanoethyl)(N,N-diisopropyl)]-phosphoramidite, dFdU-P) analogues of dFdU were synthesized and purified exactly as FIAU-DMT and FIAU-P (previously described), respectively, to give dFdU-P, as a white foam, in 47% yield.

Enzymes and DNA Preparation

Human DNA polymerase β (pol β) was obtained from Enzymax (Lexington, KY). Avian myeloblastosis virus reverse transcriptase (AMV-RT) and exonuclease-deficient Klenow fragment (exo-) polymerase were obtained from New England Biolabs (Ipswich, MA). For the polymerase incorporation assays, the primers were 5′-^{32}P-end labeled by T4 polynucleotide kinase (New England Biolabs) with [γ-^{32}P]adenosine triphosphate (MP Biomedicals, Costa Mesa, CA) under conditions recommended by the enzyme supplier. Labeled oligonucleotides were purified using G25 Sephadex columns (Roche Applied Science, Indianapolis, IN). A 2-fold excess of the complementary template strand was then added to the labeled primer mixture, incubated at 95 °C for 5 min, and allowed to cool to room temperature gradually to create the oligo-primer duplex.

Steady-State Kinetic Experiments (Polymerase Extension Assays)

Polymerase β extension reactions were performed in pol β buffer (50 mM Tris-HCl, pH 7.5, 10 mM $MgCl_2$, 2mM dithiothreitol, 20 mM NaCl, 20 mM KCl, 200 μg/ml BSA, 1% glycerol) and increasing concentrations of dGTP at 37°C. AMV-RT extension assays were performed in AMV-RT buffer (5 mM NaCl, 60 mM Tris-HCl, 8 mM $MgCl_2$,

and 0.5 mM dithiothreitol, pH 7.5) and increasing concentrations of dGTP at 37°C. Klenow (exo-) extension assays were performed in Klenow (exo-) buffer (50 mM NaCl, 10 mM Tris-HCl, 10 mM $MgCl_2$, and 1 mM dithiothreitol, pH 7.5) and increasing concentrations of dGTP at 37°C. In general, the reactions were initiated by the addition of radiolabeled primer-template substrate (5'-^{32}P-labeled) to enzyme (pol β, AMVRT, or Klenow (exo-)) and dGTP. The radiolabeled DNA concentrations were 10-fold greater than polymerase concentrations and the dGTP concentrations ranged from 0.01 to 1000 μM. Reactions (20 μL) were quenched at various times using equal volumes of "STOP" solution (98% formamide, 0.01 M EDTA, 1 mg/mL xylene cyanole, and 1 mg/mL bromophenol blue) followed by heating at 95 °C for 2 min. The reaction products were electrophoresed on denaturing polyacrylamide gels containing 20% acrylamide (19:1 acrylamide:methylenediacrylamide) and 8 M urea. The size of the gel was 19.5 cm x 16 cm x 0.4 cm and was run at 519 V for 2.5 – 3 h using a Hoeter PS 500 XT DC Power Supply (Amersheim Pharmacia Biotech). The gel was visualized and quantified using a Storm 860 PhosphorImager (Molecular Dynamics, Sunnyvale, CA) and ImageQuant 5.2 software (GE Healthcare Bio-Sciences).

Determination of k_{cat} and K_m

The previously described polymerase assays were used to measure the extension kinetics (k_{cat} and K_m) for the extension of a modified primer terminus (3'-dN) correctly paired opposite template dA) at pH 7.5 (Figure 19A). A series of reaction mixtures containing 5'-^{32}P-modified primer-template and increasing concentrations of dGTP were incubated for 0, 15, 30, 60, 120 or 180 sec. The amount of product formed by nucleotide

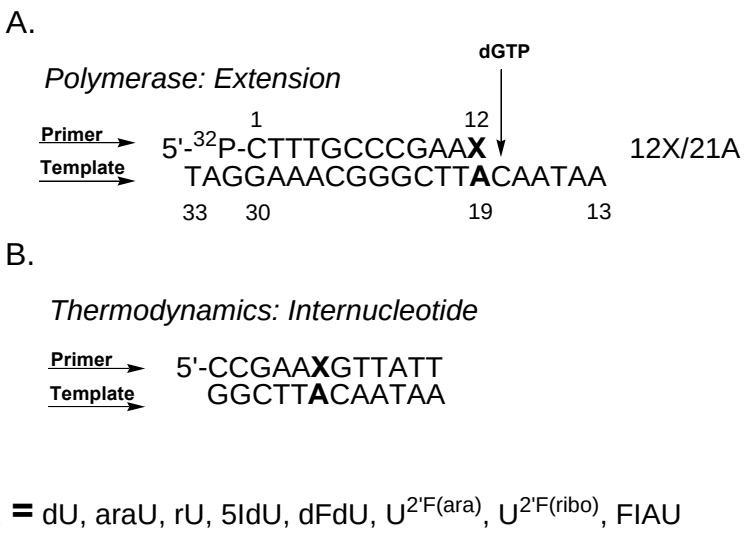

X = dU, araU, rU, 5IdU, dFdU, $U^{2'F(ara)}$, $U^{2'F(ribo)}$, FIAU

Figure 19: DNA substrates used in the present study for polymerase extension kinetics and thermodynamic studies. For polymerase kinetics studies, a ^{32}P-labeled primer (12-mer) was annealed to a 21-mer template. The steady-state kinetic parameters for (A) the extension of a sugar-modified primer terminus were measured and are presented in Table 4. For the thermodynamic studies, synthetic duplexes with sugar-modified residues at (B) an internucleotide position were used.

incorporation at the template target was determined by calculating the ratio of band intensity of the extended primer (DNA_{n+1}) to the band intensity of the un-extended primer (DNA_n). Initial velocities (V_o) were determined by plotting product formation versus time. The values of V_o were then plotted versus concentration and the data were fitted by nonlinear regression, using Prism version 5 (GraphPad Software, San Diego, CA; www.graphpad.com), to Equation 1,

$$v_o = \frac{(k_{cat})[E]_t[dGTP]}{K_m + [dGTP]} \qquad \text{Eq. 1}$$

where V_o is the initial velocity, k_{cat} is the catalytic turnover number, $[E]_t$ is the total polymerase concentration, [dGTP] is the concentration of the next correct nucleotide, 2'-deoxyguanosine-5'-triphosphate (dGTP), and K_m is the Michaelis-Menten constant.

Thermal Denaturation Studies and Assessment of Duplex Melting Behavior

Samples containing non-self-complementary oligonucleotides were prepared in buffer containing 0.1 M NaCl, 0.01 M sodium phosphate, and 0.1 mM EDTA (pH 7.0). Complexes were prepared by mixing equimolar amounts primer and template strands (Figure 19B) , and concentration dependent Tm measurements were conducted with a total strand concentration (C_T) between 2 and 60 μM in cuvettes with path lengths between 1 and 10 mm. Molar extinction coefficients of oligonucleotides were calculated [39] to determine single-strand concentrations. Oligonucleotide melting temperatures (Tm) were determined using a Varian Cary 300 Bio UV-visible spectrophotometer (Varian, Walnut Creek, CA). Five temperature ramps were performed on each sample per run while the absorbance at 260 nm was observed: (1) from 12 to 90 °C at a rate of 0.5 °C/min, (2) from 90 to 12 °C at a rate of 0.5 °C/min, (3) from 12 to 90 °C at a rate of 0.5 °C/min, (4) from 90 to 12 °C at a rate of 0.5 °C/min, and (5) from 12 to 90 °C at a rate of 0.5 °C/min. The sample was held for 3 min when the temperature reached 90 °C and for 10min when it reached 12 °C, and then the next cycle was started. Data were collected at 0.5 °C intervals while the temperature was monitored with a probe inserted into a cuvette containing only buffer. The Tm of each duplex was determined using Cary WinUV Thermal software (Varian). Theoretical Tm values for the control duplexes (A:dU) were determined [40, 41] and compared against values obtained using Cary WinUV Thermal. Thermodynamic parameters for non-self-complementary duplexes were calculated in two ways: (1) averages from fits of individual melting curves at different concentrations using the van't Hoff calculation in Cary WinUV Thermal and (2) 1/Tm versus $\ln(C_T/4)$ plots fitted to Equation 2 for the non-self-complementary sequences examined here:

$$\frac{1}{T_m} = \frac{R}{\Delta H^\circ} \ln\left(\frac{C_T}{4}\right) + \frac{\Delta S^\circ}{\Delta H^\circ} \qquad \text{Eq. 2}$$

Both methods assume a two-state model, and ΔCp = 0 for the transition equilibrium. The two-state approximation was assumed to be valid for sequences in which the ΔH° values derived from the two methods agreed within 15% [41]. The ΔH° values derived from the two methods agree within 15%, indicating that the two-state approximation is valid for all other sequences employed in this study.

Analysis of Thermodynamic Data

Thermal and thermodynamic data obtained for the ensemble of oligonucleotides examined here were expressed as the corresponding differences by comparing the measured value for the substituted duplexes with the standard A:dU containing duplex for the 3'-end and internucleotide series. The corresponding values of ΔT_m, $\Delta\Delta G^o_{37}$, $\Delta\Delta H^o$ and $\Delta\Delta S^o$ are presented in Table 5.

Results

Oligonucleotide Synthesis and Characterization

Oligonucleotide resins and phosphoramidites of the normal DNA bases were obtained from Glen Research (Sterling, VA). Oligonucleotide synthesis was conducted with a Pharmacia gene assembler (GE Healthcare Bio-Sciences, Piscataway, NJ). In general, oligonucleotides containing sugar-modified residues were deprotected with concentrated aqueous ammonia (33% as NH_3) at 60 °C for approximately 12 – 15 h, purified by HPLC, and characterized by MALDI-TOF-MS, as previously described [42,

43]. However, oligonucleotides containing C5-iodo-substituted residues (i.e. 5IdU and FIAU) were instead deprotected at room temperature for 24 h to prevent the formation of C5-amino side products as previously described [44, 45]. A synthetic approach [42], using Universal Support III PS [46, 47] available from Glen Research was used to insert dU, 5IdU, araU, rU, $U^{2'F(ara)}$, $U^{2'F(ribo)}$ FIAU and dFdU at the 3'-end (primer terminus) of synthetic duplexes. For each of the C2'-fluorine-substituted residues (i.e. FIAU, $U^{2'F(ara)}$, $U^{2'F(ribo)}$ and dFdU) it was necessary to increase the coupling times to 10 min.

Determination of Steady-State Kinetic Parameters for Extension of Modified Primer Termini.

For a modNTP analogue to persist in DNA following misincorporation, it must be extended by the addition of downstream nucleotides. Neither Klenow (exo-), AMVRT, or pol β preparations, used in this report, possess 3'→5' exonuclease activity that might remove a misincorporated modNTP analogue from the primer terminus. We therefore investigated the ability of Klenow (exo-), AMVRT, and pol β to extend a modNTP following misinsertion onto the 3'-end of a DNA strand. To accomplish this we designed 12-mer primers with a single sugar-modified residue at the primer terminus (3'-dNMP) correctly paired with template dA (Figure 19; termed 12X/21A, where X is the modified analogue) and we examined the ability of Klenow (exo-), AMVRT, and pol β to add the next correct nucleotide, dGTP (Figure 19A). Gel electrophoresis followed by autoradiographic image analysis revealed that the enzyme gradually incorporated the dGTP against a modified terminus; as primer 12-mer was elongated to a 13-mer (Figure 20A – H). Product (elongated primer) formation was plotted as a function of time to determine initial velocities. The initial velocities were then plotted as a function of

increasing dGTP concentration and a nonlinear least-squares fit of the data to the Michaelis-Menten rectangular hyperbola (equation 1), as previously described [48], was performed to obtain Km and kcat. The relative extension frequencies for pol β, AMVRT, and Klenow (exo-) extension of modified termini are summarized in Table 4 and were determined by $(kcat/Km)_{3'\text{-}dN}$ /$(kcat/Km)_{3'\text{-}dU}$, where 3'-dN is the modified primer terminus paired opposite template dA and $(kcat/Km)_{3'\text{-}dU}$ is the catalytic efficiency for extension of the reference terminus, 3'-dU.

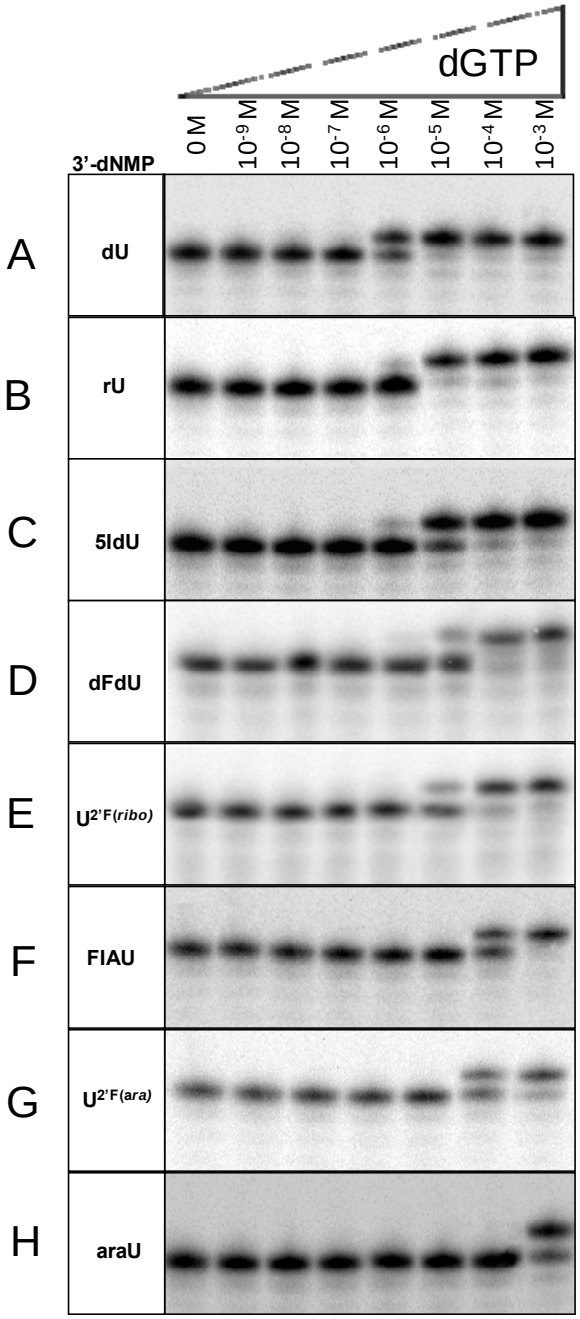

Figure 20: Polymerase β extension of sugar-modified primer termini paired opposite template A. Gel showing band intensities as a function of increasing concentrations of the next correct nucleotide, dGTP, inserted after 3'- A) dU, B) rU, C) 5IdU, D) dFdU, E) $U^{2'F(ribo)}$, F) FIAU, G) $U^{2'F(ara)}$ and H) araU modified termini.

Extension Kinetics for Primers Terminated by 3'-ribonucleosides (3'-rN)

Surprisingly, and contrary to expectations based on our incorporation studies (presented and discussed in Chapter 3 of this dissertation), we found that 3'-rU, 3'-$U^{2'F(ribo)}$, and 3'-dFdU were good substrates, *during the extension step*, for each of the polymerases examined (Table 4, Figure 21) when compared with the reference 3'-dU. When using AMVRT, extension efficiencies for 3'-rU, 3'-dFdU, and 3'-$U^{2'F(ribo)}$ were modestly reduced by 1.1-, 1.2-, and 1.6-fold, respectively. Klenow (exo-), however, appeared to be more sensitive to sugar-modified termini as its extension efficiencies of 3'-rU, 3'-dFdU, and 3'-$U^{2'F(ribo)}$ were reduced by 4-, 7.5-, and 13-fold, respectively. Significantly, when using pol β, the catalytic efficiency for dFdU- and $U^{2'F(ribo)}$-terminated primers was reduced by only 1.20 – 2.15-fold (Table 4, Figure 21). Interestingly, the extension efficiency for a rU-terminated primer was identical to the extension efficiency for the unmodified dU-terminated primer. Therefore, it appears that a ribonucleoside at the primer terminus does not significantly influence pol β primer extension. These results suggest that if a rNTP is misincorporated during the base excision repair (BER) process, it will be readily extended (buried in the DNA) by pol β.

Extension Kinetics for Primers Terminated by 3'-arabinonucleosides (3'-araNs)

Although the araNTPs investigated in these studies were readily incorporated into DNA by Klenow (exo-), AMVRT, and pol β (presented and discussed in Chapter 3 of this dissertation), they were inefficiently extended. We found that AMV-RT extension efficiency of 3'-FIAU, 3'-$U^{2'F(ara)}$, and 3'- araU was reduced by 25-, 54-, and 130-fold, respectively. Pol β extension efficiency of 3'-FIAU, 3'-$U^{2'F(ara)}$, and 3'-araU was reduced

by 30-, 50-, and 140-fold, respectively (Table 4, Figure 21). However, Klenow (exo-) exhibited greater difficulty when extending the same residues. Extension efficiency for 3'-FIAU, 3'-$U^{2'F(ara)}$, and 3'- araU was reduced by 180-, 400-, and 570-fold, respectively . The results reported thus far indicate that, perhaps paradoxically, Klenow (exo-), AMVRT, and pol β inefficiently incorporate rNTPs yet efficiently extends rN-terminated primers. However, the converse is observed with araNTPs in that they are readily incorporated by Klenow (exo-), AMVRT, and pol β yet an arabinonucleoside (araN)-terminated primer is poorly extended (Table 4).

When considering the 3'-rN/3'-araN pairs we observed that conversion of 3'-$U^{2'F(ara}$ to a 3'-$U^{2'F(ribo)}$ resulted in a 34-fold increase in extension efficiency for AMV-RT, a 32-fold increase in extension efficiency for Klenow (exo-), and 23-fold increase in extension efficiency for pol β. Likewise, conversion of 3'-araU to 3'-rU resulted in a 120-fold increase in extension efficiency for AMVRT, a 142-fold increase in extension efficiency for Klenow (exo-), and a 140-fold increase in extension efficiency for pol β. Thus, for Klenow (exo-), AMV-RT, and pol β, catalytic efficiency was recovered by 10^1 – 10^2-fold when the terminus residue was converted from a 3'-araN to a 3'-rN. Together, these data indicate that the sugar pucker of the primer terminus significantly affects the ability of DNA polymerases to complete primer extension.

Discussion

The experimental goal of this study was to examine the role of constrained ribose geometry on polymerase extension kinetics. These properties might help to explain how the configuration of the nucleoside sugar at the primer terminus impacts the ability of a

DNA polymerase to continue synthesis following misincorporation of modNTP. The nucleoside analogues analyzed here represent an important class of compounds with demonstrated anticancer and antiviral properties. Our experimental approach was to incubate Klenow (exo-), AMVRT, and pol β with primers modified at 3'-end with several sugar-modified analogues, including 2'-fluoro- and 2'-OH-modification, constrained to the either the C2'-endo (DNA-like) configuration or C3'-endo (RNA-like) configuration (Figure 18), and examine how efficiently Klenow (exo-), AMVRT, and pol β extended them by incorporation of the next correct nucleotide dGTP (Figure 19A). The data reported here might facilitate an improved understanding of the actions of this class of nucleoside analogues.

Klenow (exo-), AMVRT, and pol β readily extend primers terminated by ribonucleosides (3'-rNs). During the incorporation step we observed that Klenow (exo-), AMVRT, and pol β exhibited difficulty incorporating yet readily incorporated an araNTP (Table 4). Interestingly, the inverse was observed during the extension step, namely, we observed that pol β exhibited difficulty when extending a 3'-araN yet readily extended a 3'-rNMP by incorporation of the next correct nucleotide, dGTP.

During the extension step, the electron-rich 3'-O^- of the primer terminus has to be appropriately positioned to perform a nucleophilic attack on the αP of the incoming NTP (phosphoryl transfer). Klenow (exo-), AMVRT, and pol β extended 3'-rU with catalytic efficiencies that were nearly identical to the extension efficiencies for the reference 3'-dU (Table 4, Figure 21). Moreover, extension efficiency of 3'-dFdU and 3'-$U^{2'F(ribo)}$ was only reduced by 1.2 and 2.1-fold, respectively, when using AMVRT and 7.5- and 13-fold, respectively, when using Klenow (exo-) (Table 4). These data imply that the sugar

moieties of the 3'-rU, 3'-dFdU, and 3'-$U^{2'F(ribo)}$ residues are in the proper geometry and, consequently, their 3'-O^- is well positioned to allow further catalysis. Previously, Batra V.K. et al were able to develop a high resolution structure for a precatalytic complex of pol β with a single-nucleotide gapped substrate whose primer terminus had an intact C3'-OH, catalytic Mg^{2+} and a nonhydrolyzable dUTP analogue, 2'-deoxyuridine-5'-(α, β)-imido triphosphate [49]. Several intriguing features were revealed regarding pol β catalyzed phosphoryl transfer: 1) the sugar geometry of the primer terminus is C3'-endo when catalytic metal ion sites are occupied by Mg^{2+}; 2) when Mg^{2+} occupies metal binding site A it coordinates the 3'-O^-, the αP of the incoming NTP, three aspartate residues and exhibits octahedral geometry. This coordination geometry, in turn, influences the geometry of the primer terminus; 3) the identity of the catalytic metal influences the geometry of the sugar pucker of the primer terminus; whereas Mg^{2+} induces a C3'-endo geometry, Na^+ induces a conformation geometry that is closer to C2'-endo; 4) the Mg^{2+}-induced C3'-endo conformation of the primer terminus shifts the 3'-O^- 1.3 Å closer to both the catalytic metal and the αP when compared with the Na^+-induced C2'-endo like terminus.

Table 4: Kinetic parameters (k_{cat}, K_m and k_{cat}/K_m) for extension of sugar-modified primer termini, paired opposite dA, using pol β, AMV-RT and Klenow (exo-) at pH 7.5.

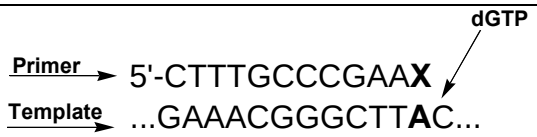

Polymerase	Template	3'-NMP	Km (M)	kcat (s^{-1})	kcat/Km (M^{-1} s^{-1})	Extension Efficiency
Pol β	A	dU	7.47±0.10 X 10^{-6}	2.31±0.17 X 10^{-3}	3.09±0.23 X 10^{2}	1.00
		rU	2.13±0.48 X 10^{-5}	6.60±0.90 X 10^{-3}	3.10±0.82 X 10^{2}	1.00
		5IdU	9.05±0.42 X 10^{-6}	2.66±0.35 X 10^{-3}	2.94±0.41 X 10^{2}	9.52*10^{-1}
		dFdU	2.11±0.07 X 10^{-5}	5.44±0.19 X 10^{-3}	2.58±0.12 X 10^{2}	8.35*10^{-1}
		$U^{2'F(ribo)}$	3.39±0.53 X 10^{-5}	4.88±0.27 X 10^{-3}	1.44±0.24 X 10^{2}	4.66*10^{-1}
		FIAU	5.73±0.57 X 10^{-4}	6.41±0.30 X 10^{-3}	1.12±0.12 X 10^{1}	3.62*10^{-2}
		$U^{2'F(ara)}$	5.00±0.47 X 10^{-4}	3.04±0.20 X 10^{-3}	0.61±0.06 X 10^{1}	1.97*10^{-2}
		araU	7.87±0.82 X 10^{-4}	1.73±0.05 X 10^{-3}	0.22±0.02 X 10^{1}	7.12*10^{-3}
AMV-RT	A	dU	7.27±0.23 X 10^{-7}	3.39±0.40 X 10^{-3}	4.66±0.57 X 10^{3}	1
		5IdU	6.98±0.17 X 10^{-7}	3.10±0.23 X 10^{-3}	4.44±0.35 X 10^{3}	9.53 X 10^{-1}
		rU	6.63±0.29 X 10^{-7}	2.79±0.23 X 10^{-3}	4.21±0.39 X 10^{3}	9.03 X 10^{-1}
		dFdU	4.57±0.15 X 10^{-7}	1.80±0.21 X 10^{-3}	3.94±0.48 X 10^{3}	8.45 X 10^{-1}
		$U^{2'F(ribo)}$	3.39±0.22 X 10^{-7}	9.87±0.16 X 10^{-4}	2.91±0.51 X 10^{3}	6.24 X 10^{-1}
		FIAU	5.43±0.30 X 10^{-6}	1.02±0.10 X 10^{-3}	1.88±0.21 X 10^{2}	4.03 X 10^{-2}
		$U^{2'F(ara)}$	9.65±0.14 X 10^{-6}	8.34±0.10 X 10^{-4}	8.64±0.12 X 10^{1}	1.85 X 10^{-2}
		araU	2.48±0.12 X 10^{-5}	8.83±0.23 X 10^{-4}	3.56±0.19 X 10^{1}	7.64 X 10^{-3}
Klenow (exo-)	A	dU	3.71±0.12 X 10^{-8}	3.03±0.10 X 10^{-3}	8.17±0.38 X 10^{4}	1
		5IdU	5.12±0.27 X 10^{-8}	1.96±0.13 X 10^{-3}	3.83±0.32 X 10^{4}	4.69 X 10^{-1}
		rU	5.87±0.11 X 10^{-8}	1.19±0.16 X 10^{-3}	2.03±0.28 X 10^{4}	2.48 X 10^{-1}
		dFdU	7.64±0.23 X 10^{-8}	8.31±0.02 X 10^{-4}	1.09±0.03 X 10^{4}	1.33 X 10^{-1}
		$U^{2'F(ribo)}$	9.03±0.52 X 10^{-7}	5.80±0.21 X 10^{-4}	6.42±0.44 X 10^{3}	7.86 X 10^{-2}
		FIAU	7.15±0.42 X 10^{-7}	3.26±0.37 X 10^{-4}	4.56±0.58 X 10^{2}	5.58 X 10^{-3}
		$U^{2'F(ara)}$	1.42±0.14 X 10^{-6}	2.85±0.24 X 10^{-4}	2.01±0.26 X 10^{2}	2.46 X 10^{-3}
		araU	1.53±0.17 X 10^{-6}	2.17±0.24 X 10^{-4}	1.42±0.22 X 10^{2}	1.74 X 10^{-3}

[a.] Extension efficiency, is defined as $(kcat/Km)_{3'\text{-dNMP}}$ /$(kcat/Km)_{3'\text{-dUMP}}$, where 3'dNMP is the modified primer terminus paired opposite template dA.

Thus, catalytic Mg^{2+} induces additional conformational changes within the pol β active site leading to optimal positioning of the 3'-O^- necessary for efficient phosphoryl transfer during the extension step. Consequently, this optimal positioning is brought about when the sugar pucker of the primer terminus is inverted to C3'-endo. The unencumbered extension of the 3'-rU-, 3'-dFdU-, and 3'-$U^{2'F(ribo)}$-terminated primers examined (Table 4) is in support of primer terminus sugar pucker inversion at the polymerase active site. Indeed, X-ray crystal structures for DNA at the active sites of bacteriophage T7, thermostable *Bacillus stearothermophilus*, and *Thermus aquaticus* (Taq) DNA polymerases reveal that the base pairs at the primer terminus exhibit a widened minor groove, a decreased helical twist, and C3'-endo configured sugars [50-52], suggesting that primer terminus sugar pucker inversion is commonly employed by DNA polymerases. Further, Arnold, E. et al have solved the crystal structure for human immunodeficiency virus type 1 (HIV-1) reverse transcriptase (HIV-RT) with a double-stranded DNA (dsDNA) template-primer [53, 54]. This structure revealed that the base pairs of dsDNA at the reverse transcriptase active site adopted a conformation like A-form DNA, whereas the base pairs outside of the active site conformed to B-form DNA geometry. This observation is reasonable when one considers that the polymerase active site is hydrophobic when the polymerase-primer/template-dNTP complex is in the "closed" form and that under hydrophobic conditions (i.e. reduced water activity) DNA is known to conform to A-form geometry [55, 56]. Thus, in the context of the hydrophobic active site the preferred nucleoside sugar geometry at the primer terminus is predicted to be C3'-endo (A-form). Thus, an rN-terminated exists in the preferred extension geometry and, consequently, a lower energy penalty is incurred when aligning its 3'-O^- for

nucleotidyl transfer. It is apparent that the incorporation step is critical to avoid rNTP accumulation in DNA since once incorporated, a ribonucleoside is readily extended and buried into the growing DNA strand.

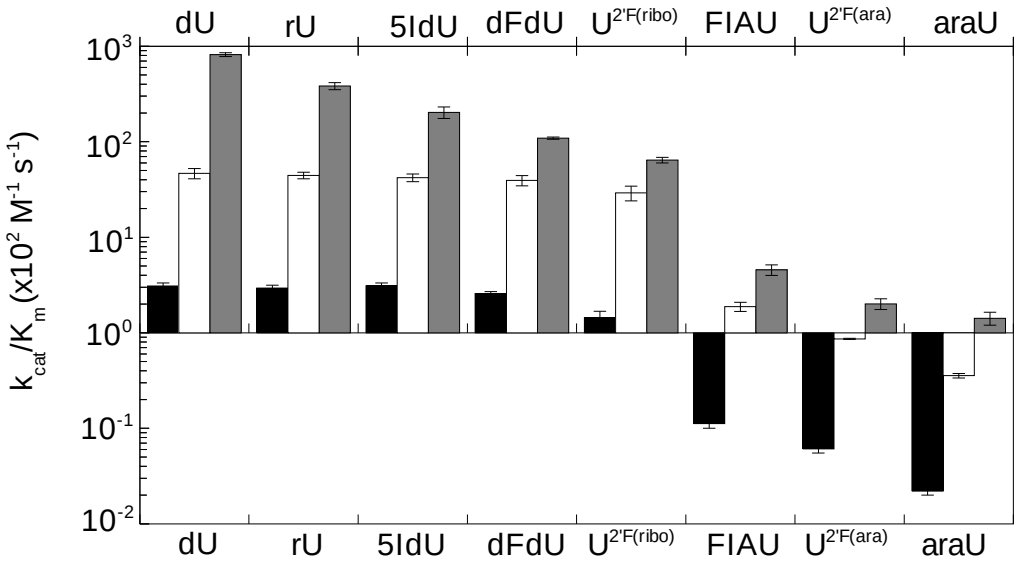

Figure 21: A log plot comparing the extension efficiencies for sugar-modified primer termini using the following polymerases: polymerase β (*black-filled bars*), AMV reverse transcriptase (*open-bars*), and Klenow (exo-) (*gray-filled bars*). The base line represents a catalytic efficiency of 10^2 M^{-1} s^{-1}. The catalytic efficiencies are tabulated in Table 4.

Klenow (exo-), AMVRT, and pol β inefficiently extend primers terminated by arabinonucleosides (3'-araNs). It has been observed that several DNA polymerases including DNA pol α-Primase, *Escherichia coli* polymerase I (Klenow fragment) (Pol I), T4 polymerase and avian myeloblastosis virus reverse transcriptase (AMVRT) [20, 21, 26, 57] exhibit difficulty when extending araC-terminated primers. Consistent with literature, we observed that AMV-RT extension efficiency of 3'-FIAU, 3'-$U^{2'F(ara)}$, and 3'-

araU was reduced by 25-, 54-, and 130-fold, respectively. Pol β extension efficiency of 3'-FIAU, 3'-$U^{2'F(ara)}$, and 3'-araU was reduced by 30-, 50-, and 140-fold, respectively (Table 4, Figure 21). However, Klenow (exo-) exhibited greater difficulty when extending the same residues. Extension efficiency for 3'-FIAU, 3'-$U^{2'F(ara)}$, and 3'- araU was reduced by 180-, 400-, and 570-fold, respectively .The exact mechanism by which an araN-terminated primer impedes further extension is not known, though, several structural studies on araN-substituted duplexes likely offer insight into the difficulty polymerases exhibit when elongating araN-terminated primers. These studies are discussed below.

Gmeiner and co-workers have investigated the structural consequences of araC substitution in DNA using NMR spectroscopy and temperature dependent UV spectroscopy [35, 58]. These studies revealed that substitution of araC in the DNA duplex region (DDR) of a model Okazaki fragment: 1) resulted in reduced base stacking in adjacent purines located 5' of the site of substitution in the DNA strand, 2) decreased the melting temperature of the duplex by 4.4 °C, and 3) resulted in a pronounced 19° increase in the helical bend at the site of substitution. This increase in helical bend is likely the result of the C2'-OH group of araC projecting into the major groove of the DNA helix [59, 60], sterically interacting with the C5-CH_3 and H6 atoms of the dT residue immediately 3' of the araC substitution, and pushing the dT base further away from the araC base causing destacking between the two bases. Beardsley and co-workers [61] also investigated the impact of araC substitution on DNA dodecamer structure and formation. In the sequence used in these studies a dG residue is immediately 3' of the araC substitution. It was determined that the C2'-OH of the araC residue was within ~2.5 Å of

the guanine base of dG. This would have the effect of pushing against the dG residue causing a loss of interstrand stacking. Together, these studies imply that the C2' substituent of an arabinonucleoside is in close contact with the entire base moiety of the 3' nucleoside not just the C5/C6 substituent of the 3' base.

These findings likely have implications regarding our extension results. In the extension model investigated in this report, AMVRT, Klenow (exo-), and pol β extended a modified primer by incorporation of dGTP (Figure 19B). It is predicted, therefore, that stacking dG on the 3'-araU led to the C2'-OH of 3'-araU sterically interacting with, and pushing against, the base moiety of dG which resulted in increased buckling in the araU12-dA19 base pair. This would have the effect of reducing van der Waals interactions between the araU12 base and the 3' adjacent dG base (Figure 19B). Displacement of the araU12-dA19 base pair from its original position would have the domino effect of displacing the adjacent dA11-dT18 base pair and so on, consequently, increasing helical bend, reducing stacking interactions, and destabilizing the duplex. Loss of stacking interactions between the terminal 3'-araU and the 3'-dG could affect the stabilization of the dGTP when araU is at the primer terminus. We therefore proposed that reducing the steric size of the C2' substituent of the 3'-araN would lessen steric interactions between it and the base of the incoming dGTP and avoid duplex destabilization resulting from increased helical bend and interstrand destacking at the site of substitution. Consistent with these expectations, conversion of the C2'-OH to a C2'-F resulted in a 3 – 5-fold recovery in extension efficiency with pol β, a 3-fold recovery in extension efficiency with Klenow (exo-), and 2 – 5-fold recovery in extension efficiency

with AMVRT (Table 4), implying that the smaller fluorine group is less detrimental to duplex formation and stability.

The conformational flexibility of the 3'-araN sugar may also impact polymerase extension efficiency. Damha et al [62, 63] observed that 2'-deoxy-2'-fluoroarabinosyladenine (2'F(ara)A), when incorporated into DNA/RNA hybrid duplexes, was capable of adopting RNA compatible sugar pucker conformations, including C4'-endo. Conversely, arabinosyladenine (araA) was incapable of exploring as much conformational space and generally maintained DNA compatible conformations including C1'-exo. It was reasoned that this inability to explore conformational space was the result of araA being a more "rigid" molecule than 2'F(ara)A and that this rigidity was derived from intramolecular hydrogen bonding between the C2'-OH and H8 group of the nucleobase that rendered araA unlikely to adopt a C3'-endo or A-form like conformation [64]. Indeed, X-ray crystal studies of araC-substituted decamers indicate that the C2'-OH of araC is able to form stable hydrogen bonds with the H6 of its own cytosine base and the C2'-H and C4'-H of its own sugar [59]. In addition, several lines of research indicate that a hydrogen bond between the C2'-OH and C5'-oxgen also contributes to the rigidity of C2'-endo arabinosides [60, 65, 66]. Taken together, these structural studies imply that the arabino C2'-OH is close enough in space to stably hydrogen bond with its own sugar and base moieties thus "locking" the sugar in a C2'-endo conformation and predisposing it to a B-form-like geometry.

Again, these observations likely have implications regarding the Klenow (exo-), AMVRT, and pol β extension models investigated in this report. As previously discussed in Chapter 3 of this dissertation, Klenow (exo-), pol β, and AMVRT (and other DNA

polymerases) convert the primer terminus sugar pucker from C2'-endo to C3'-endo and in doing so the terminus 3'-O^- is geometrically positioned for in-line attack on the αP of the incoming modNTP. In addition the desolvated hydrophobic active site will likely favor A-form nucleoside sugar conformations [55, 56]. The 3'-araU is predicted to be the most rigid of the 3'-araNs investigated in this report and this increased rigidity likely rendered the 3'-araU more resistant to sugar pucker inversion at the active sites of Klenow (exo-), AMVRT, and pol β. Thus, the 10^2-fold reduction in the extension efficiency of 3'-araU exhibited by each of the polymerases examined reflects the greater energetic penalty incurred by Klenow (exo-), AMVRT, and pol β to invert the sugar pucker of 3'-araU to a suitable C3'-endo-like conformation for the extension step likely resulting in reduced phosphodiester bond formation. On the other, 3'-rU exists in the preferred geometry, as such, a lower energy penalty is incurred with extending a primer terminated by rU (Table 4, Figure 21).

Net thermodynamic differences between 3'-end-modified duplexes and internally modified duplexes might explain why polymerase exhibit difficulty when extending sugar-substituted primer termini. One of the paradoxical findings of these studies is that araNTPs are readily incorporated by DNA polymerases, yet, difficult to extend. Conversely, rNTPs are difficult to incorporate, yet, readily extended. In our previous report [42] we observed that the $U^{2'F(ribo)}$ substitution was more destabilizing, with larger magnitude ΔΔH° (enthalpy) and ΔΔS° (entropy) when on the 3'-end, relative to the internucleotide linkage (Table 5).

Table 5: Experimental thermodynamic parameters of duplex formation. The values include measured free energy of duplex formation ($\Delta G°_{37}$), enthalpy ($\Delta H°$), entropy ($\Delta S°$) and melting temperature with a strand concentration of 28 μM ($T_{m\ 28\ \mu M}$). The thermodynamic parameters for the A:dU oligonucleotide was used as the reference when calculating $\Delta\Delta G°_{37}$, $\Delta\Delta H°$, and $\Delta\Delta S°$ in the 3'-terminal position. Measured free energy, enthalpy and entropy differences that exceed experimental error are indicated in bold.

	$\Delta G°_{37}$ (kcal/mol)	$\Delta\Delta G°_{37}$ (kcal/mol)	$T_{m\ 28\mu M}$ (°C)	$\Delta T_{m\ 28\mu M}$ (°C)	$\Delta H°$ (kcal/mol)	$\Delta\Delta H°$ (kcal/mol)	$\Delta S°$ (cal mol^{-1} K^{-1})	$\Delta\Delta S°$ (cal mol^{-1} K^{-1})
3'-Terminal								
A:dU	-9.5±0.2	-	49.4±0.3	-	-89.0±4.6	-	-251.2±14.2	-
A:U$^{2'F(ara)}$	-9.5±0.2	0.0±0.3	50.3±0.1	0.9±0.3	-84.8±3.2	4.2±5.6	-238.4±9.7	12.8±17.2
A:U$^{2'F(ribo)}$	-9.0±0.2	**0.5±0.3**	49.2±0.2	-0.2±0.4	-79.9±3.9	**9.1±6.0**	-224.3±12.2	**26.9±18.7**
A:dFdU	-9.5±0.2	0.0±0.3	51.0±0.4	1.6±0.5	-85.5±3.3	3.5±5.7	-240.4±10.1	10.8±17.4
A:araU	-9.4±0.1	0.1±0.2	49.8±0.4	0.4±0.5	-85.9±2.6	3.1±5.3	-242.1±7.8	9.1±16.2
A:rU	-9.2±0.1	**0.3±0.1**	49.2±0.2	-0.2±0.4	-83.7±2.2	**5.3±5.1**	-235.7±6.5	15.5±15.6
A:5IdU	-9.4±0.2	0.1±0.3	50.2±0.2	0.8±0.4	-80.3±3.9	**8.7±6.1**	-224.5±12.2	**26.7±18.7**
A:FIAU	-9.7±0.1	-0.2±0.2	51.3±0.2	1.9±0.4	-85.3±3.6	3.7±5.8	-238.9±11.2	12.3±18.1
Internucleotide								
A:dU	-8.1±0.2	-	43.8±0.2	-	-93.2±5.1	-	-271.4±14.9	-
A:U$^{2'F(ara)}$	-8.0±0.1	0.1±0.2	43.8±0.3	0.0±0.4	-85.4±3.0	**7.8±5.9**	-245.7±9.5	**25.7±17.6**
A:U$^{2'F(ribo)}$	-7.8±0.1	**0.3±0.2**	42.9±0.1	-0.9±0.2	-86.7±3.5	**6.4±6.2**	-250.7±11.1	**20.7±18.6**
A:dFdU	-6.9±0.1	**1.2±0.2**	39.5±0.1	-4.3±0.2	-84.7±2.4	**8.5±5.6**	-247.5±7.5	**24.0±16.7**
A:araU	-7.3±0.1	**0.8±0.2**	40.2±0.1	-3.6±0.2	-86.1±2.7	**7.1±5.8**	-250.8±8.5	**20.6±17.2**
A:rU	-7.2±0.1	**0.9±0.2**	41.0±0.1	-2.8±0.2	-82.6±4.2	**10.6±6.6**	-239.5±13.6	**31.9±20.2**
A:5IdU	-8.0±0.2	0.1±0.3	43.7±0.2	-0.1±0.3	-85.3±3.4	**7.9±6.1**	-245.3±10.8	**26.1±18.4**
A:FIAU	-8.1±0.1	0.0±0.3	44.8±0.2	1.0±0.3	-85.9±3.7	**7.3±6.3**	-246.7±11.6	**24.8±18.9**

The impact of the sugar constraint on ΔΔS° has been attributed to a conformational preorganization, reducing the net conformational entropy change upon duplex formation [12]. The impact on ΔΔH° would be attributed to the constrained sugar preventing the formation of the most favorable base stacking geometry. In contrast, $U^{2'F(ara)}$ was substantially less destabilizing than $U^{2'F(ribo)}$ on the 3'-end. However, upon comparison of the impact of $U^{2'F(ara)}$ substitution on the 3'-end to the internucleotide position, $U^{2'F(ara)}$ was more destabilizing in the internucleotide position than on the 3'-end. Put another way, these results predict that the $U^{2'F(ara)}$ nucleoside analogue will be more destabilizing when converted to an internucleotide position through polymerase extension and, consequently, will be difficult to extend. On the other hand, the $U^{2'F(ribo)}$ analogue is less destabilizing at an internucleotide position and will likely be extended by a polymerase. Based on the thermodynamic parameter ΔΔH°, the extent to which a modified analogue will increase or decrease duplex stability when converted to an internucleotide position can be computed by taking the difference between ΔΔH° for duplex formation with the modified nucleoside at an internucleotide position ($\Delta\Delta H°_{Intern}$) and ΔΔH° or for duplex formation with the modified nucleoside at the 3'-terminal position ($\Delta\Delta H°_{3'\text{-}Terminal}$). Thus, positive values of $\Delta\Delta H°_{Intern.} - \Delta\Delta H°_{3'\text{-}Terminal}$ would predict that converting the modified nucleoside analogue to an internucleotide position would decrease duplex stability. Conversely, negative values of $\Delta\Delta H°_{Intern.} - \Delta\Delta H°_{3'\text{-}Terminal}$ would predict that converting the modified nucleoside analogue to an internucleotide position would increase duplex stability. The same analysis can be performed for values of ΔΔS° (Table 6)

Table 6: Comparison of the differences in enthalpy (ΔΔH°) and entropy (ΔΔS°) between 3'-terminal substituted duplexes and duplexes with a substitution at an internucleotide position. The experimental thermodynamic parameters of duplex formation, namely, the measured free energy of duplex formation ($\Delta G°_{37}$), enthalpy (ΔH°), entropy (ΔS°) and melting temperature with a strand concentration of 28 μM ($T_{m\ 28\ \mu M}$) are listed in Table 5.

	$\Delta\Delta H°_{Intern.} - \Delta\Delta H°_{3'\text{-}Terminal}$ (kcal/mol)	$\Delta\Delta S°_{Intern} - \Delta\Delta S°_{3'\text{-}Terminal}$ (cal mol^{-1} K^{-1})
A:dU	-	-
A:$U^{2'F(ara)}$	+3.6[a]	+12.9
A:$U^{2'F(ribo)}$	-2.7[b]	-6.2
A:dFdU	+5.0	+13.2
A:araU	+4.0	+11.5
A:rU	+5.3	+16.4
A:5IdU	-0.8	-0.6
A:FIAU	+3.6	+12.5

[a.] Positive values of $\Delta\Delta H°_{Intern.} - \Delta\Delta H°_{3'\text{-}Terminal}$ and $\Delta\Delta S°_{Intern.} - \Delta\Delta S°_{3'\text{-}Terminal}$ predict that converting the modified nucleoside analogue to an internucleotide position would decrease duplex stability.
[b.] Negative values of $\Delta\Delta H°_{Intern.} - \Delta\Delta H°_{3'\text{-}Terminal}$ and $\Delta\Delta S°_{Intern.} - \Delta\Delta S°_{3'\text{-}Terminal}$ predict that converting the modified nucleoside analogue to an internucleotide position would increase duplex stability.

Upon computing values of $\Delta\Delta H°_{Intern.} - \Delta\Delta H°_{3'\text{-}Terminal}$ and $\Delta\Delta S°_{Intern.} - \Delta\Delta S°_{3'\text{-}Terminal}$ (Table 6), it is apparent that each of the arabinonucleosides (FIAU, $U^{2'F(ara)}$, araU) yield positive values. As such, one would predict that these analogues would be difficult to extend. Consistent with these predictions we observed that Klenow (exo-), AMVRT, pol β exhibited difficulty when extending 3'-FIAU, 3'-$U^{2'F(ara)}$, and 3'-araU (Table 4, Figure 21). When these same calculations are performed for duplexes containing 5IdU, small negative values are obtained for $\Delta\Delta H°_{Intern.} - \Delta\Delta H°_{3'\text{-}Terminal}$ and $\Delta\Delta S°_{Intern.} - \Delta\Delta S°_{3'\text{-}Terminal}$ (Table 6). As such, one would predict that 3'-5IdU would be extended nearly as well as 3'-dU. The kinetic results for pol β and Klenow (exo-) extension of 5IdU are

consistent with this prediction. Finally, this model correctly predicts that 3'-$U^{2'F(ribo)}$ will be readily extended as it yields large negative values of $\Delta\Delta H°_{Intern.} - \Delta\Delta H°_{3'\text{-}Terminal}$ and $\Delta\Delta S°_{Intern.} - \Delta\Delta S°_{3'\text{-}Terminal}$ (Table 6). However, whereas this thermodynamic model correctly predicts the extension behavior of six out of eight nucleoside analogues investigated (dU, 5IdU, $U^{2'F(ara)}$, $U^{2'F(ribo)}$, araU, and FIAU) it does not correctly predict the extension behavior the remaining two (dFdU, rU). Whereas our thermodynamic model predicts that 3'-dFdU and 3'-rU would be poorly extended, our kinetic data demonstrates that they are readily extended. Thus, additional factors, perhaps unique to dFdU and rU and their interaction with the polymerase active site, take precedence over net thermodynamic differences during the extension step.

Concluding Remarks.

We found that surprisingly Klenow (exo-), pol β, and AMVRT extended a 3'-rN more efficiently than a normal 3'-dN or modified 3'-araN. However, the opposite was observed during the incorporation step, namely, each of the three polymerases inefficiently incorporated a rNTP yet readily inserted an araNTP opposite template dA. Our data suggests that selection criteria for nucleotide incorporation might be different from that required for primer extension . Taken together, these data directly demonstrate that sugar modification impacts duplex stability and, consequently, polymerase extension ability. Whereas rigid geometrical constraints imposed by the polymerase active site are believed to be the primary contributor to sugar fidelity at the insertion and extension steps, we also present a basic thermodynamic model for sugar discrimination. Consistent with expectations based on kinetic data, arabinonucleosides form the most stable

duplexes when incorporated onto the primer terminus. However, those same arabinonucleosides are more thermodynamically destabilizing when converted to an internucleotide position, explaining, in part, why polymerases exhibit difficulty extending araNTPs following incorporation. We also reported that, significantly, the deaminated metabolites of Gemcitabine (dFdC) and Cytarabine (araC) reduce duplex melting temperatures by ~ 4 °C when located at an internucleotide position. FIAU- and, surprisingly, dFdU-terminated primers increase duplex stability by ~2 °C. The increased duplex thermal stability resulting from misincorporation of FIAU and dFdU (or the parent compound dFdC) onto the 3'-end likely allows these analogues to elude exonuclease editing mechanisms.

References

(1) Kunkel, T. A. (2004) DNA replication fidelity. J. Biol. Chem. 279, 16895-16898.

(2) Goodman, M. F., Creighton, S., Bloom, L. B., and Petruska J. (1993) Biochemical basis of DNA replication fidelity. Crit. Rev. Biochem. Mol. Biol. 28, 1559-1562.

(3) Joyce, C. M., Sun, X. C., and Grindley, N. D. F. (1992) Reactions at the polymerase active site that contribute to the fidelity of Escherichia coli DNA polymerase I (Klenow Fragment). J. Biol. Chem. 267, 24485–24500.

(4) Petruska, J., Goodman, M.F., Boosalis, M.S., Sowers, L.S., Cheong, C. and Tinoco, I. (1988). Comparison between DNA melting thermodynamics and DNA polymerase fidelity. Proc. Natl. Acad. Sci. USA. 85, 6252-6256.

(5) Perrino, F.W., Preston, B.D., Sandell, L.L. and Loeb, L.A. (1989). Extension of mismatched 3' termini of DNA is a major determinant of the infidelity of human immunodeficiency virus type 1 reverse transcriptase. Proc. Natl. Acad. Sci. 86, 8343-8347.

(6) Zinnen, S., Hsieh, J-C. and Modrich, P. (1994). Misincorporation and mispaired primer extension by human immunodeficiency virus reverse transcriptase. J. Biol. Chem. 269, 24195-24202.

(7) Mendelman, L.V., Petruska, J., and Goodman, M.F. (1990) base pair extension kinetics. Comparision of DNA polymerase α and reverse transcriptase. J. Biol. Chem. 265, 2338-2346.

(8) Shah, A.M., Maitra, M. and Sweasy, J.B. (2003). Variants of DNA polymerase β extend mispaired DNA due to increased affinity for nucleotide substrate. Biochemistry 42, 10709-10717.

(9) Berger, I., Tereshko, V., Ikeda, H., Marquez, V.E. and Egli, M. (1998). Crystal structure of B-DNA with incorporated 2' –deoxy-2' –fluoro-arabino-furanosyl thymines: implications of conformational preorganization for duplex stability. Nucleic Acids Res. 26, 2473-2480.

(10) Damha, M.J., Wilds, C.J., Noronha, A., Brukner, I., Borkow, G., Arion, D. and Parniak, M.A. (1998). Hybrids of RNA and arabinonucleic acids (ANA and 2'F-ANA) are substrates of Ribonuclease H. J. Am. Chem. Soc. 120, 12976-12977.

(11) Ikeda, H., Fernandez, R., Wilk, A., Barchi, J.J., Jr., Huang, X. and Marquez, V.E. (1998). The effect of two antipodal fluorine-induced sugar puckers on the conformation and stability of the Dickerson-Drew dodecamer duplex [d(CGCGAATTCGCG)]2. Nucleic Acids Res. 26, 2237-2244.

(12) Wilds, C.J. and Damha, M.J. (1999). Duplex recognition by oligonuclotides containing 2'-Deoxy-2'-fluoro-D-arabinose and 2'-Deoxy-2'-fluoro-D-ribose. Intermolecular 2'-OH- phosphate contacts versus sugar puckering in the stabilization of triple-helical complexes. Bioconjugate Chem. 10, 299-305.

(13) Schultz, R. G. and Gryaznov, S.M. (2000). Arabino-fluorooligonucleotide N3' →P5' phosphoramidites: synthesis and properties. Tetrahedron Lett. 41, 1895-1899.

(14) Wilds, C.J. and Damha, M.J. (2000). 2' –Deoxy-2' –fluoro-β-D-arabinonucleosides and oligonucleotides (2'F-ANA): synthesis and physicochemical studies. Nucleic Acids Res. 28, 3625-3635.

(15) Trempe, J-F., Wilds, C.J., Yu, Denisov, A.Y., Pon, R.T., Damha, M.J. and Gehring, K. (2001). NMR solution structure of an oligonucleotide hairpin with a 2'F-ANA/RNA stem: Implications for RNase H specificity toward DNA/RNA hybrid duplexes. J. Am. Chem. Soc. 123, 4896-4903.

(16) Kalota, A., Karabon, L., Swider, C.R., Viazovkina, E., Elzagheid, E., Damha, M.J. and Gewirtz, A.M. (2006). 2'-Deoxy-2'-fluoro- β-D-arabinonucleic acid (2'F-ANA) modified oligonucleotides (ON) effect highly efficient, and persistent, gene silencing. Nucleic Acids Res. 34, 451-461.

(17) Peng, C.G. and Damha, M.J. (2007). G-quadruplex induced stabilitization by 2' –deoxy-2' –fluoro-D-arabinonucleic acids (2'F-ANA). Nucleic Acids Res. 35, 4977-4988.

(18) Ziemkowski, P., Felczak, K., Poznanski, J., Kulikowski, T., Zielinski, Z., Ciesla, J. and Rode, W. (2007). Interactions of 2'-fluoro-substituted dUMP analogues with thymidylate synthase. Biochem. Biophys. Res. Comm. 362, 37-43.

(19) Pinto, D., Sarocchi-Landousy, M-T. and Guschlbauer, W. (1979). 2'-Deoxy-2'-fluorouridine-5'-triphosphates: a possible substrate for E. coli RNA polymerase. Nucleic Acids Res. 6, 1041-1048.

(20) Mikita, T. and Beardsley, G.P. (1988). Functional consequences of the arabinosylcytosine structural lesion in DNA. Biochemistry 27, 4698-4705.

(21) Kuchta, R.D., Ilsley, D., Kravig, K.D., Schubert, S., Harris, B. (1992). Inhibition of DNA primase and polymerase alpha by

arabinofuranosylnucleoside triphosphates and related compounds. Biochemistry 31, 4720-4728.

(22) Perrino, F.W. and Mekosh, H.L. (1992). Incorporation of cytoside arabinoside monophosphate into DNA at internucleotide linkages by human DNA polymerase α. J. Biol. Chem. 267, 23043-23051.

(23) Lewis, W., Meyer, R.R., Simpson, J.F., Colacino, J.M., Perrino, F.W. (1994). Mammalian DNA polymerases alpha, beta, gamma, delta, and epsilon incorporate fialuridine (FIAU) monophosphate into DNA and are inhibited competitively by FIAU triphosphate. Biochemistry 33, 14620-14624.

(24) Ono, T., Scalf, M. and Smith, L.M. (1997). 2' –Fluoro modified nucleic acids: polymerase-directed synthesis, properties and stability to analysis by matrix-assisted laser desorption/ionization mass spectrometry. Nucleic Acids Res. 25, 4581-4588.

(25) Perrino, F.W., Mazur, D.J., Ward H. and Harvey, S. (1999). Exonucleases and the incorporation of aranucleotides into DNA. Cell. Biochem. Biophys. 30, 331-352.

(26) Richardson, K.A., Vega, T.P., Richardson, F.C., Moore, C.L., Rohloff, J.C., Tomkinson, B., Bendele, R.A. and Kuchta, R.D. (2004). Polymerization of the triphosphates of AraC, 2', 2' –difluorodeoxycytidine (dFdC) and OSI-7836 (T-araC) by human DNA polymerase alpha and DNA primase. Biochem. Pharmacol. 68, 2644-3647.

(27) Pankiewicz K.W. (2000) Fluorinated nucleosides. Carbohyd. Res. 327, 87-105.

(28) Lai, Y., Tse, C.M., Unadkat, J.D. (2004) Mitochondrial expression of the human equilibrative nucleoside transporter 1 (hENT1) results in enhanced mitochondrial toxicity of antiviral drugs. J. Biol. Chem. 279, 4490-4497.

(29) Pastor-Anglada, M., Molina-Arcas, M., Casado, F.J., Bellosillo, B., Colomer, D., and Gil, J. (2004) Nucleoside transporters in chronic lymphocytic leukaemia. Leukemia 18, 385-393.

(30) Zhang, J., Visser, F., King, K.M., Baldwin S.A., Young, J.D., Cass, C.E. (2007) The role of nucleoside transporters in cancer chemotherapy with nucleoside drugs. Cancer Metastasis Rev. 26, 85-110.

(31) Heinemann, V., Schulz, L., Issels, R.D., and Plunkett, W. (1995) Gemcitabine: a modulator of intracellular nucleotide and deoxynucleotide metabolism. Semin Oncol. 4, Suppl. 11, 11-18.

(32) Huang, P., Chubb, S., Hertel, L.W., Grindey, G.B., Plunkett, W. (1991) Action of 2',2'-difluorodeoxycytidine on DNA synthesis. Cancer Res. 51, 6110-6117.

(33) Iwasaki, H., Huang, P., Keating, M.J., Plunkett, W. (1997) Differential incorporation of ara-c, gemcitabine, and fludarabine into replicating and repairing DNA in proliferating human leukemia cells. Blood 90, 270-278.

(34) Konerding, D., James, T.L., Trump, E., Soto, A.M., Marky, L.A., and Gmeiner, W.H. (2002) NMR structure of a Gemcitabine-substituted model Okazaki fragment. Biochemistry 41, 839-846.

(35) Gmeiner, W.H., Konerding, D., and James, T.L. (1999) Effect of Cytarabine on the NMR structure of a model Okazaki fragment from the SV40 genome. Biochemistry 38, 1166-1175.

(36) Hamamoto, S and Takaku, K. (1986) New approach to the synthesis of deoxyribonucleoside phosphoramidite derivatives. Chem. Lett., 1401-1404.

(37) Barone, A.D., Yang, J.-Y. Caruthers, M.H. (1984) In situ activation of bis-dialkylaminophosphines - a new method for synthesizing deoxyoligonucleotides on polymer supports.

(38) Gait, M.J. (1984) Oligonucleotide synthesis: a practical approach, Oxford, IRL Press, Washington, DC.

(39) Puglisi, J. D., and Tinoco, I., Jr. (1989) Absorbance melting curves of RNA. Methods in Enzymology (Dahlberg, J. E., and Abelson, E. N., Eds.) Vol. 180, pp 304-325, Academic Press, Orlando, FL.

(40) SantaLucia, J., Jr., Allawi, H. T., and Seneviratne, P. A. (1996) Improved nearest-neighbor parameters for predicting DNA duplex stability. Biochemistry 35, 3555–3562.

(41) Allawi, H. T., and SantaLucia, J., Jr. (1997) Thermodynamics and NMR of internal G●T mismatches in DNA. Biochemistry 36, 10581–10594.

(42) Williams, A.A., Darwanto, A., Theruvathu, J.A., Burdzy, A., Neidigh, J.W., Sowers, L.C. (2009) Impact of sugar pucker on base pair and mispair stability. Biochemistry 48, 11994-12004.

(43) Cui, Z., Theruvathu, J.A., Farrel, A., Burdzy, A., Sowers, L.C. (2008) Characterization of synthetic oligonucleotides containing biologically important modified bases by matrix-assisted laser desorption/ionization time-of-flight mass spectrometry. Anal. Biochem. 379, 196-207.

(44) Ferrer, E., Wiersma, M., Kazimierczak, B., Muller, C.W., Eritja, R. (1997) Preparation and properties of oligodeoxynucleotides containing 5-iodouracil and 5-bromo- and 5-iodocytosine. Bioconjugate Chem. 8, 757-761.

(45) Sheardy, R.D., and Seeman, N.C. (1986) Synthesis of a deoxyoligonucleotide incorporating 5-iododeoxyuridine. J. Org. Chem. 51, 4301-4303.

(46) Pon, R. T., and Yu, R. (1997) Hydroquinone-O,O-diacetic acid as a more labile replacement for succinic acid linkers in solid-phase oligonucleotide synthesis. Tetrahedron Lett. 38, 3327–3330.

(47) Azhayev, A. V., and Antopolsky, M. L. (2001) Amide group assisted 3'-dephosphorylation of oligonucleotides synthesized on universal A-supports. Tetrahedron 57, 4977–4986.

(48) Boosalis, M.S., Petruska, J., Goodman, M.F. (1987) DNA polymerase insertion fidelity: gel assay for site-specific kinetics. J. Biol. Chem. 262, 14689-14696.

(49) Batra V.K., Beard, W.A., Shock, D.D., Krahn, J.M., Pedersen, L.C., Wilson, S.H. (2006) Magnesium-induced assembly of a complete DNA polymerase catalytic complex. Structure 14, 757-766.

(50) Kiefer, J.R., Mao, C., Braman, J.C., Beese, L.S. (1998) Visualizing DNA replication in a catalytically active Bacillus DNA polymerase crystal. Nature 391, 304-307.

(51) Doublie, S., Tabor, S., Long, A.M., Richardson, C.C., Ellenberger, T. (1998) Crystal structure of a bacteriophage T7 DNA replication complex at 2.2 Å resolution. Nature 391, 251-255

(52) Li, Y., Korolev, S., Waksman, G. (1998) Crystal structures of open and closed forms of binary and ternary complexes of the large fragment of Thermus aquaticus DNA polymerase I: structural basis for nucleotide incorporation. EMBO J. 17, 751-7525.

(53) Jacobo-Molina, A., Ding, J., Nanni, R.G., Clark Jr., A.D., Lu, X., Tantillo, Ch., Williams, R.L., Kamer, G., Ferris, A.L., Clark, P., Hizi, A., Hughes, S.H., Arnold, E. (1993) Crystal structure of human immunodeficiency virus type 1 reverse transcriptase complexed with double-stranded DNA at 3.0 Å resolution shows bent DNA. Proc. Natl. Acad. Sci. USA 90, 6320-6324.

(54) Ding, J., Hughes, S.H., Arnold, E. (1998) Protein-nucleic acid interactions and DNA conformation in a complex of human immunodeficiency virus type 1 reverse transcriptase with a double-stranded DNA template-primer. Biopolymers 44, 125-138.

(55) Saenger, W., Hunter, W.N., Kennard, O. (1986) DNA conformation is determined by economics in the hydration of phosphate groups. Nature 324, 385-388.

(56) Feig, M. and Pettitt, B.M. (1998) A molecular simulation picture of DNA hydration around A- and B-DNA. Biopolymers 48, 199-209.

(57) Harrington, C. and Perrino, F.W. (1995) The effects of cytosine arabinoside on RNA-primed DNA synthesis by DNA polymerase α-primase. J. Biol. Chem. 270, 26664-26669.

(58) Gmeiner, W.H., Skardis, A., Pon, R.T., Liu, J. (1998) Cytarabine-induced destabilization of a model Okazaki fragment. Nucleic Acids Res. 26, 2359-2365.

(59) Gao, Y.-G., van der Marel, G.A., van Boom, J.H., Wang A.H.-J. (1991) Molecular structure of a DNA decamer containing an anticancer nucleoside arabinosylcytosine: conformational perturbation by arabinosylcytosine in B-DNA. Biochemistry 30, 9922-9931

(60) Noronha, A.M., Wilds, C.J., Lok, C.-N., Viazovkina, K., Arion, D., Parniak, M.A., Damha, M.J. (2000) Synthesis and biophysical properties of arabinonucleic acids (ANA): circular dichroic spectra, melting temperatures, and ribonuclease H susceptibility of ANA.RNA hybrid duplexes. Biochemistry 39, 7050-7062.

(61) Schweitzer, B.I., Mikita, T., Kellogg, G.W., Gardner, K.H., Beardsley, G.P. (1994) Solution structure of a DNA dodecamer containing the anti-neoplastic agent arabinosylcytosine: combined use of NMR, restrained molecular dynamics, and full relaxation matrix refinement. Biochemistry 33, 11460-11475

(62) Wilds, C.J. and Damha, M.J. (2000) 2'-Deoxy-2'-fluoro-β-D-arabinonucleosides and oligonucleotides (2'F-ANA): synthesis and physiochemical studies. Nucleic Acids Res 28, 3625-3635.

(63) Watts, J.K., Martin-Pintado, N., Gomez-Pinto, I., Schwartzentruber, J., Portella, G., Orozco, M., Gonzalez, C., Damha, M.J. (2010) Differential stability of 2'F-ANA●RNA and ANA●RNA hybrid duplexes: roles of structure, pseudohydrogen bonding, hydration, ion uptake and flexibility. Nucleic Acids Res. 38, 2498-2511.

(64) Li, F., Sarkhel, S., Wilds, C.J., Wawrzak, Z., Prakash, T.P., Manoharan, M., Egli, M. (2006) 2'-Fluoroarabino- and arabinonucleic acid show different

conformations, resulting in deviating RNA affinities and processing of their heteroduplexes with RNA by RNase H. Biochemistry 45, 4141-4152.

(65) Tollin, P., Wilson, H.R., Young, D.W. (1973) The crystal and molecular structure of uracil-β-D-arabinofuranoside. Acta Cryst B29, 1641-1647.

(66) Yathindra, N. and Sundaralingam, M. (1979) Conformational analysis of arabinonucleosides and nucleotides: a comparison with the ribonucleosides and nucleotides. Biochim Biophys Acta 564, 301-310 Momparler, R. L., and J. Goodman. "In Vitro Cytotoxic and Biochemical Effects of 5-Aza-2'-Deoxycytidine." *Cancer Res* 37, no. 6 (1977): 1636-9.